Solid-State Microwave Heating for Biomedical Applications

A thesis submitted to the Cardiff University in candidature for the degree of

Doctor of Philosophy

By

Azeem Imtiaz
April 2015

Department of Electrical and Electronic Engineering, Cardiff University, United Kingdom

Declaration

This work has not previously been accepted in substance for any degree and is not concurrently submitted in candidature for any other higher degree.

Signed:……..(Candidate) Date:…….

Statement 1

This thesis is being submitted in partial fulfilment of the requirements for the degree of ……..(insert as appropriate PhD, MPhil, EngD)

Signed:……..(Candidate) Date:…….

Statement 2

This thesis is the result of my own independent work/investigation, except where otherwise stated. Other sources are acknowledged by explicit references.

Signed:……..(Candidate) Date:…….

Statement 3

I hereby give consent for my thesis, if accepted, to be available for photocopying, inter-library loan and for the title and summary to be made available to outside organisations.

Signed:……..(Candidate) Date:…….

Copyright © 2015 Azeem Imtiaz

Cardiff School of Engineering, Trevithick Building, 14-17

The Parade, Cardiff, South Glamorgan CF24 3AA

United Kingdom.

Abstract

The research conducted in this thesis aims to develop an efficient microwave delivery system employing miniature resonant microwave cavities, targeted at compact, flexible and ideally field-deployable microwave-assisted diagnostic healthcare applications. The system comprises a power amplifier as a solid-state microwave source and a load - as a single mode cavity resonator to hold the sample. The compactness of the practical microwave delivery system relies on the direct integration of the sample-holding cavity resonator to the power amplifier and inclusion of the built-in directional coupler for power measurements. The solid state power transistors used in this research (10W-LDMOS, 10W-GaN) were provided by the sponsoring company NXP Inc.

In practical microwave delivery applications, the impedance environment of the cavity resonators change significantly, and this thesis shows how this can be systematically utilized to present the optimal loading conditions to the transistor by simply designing the series delay lines. This load transfer technique, which critically can be achieved without employing bulky, lossy and physically larger output matching networks, allows high performance of the power amplifier to be achieved through waveform engineering at the intrinsic plane of the transistor.

Starting with the impedance observation of a rectangular cavity, using only series delay lines allowed the practical demonstration of the high power and high efficiency fully integrated inverse class-F (F^{-1}) power amplifier.

Temperature is an important factor in a microwave heating and delivery system as it changes the impedance environment of the cavity resonator. This natural change in both cavity and sample temperature can be accommodated through simplified series matching lines and the microwave heating system capable of working over substantial bandwidth was again practically demonstrated. The inclusion of the coupler maintained the compactness of the system.

In the practical situations envisaged, the microwave delivery system needs to accommodate natural variation between sample volumes and consistencies for heating. The experimental work considered the heating of different sample volumes

of water, and characterizing the change in the natural impedance environment of the cavity as a result. It was shown how the natural impedance variation can not only be accommodated, but also exploited, allowing 'continuous', high-efficiency performance to be achieved while processing a wide range of sample volumes. Specifically, using only transistor package parasitic, the impedance of the cavity itself together with a single series microstrip transmission line allows a continuous class-F^{-1} mode loading condition to be identified.

Through different experiments, the microwave delivery systems with high-performance are demonstrated which are compact, flexible and efficient over operational bandwidth of the cavity resonators.

Acknowledgements

I begin by thanking Allah (the exalted) for blessing me with the excellent opportunity to pursue my doctoral research studies at Cardiff University in the supervision of the distinguished scientists.

From the formative stages of this thesis to the final draft, I owe an immense debt of gratitude to my supervisor Dr. Jonathan Lees. I acknowledge that his sound advice, wisdom and commitment; kept my thesis on track during this time. Besides that, his insightful criticism and appreciation to my work was such an amazing blend that I found myself motivated throughout my studies.

I am thankful to NXP, Nijmegen area, Netherlands for sponsoring my doctoral studies and I acknowledge the support of Dr. Klause Werner and Richard John Marlow for always expressing their interests and appreciation to my research work during conference meetings and informal telephone calls. Also I pay my sincere thankfulness to Dr. Aamir Sheikh and Dr. Akmal for many hours of academic discussions.

I pay my sincere thankfulness to Professor Adrian Porch and for Professor Steve Cripps for always being very supportive and explaining me with difficult RF concepts in very simple words.

During my work at school of engineering, I enjoyed the amazing company of my colleagues particularly Zulhazmi, David, Jerome and Jon who were always friendly and supportive. I'm grateful to everyone in the RF research group for several academic and nonacademic useful discussions throughout my studies.

My special gratitude is for my family members particularly, my father and my brother Ijaz, who always helped me to improve the positive sides of myself.

I'm lacking words to pay my sincere thankfulness to my wife Sara and my son Khalid who always stood beside me and supported me during difficult times. You both are simply great and I thank you for your ever green smiles.

Cardiff, United Kingdom, April 2015

Dedicated to my parents,

Mr. Muhammad Aslam & Mrs. Shehnaz Akhtar

List of Publications

First Author Papers

1 **Azeem Imtiaz**, Zulhazmi A.Mokhti, Jerome Cuenca and Jonathan Lees, "An Integrated Inverse-F power amplifier design approach for heating applications in a microwave resonant cavity" *IEEE Asia Pacific Microwave Conference*, pp.756-758, Nov 2014.

2 **Azeem Imtiaz**, Jon Hartley, Heungjae Choi and Jonathan Lees, "A High Power High Efficiency Integrated Solid-State Microwave Heating Structure for Portable Diagnostic Healthcare Applications", *IEEE-MTT-S IMWS-Bio Conference*, pp.147-149, Dec 2014

3 **Azeem Imtiaz**, Jonathan Lees and Heungjae Choi, "An Integrated Continuous F^{-1} Mode Power Amplifier Design Approach for Microwave Enhanced Portable Health-Care Applications", *IEEE-MTT-S IMWS-Bio Mini Special Issue*, no.1,vol.1, Apr 2015 US (Accepted –awaiting publication)

Additional Papers

1 Hana Dobšíček Trefna, **Azeem Imtiaz**, Hoi-Shun Lui and Mikael Persson ,"Evolution of an UWB Antenna for Hyperthemia Array Applicator" *6th European Conference on Antennas and Propagation*, pp.1046-1048, March 2012.

List of Terms

- RF — Radio Frequency
- LDMOS — Laterally diffused metal-oxide semiconductor
- GaN — Gallium Nitride
- PA — Power Amplifier
- E-Field — Electric Field
- H-Field — Magnetic Field
- ISM — Industrial Scientific and Medical
- TE — Transverse Electric
- TM — Transverse Magnetic
- EM — Electromagnetic
- CAD — Computer Aided Design
- Q-Factor — Quality Factor
- RLC — Resistor-Inductor-Capacitor
- PAE — Power Added Efficiency
- MAG — Maximum Available Gain
- OMN — Output Matching Network
- VDS — Drain-Source Voltage
- VGS — Gate-Source Voltage
- V_{Knee} — Knee Voltage
- CW — Continuous Wave
- DUT — Device Under Test
- VNA — Vector Network Analyzer
- DAQ — Data Acquisition
- I_{GEN}-Plane — Current Generator Plane
- DAC — Data Access Component
- CF^{-1} — Continuous F Inverse
- DNA — Deoxyribonucleic Acid
- *C-difficile* — Clostridium Difficile
- RT PCR — Reverse Transcription-Polymerase Chain Reaction
- MAMEF — Microwave-Accelerated Metal-Enhanced Fluorescence

Contents

CHAPTER.1 INTRODUCTION 1

1.1 SOLID-STATE MICROWAVE HEATING 1
1.2 RESEARCH MOTIVATION 3
1.3 THESIS OUTLINE 3

CHAPTER.2 LITERATURE REVIEW 5

2.1 MICROWAVE HEATING 6
2.2 CONVENTIONAL MICROWAVE HEATING 7
2.3 SOLID-STATE MICROWAVE HEATING 13
2.4 POWER AMPLIFIER MODES OF OPERATION 23
2.5 POWER AMPLIFIER DESIGN LIMITATIONS AND SOLUTIONS 31
2.6 BIOMEDICAL HEALTHCARE DIAGNOSTIC APPROACHES 35
2.7 CHAPTER SUMMARY 39
REFERENCES 41

CHAPTER.3 TRANSISTOR TECHNOLOGY AND CHARACTERIZATION 44

3.1 POWER TRANSISTOR 44
3.2 TRANSISTOR DE-EMBEDDING 46
3.3 TRANSISTOR CHARACTERIZATION AND LOAD LINE 60
3.4 ACTIVE HARMONIC LOAD-PULL MEASUREMENT SETUP 66
3.5 INVERTED CLASS-F WAVEFORM ENGINEERING (AT 900MHZ) 71
3.6 SUMMARY 79
REFERENCE 80

CHAPTER.4 INTEGRATED INVERSE-F POWER AMPLIFIER FOR MICROWAVE HEATING 81

4.1 INTRODUCTION 81
4.2 DESIGN PROCESS 82
4.3 TRANSISTOR CHARACTERIZATION (AT 2.45GHZ) 84
4.4 RECTANGULAR CAVITY RESONATOR 94
4.5 INTEGRATED F^{-1} POWER AMPLIFIER DESIGN 107
4.6 SUMMARY 111
REFERENCES 112

CHAPTER.5 INTEGRATED CONTINUOUS MODE POWER AMPLIFIER FOR MICROWAVE HEATING 113

5.1 INTRODUCTION 113
5.2 GAN POWER TRANSISTOR TECHNOLOGY AND ANALYSIS 114
5.3 LARGE SIGNAL ANALYSIS OF 10W-GAN POWER TRANSISTOR (AT 2.45GHZ) 118
5.4 TM_{010} MODE SPLIT CIRCULAR CAVITY RESONATOR 124
5.5 UNDERSTANDING CONTINUOUS-F^{-1} MODE 132
5.6 THE DIRECT INTEGRATED CONTINUOUS CLASS-F^{-1} POWER AMPLIFIER 135
5.7 SUMMARY 141
REFERENCE 142

CHAPTER.6 THE EFFECT OF TEMPERATURE IN SOLID-STATE MICROWAVE HEATING.....145

6.1 INTRODUCTION 145
6.2 DESIGN PROCESS 146
6.3 CAVITY RESONATORS AND MICROWAVE HEATING.....147
6.4 CAVITY PERTURBATIONS.....147
6.5 CONTROLLED HEATING ARRANGEMENT 154
6.6 TM_{010} MODE CIRCULAR CAVITY CHARACTERIZATION 156
6.7 TRANSISTOR CHARACTERIZATION 159
6.8 INTEGRATED NARROWBAND F^{-1} POWER AMPLIFIER DESIGN.....160
6.9 INTEGRATED BROADBAND POWER AMPLIFIER DESIGN 162
6.10 SUMMARY.....165
REFERENCE.....166

CHAPTER.7 CONCLUSION AND DISCUSSION 168

CHAPTER.8 FUTURE WORK 171

8.1 COAXIAL CONNECTION REMOVAL 171
8.2 MEASUREMENT TECHNIQUE 171
8.3 COAXIAL CONNECTOR VS T.L CONNECTOR MEASUREMENTS 173

APPENDIX-A 175

APPENDIX-B 177

APPENDIX-C 178

Chapter.1 INTRODUCTION

1.1 Solid-state Microwave Heating

During the last decade, the need for configurable, flexible and mobile electrical equipment has become an inevitable phenomenon. The electrical industry in its various forms is growing with each new day. A small part of this industry focuses on microwave or microwave-assisted heating applications, dominated by domestic microwave ovens. In such ovens, the heat is typically generated using a magnetron operating at 2.45GHz. The magnetron converts high-voltage electrical energy into microwave energy which is then used to excite polar water molecules within the food. The frequency of operation (2.45GHz) is important for two reasons:

Firstly, because it lies within the dedicated ISM (industrial scientifc and medical) frequency band and *secondly*, at this frequency the penetration depth of the microwaves is sufficient to excite the water molecules contained in the food for microwave heating.

Although the magnetron is a tried and tested solution, it is not always the best solution. This is the case in the healthcare application that is the focus of this work. The uneven and unpredictable field distrubtion that results when multi-mode cavities, such as those used in domestic microwave ovens, are excited using magnetrons that are inherently broadband (20MHz) make them less than ideal for operation in applications where precise delivery of microwave energy is important. The high-power / high-voltage requirements (kW and kV levels respectively) associated with magnetrons also present problems when applications are required to be small-size, low-energy, battery-operated and portable. In addition, commercial size microwave ovens possess extremely complex impedance environments due to their multimode nature, and this makes it very difficult to target and identify specific resonant modes under varying loading conditions. An unpredictable field complexity of the cavity and high input power requirements of the magnetron therefore limit their use in the research sector where precise delivery of microwave energy is key.

In contrast, single mode resonant cavities have well defined behaviour in terms of their field distribution and impedance environments, and it is possible to identify and design

specific resonant modes of interest. Single mode resonators, either used for material characterization using low power (μW-mW) signals or used for microwave heating / disruption using larger signal levels (>10W) possess specific impedance environments at fundamental and harmonic frequencies. This not only allows accurate modal and impedance analysis of the fundamental signal component but also offers specific power amplifier possibilities when considering the harmonic components and terminations.

Replacing magnetrons with solid-state power amplifiers and commercial size cavities with the single mode microwave cavities has attracted the interest of both industry and academia because, they offer design flexibility, energy efficiency and portability for various microwave eapplications. A significant stake holder in favour of this new technology is the biomedical industry, demanding compact, light-weight, portable and efficient apparatus for health-care applications. With the emergance and development of modern-day biomedical systems, one motivation is for diagnostic equipment that may be needed at the bedside, for rapid diagnosis of infection. In this particular example, a sample containing a bacteria of interest is held inside the cavity resonator and exposed to high electric field microwave signals. This causes the bacterium and bacterial spore to rupture and for DNA to 'leak out' allowing subsequent detection.

In such systems the reliability and cost-effectivenss are two other important parameters that need to be carefully considered before practically deploying the equipment. For example, in 2014, an expensive and narrowband solid-state microwave generation system was introduced by Emblation microwave Inc. in which GaN power transistor was used for generating high power RF signals at 2.45GHz. The power generation stage of the system was designed to operate in a fixed 50Ω impedance environment without high efficiency output matching network synthesis thus, approxiamately 50% efficiency was demonstrated. Most of the present age equipments are integrated with the radio frequency technology such as power amplifiers, microwave antennas or both. In each case, the equipment efficiency with respect to output power, flexibility and cost effectiveness is paramount. For example, in microwave power generation systems, the main power consuming part is the Power Amplifier which broadly identifies the system performance, reliability and cost.

1.2 Research Motivation

The focus of the research is:

- To design a compact, physically small and field deployable solid-sate microwave heating apparatus, employing high-efficiency power amplifier modes of operation and suitable for diagnostic healthcare applications.
- To extend the above and to consider how continuous modes design techniques can be employed to achieve high performance over varying resonant frequency and cavity loading conditions.
- To adopt a direct-integrated power amplifier design approach, by eliminating the need for an additional physically large and lossy output matching network, for a compact heating structure.

1.3 Thesis Outline

Chapter 2 outlines the literature review, encompassing cavity resonators, high-efficiency power amplifier modes of operation, direct integrated PA design approaches and the conventional biomedical healthcare systems with a final comparison.

Chapter 3 describes an in-depth understanding of the transistor technologies used, transistor de-embedding, DC and RF characterization, loadpull measurement working principles and waveform engineering. The last part of this chapter includes the nonlinear chracterization of 10W-LDMOS power device at 900MHz to identify an inverted class-F (F^{-1}) mode of operation through waveform engineering.

Chapter 4 practically demonstrates a novel methodology for designing the direct integrated, high-power, high-efficiency and portable solid state microwave heating arrangement suitable for the targeted diagnostic healthcare application. In this method, a 300 µl water loaded rectangular cavity resonator together with simple series delay lines work as part of an integrated F^{-1} power amplifier matching network designed at 2.45GHz. This design technique also demonstrates the high efficiency F^{-1} power amplifier waveforms at the intrinsic plane of the 10W-LDMOS power transistor.

Chapter 5 further extends the work presented in chapter 4. The solid state microwave heating arrangement has been designed to accommodate a range of water sample volumes and temperatures, whilst maintaining a continuous microwave efficiency

over the operational bandwidth of the cavity resonator. Direct integration of the power amplifier into the cavity resonator significantly reduces the physical size of the structure. Anti-phasing of the fundamental and 2nd harmonic loads at the intrinsic plane of the 10W-GaN power transistor makes it a true continuous-Inverse-F Power Amplifier.

Chapter 6 describes the effect of temperture on the resonance and impedance properties of the sample holding cavity during microwave heating process. The natural change appearing in the resonance and impedance environment of the cavity during microwave heating process has been systematically accommodated to formulate the integrated microwave heating apparatus. The compact, flexible and broadband microwave heating structure operates efficiently over the functional bandwidth of the cavity resonator.

Conclusion and discussion of this thesis is outlined in chapter 7. In this chapter the complete summary of the thesis and the detalied discussion about three novel experiments have been outlined. This chapter starts off with the transistor technology and the cavity resonators used in this research. The three novel experiments conducted in Chapter-4, Chapter-5 and Chapter-6 have been discussed briefly. The main concept of integrated power amplifier design for microwave heating applications have been outlined. Most importantly the importance of the direct integrated PA design for biomedical applications have been emphasized In conclusion, high-efficiency PA mode impedances have been achieved by utilizing the natural impedance environment of the sample holding cavity and fundamental, 2nd and 3rd harmonic loads have been transformed to the optimum impedance locations of the transistor by using simple series delay lines. The cavity impedance exploitation and load transformation procedure has been adopted by taking motivation from passive laodpull techniques.

and future work is presented in chapter 8 that explains the implementation of a fully integrated PA structure by completely removing the coaxial connector. in this chapter it has been shown that the delay lines printed on the substrate can be directly mounted on the top surface of the cavity such that the cavity surface acts as a natural ground. Three experiments demonstarted in this thesis can be performed again by using this new technique.

Chapter.2 LITERATURE REVIEW

This chapter outlines the existing literature on magnetron based microwave heating approaches and compares it with the application based solid-state microwave heating method that can offer significant improvements to the established heating techniques. The motivation of this research is to replace the magnetron and multimode cavities with high-power amplifiers (PAs) and at least for this work, single mode cavity resonators respectively.

As briefly outlined earlier that, solid-state microwave heating arrangement can be used in biomedical applications, opening a door to portable, and field deployable diagnostic equipment. It is believed that by adopting this approach, energy efficient and battery operated flexible microwave heating structures can be introduced to initially meet the needs of specific healthcare requirements, and at high volume in future in applications such as domestic cooking.

Such a microwave heating apparatus contains a microwave energy *'source'* as transistor and a *'load'* as coupling structure assisted microwave '*cavity resonator'*.

The biomedical application based microwave heating arrangement presented in this thesis can be visualized in two ways:

- A compact, field deployable, efficient '*microwave heating arrangement*' using a solid-state power source, and a single mode microwave cavity resonator.
- A highly compact '*high efficiency mode power amplifier'* using waveform engineering techniques.

The new two-way design approach, looking seperately at the resonator and then the PA offers a solution to the limitations imposed by the traditional methods in both cases. In the next section we will discuss the performance limitations in the microwave heating arrangements using conventional approach and how the new design approach can offer improved solutions. Therefore, to understand the basic difference between the magnetron based microwave heating and solid-state microwave heating; it is important to know the working principle of the microwave energy source (*magnetron*), the energy guiding structure (*wave guide*), the load (*oven*) and the resulting E-Field distribution in the cavity.

2.1 Microwave Heating

Heating produced due to the friction between the water molecules by the application of electromagnetic energy is called the microwave heating. Water is an important factor behind microwave heating of many samples. In conventional microwave ovens, microwave heating results due to the back and forth motion of the polar water molecules. A water molecule consists of one oxygen atom and two hydrogen atoms which are tightly bound through covalent bonding such that due to the force of repulsion the angle between two hydrogen atoms is 104°[1]. Water molecules, in the absence of any external applied electric field, are spread evenly and have their random slow motion. However, in the presence of an external static E-Field, the randomly moving water molecules align themselves with the external electric field in the direction of electric lines of force [2]. In case of alternating electric field, the water molecules move back and forth along the alternating waves and again try to align themselves with the alternating electric field. Magnetron based microwave ovens make use of this natural property of water and force water molecules to move along the alternating electric field component.

Commercial microwave ovens work at 2.45GHz for heating of the food, the reason for this frequency choice is this frequency lies conveniently within an ISM band, whilst sufficient penetration depth of microwaves into the food is achieved.

The loss tangent of a material is another important factor in heating, given by

$$\tan(\delta) = \frac{\varepsilon_2}{\varepsilon_1} \tag{2.1}$$

Where ε_2 is the imaginary part of the complex permitivity and quantifies the conversion of electromagnetic energy to heat, and ε_1, the real part describes the ability of the material to store energy, or the polarization ability of the material under applied E-Field. Loss-factor is responsible for microwave heating and its maximum value occurs at nearly 20GHz as shown in Fig.2.1.

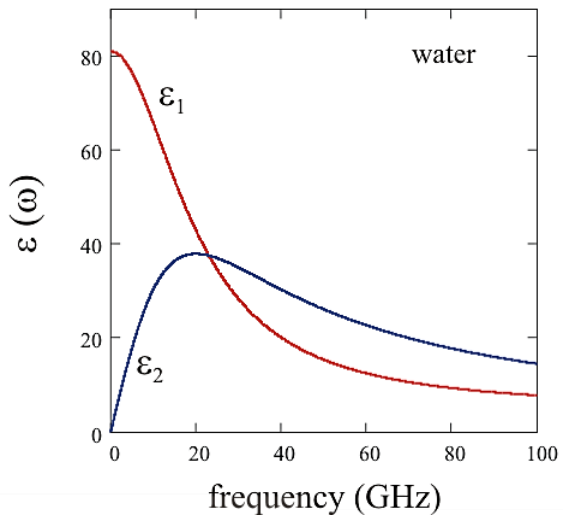

Figure 2.1: Dielectric constant and dielectric loss as function of frequency [2]

Therefore, frequency selection is a very important parameter in microwave heating because it is related to the dipole moment of water molecules. For example, a low frequency E-Field will result in slower dipole moments resulting in lower heat dissipation. This phenomenon will be explained in chapter 6 in Fig.6.1. Similarly at very high frequency of operation, water molecules will fail to align themselves with the alternating electric field and their relaxation time will be too short for efficient heating, this fact has also been elaborated further in chapter 6. Penetration depth is the length from the outer layer to the inner layer of a material where microwave power attenuates 37% from the outer layer [2]. At very high frequencies, the penetration depth of the electromagnetic radiations is too small to reach sufficient depth, thus the outer surface of material gets hot while the inner water layers still remain cold. Therefore, the magnetrons are designed to operate at 2.45GHz firstly because of the deep penetration and secondly this frequency lies within ISM band[2] which is specific for short range ultra-wideband operations only and does not interfere with other frequency allocated bands.

2.2 Conventional Microwave Heating

A typical microwave oven contains three main components; a magnetron, a waveguide and a chamber for microwave heating. The magnetron generates microwave energy, the waveguide directs that energy and the metal chamber safely reflects and 'holds' the resulting standing wave field pattern needed for heating . In principle, a microwave

oven heats no differently to any other type of heat transfer. At molecular level, heat is a transfer of energy that results in increased motion of molecules in a substance. In a traditional oven the food is heated by placing a pan on a burner or in the oven where the walls radiate heat which cooks the outside of the food. The insides cook when heat transfers from the surface of the food to interior. In contrast, the energy from the magnetron penetrates into the food which means the whole of the food can potentially be cooked simultaneously, although conduction also plays a role. Thus in magnetron based heating systems the food cooks from inside to outside.

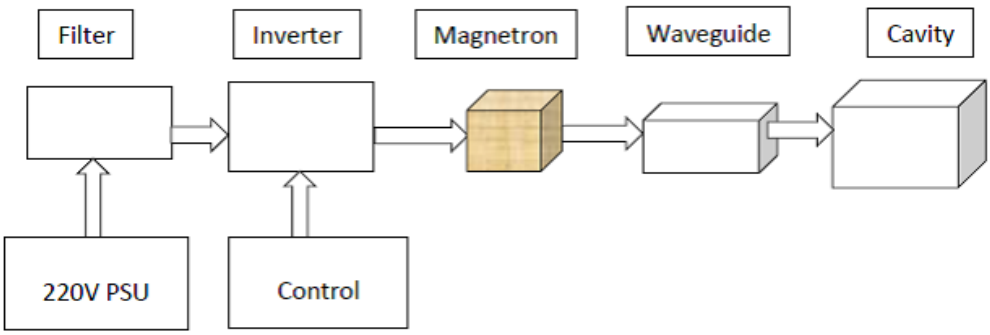

Figure 2.2: Block diagram: microwave oven components and working principle

2.2.1 The Magnetron

The magnetron is an oscillatory device which generates high power microwave signals from DC supply to the cavity. A high density stream of electrons passing by the applied magnetic field in magnetron generates microwave radiation. A magnetron is also sometimes called a cross-field device because it employs both E and H fields in its operation at the same time. The modern resonant cavity magnetron was invented by John Randall and Harry Boot in 1940 [3] and operated at a high DC voltage. The AC line voltage is converted to higher DC voltage so that the high density stream of electrons should be able to generate enough microwave energy for cooking.

Within the Magnetron, there is a vacuum tube located inside the cooling fins which are thin pieces of metal that dissipate heat due largely to refelcted energy as the magnetron operates. The key parts are two magnets and the vacuum tube. A large voltage is applied across both the inner filament and the circular copper outside. This voltage 'boils' electrons off the center filament and they then rapidly progress to the circular copper section. The filament is made from tungsten and thorium; tungsten

because it can withstand high temperatures and thorium because it is good source of electrons. The permenent magnet's field bends the electron stream so the electrons swing back towards center filament. The magnetic field strength is constant but can be finely adjusted so that the now orbiting electrons just pass over the opening of the cavities, a little like blowing over a half filled bottle to make a note.

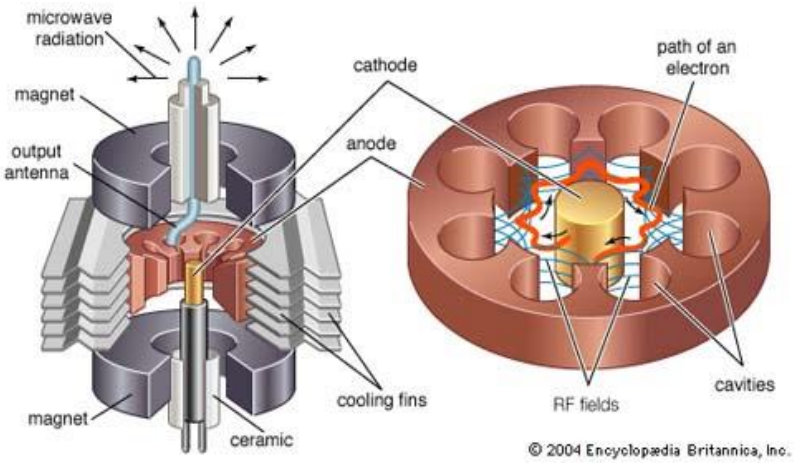

Figure 2.3: Cavity magnetron inside view [4]

2.2.2 The Waveguide

A physical structure used to carry the waves is called waveguide. It is a guiding structure that constrains the scattered waves and propagates them in a particular direction. The function of a waveguide can be estimated by its structure. For example, slab waveguide restricts the electromagnetic energy for unidirectional propagation. Similarly, there are other waveguides that allow the energy to flow in two dimensions such as fiber or channel waveguide. According to inverse square law, the power of the wave falls as square of the distance from the source so, under ideal conditions, the wave doesn't lose any power once travelling in one dimensional guided medium. For a lossless propagation under ideal conditions, the width of the waveguide should be equal to the wavelength of the propagating wave. Generally, rectangular waveguides are used in commercial microwave ovens for energy guidance into the cavity. Rectangular waveguides work either in their TE or TM modes such that at a time only one field component can take the dominating role. In TE mode for example, the electric field is normal to the direction of propagation and magnetic field component is responsible for overall energy propagation. Similarly in TM mode, the magnetic

field component is normal to the direction of propagation. The frequency below which a waveguide cannot propagate a microwave signal is called the *cut-off* frequency of the waveguide. Cut-off frequency of waveguides depends upon their dimensions given in equation (2.2).

To allow the microwaves to pass at 2.45GHz, one must bear in mind the industrial standards adopted for guiding structures. Typical rectangular waveguide employed in microwave oven works in 'TE_{01}' mode which means,

$$E_y = 0, E_x \neq 0$$

$$f_c = \frac{c}{2b} \tag{2.2}$$

Where c is the speed of light and b is the width of the waveguide.

Frequency Band	Waveguide Standard	Frequency Limit(GHz)	Inside Dimensions(mm)
R-Band	WR-430	1.7-2.60	109.22×54.61
D-Band	WR-340	2.2-3.30	86.360×43.18

Table 2.1: Design parameters of the rectangular waveguide to work at 2.45GHz

Cut-off frequency of TE_{mn}/TM_{mn} mode is given in equation (2.3)

$$f_c = \frac{c}{2}\sqrt{\frac{m^2}{a^2} + \frac{n^2}{b^2}} \tag{2.3}$$

Mode	*m*	*n*
$TE_{mn}(E_z=0, H_z\neq0)$	Half wavelengths of E_y along x	Half wavelengths of E_x along y
$TM_{mn}(H_z=0, E_z\neq0)$	Half wavelengths of H_x along y	Half wavelengths of H_y along x

Table 2.2: TE/TM modes and wave propagation

The values of the other field components Ex, Ey, Hx, Hy in both TEmn and TMmn can be found in [5]

2.2.3 The Cavity

The third and last fundamental part of the microwave oven is the chamber or cavity to contain the microwave energy. It is generally a bulky rectangular metalic box with commercial dimensions (35×22.5×27.1) cm^3. The 'hot-spots' of electric field intensity inside the oven appear at the locations of the anti nodes and the 'cold-spots' appear at the nodes of the standing waves. In real experimentation, the 3-D pattern is difficult to see but the principle can be seen by simulating the metalic chamber in any electromagnetic simulator. With reference to Fig 2.4, the red spots represent the greatest E-field of the standing wave, while the yellow and blue spots correspond to the cold spots or minima inside the chamber.

The wavelength of the microwave energy emitted from the magnetron is obviously precise, but can be estimated by simply placing a foodstuff such as cheese inside the oven. A close observation will reveal sections where the cheese has completely melted and the section where it is completely unheated. the distance between the melted cheese will be approximately 6.4cm which is equal to the half wave length at 2.45GHz. Once the high power microwaves are generated by the magnetron, these waves are then injected into the metallic rectangular waveguide structure approx 6.4cm from the closed end. The other end of the waveguide extends into an opening into the chamber. Thus magnetron acts as a power generator, the waveguide as a power carrier and the metal cavity as microwave energy handler.

2.2.4 E-Field Analysis of Conventional Microwave Oven

As mentioned earlier, it is very difficult to measure the radiation level and field distribution of the microwave radiation around the food unless, for example, an infrared camera is installed that can see inside the cavity. The other, increasingly robust and very accurate way to observe the electromagnetic behavior within the cavity is to draw offline in a CAD electromagnetic simulation environment. Finely modelled and meshed objects in finite element method (FEM) solvers allow their accurate field distribution analysis under certain boundary conditions [6]. The complex objects are modelled and meshed in electromagnetic solvers such that the approximations made on spatial dimensions lead to the finite element for accurate field distribution analysis in three dimensions. Therefore, to properly analyze the field

distribution inside the commercial size microwave oven, an estimation was made by designing the cavity of the same dimensions in electromagnetic simulation environment and its electromagnetic properties were observed for proper analysis. The cavity of the actual size was designed in COMSOL multiphysics simulation environment to operate at 2.45GHz and an Eigen-mode analysis was made by adopting 9 frequencies on either side of 2.45GHz. The results of the field patterns depicted in Fig.2.4.clearly indicates an uneven and unpredictable microwave energy distribution at different Eigen frequencies. This is because the magnetron is a relatively broadband (20 MHz) and unintelligent microwave device that simply generates massive amount of microwave energy guided into the cavity without caring for its distribution. This is actually an advantage in a commercial multi-mode cavity as there are many modes that can be excited by the 'noisy' magnetron, all closely grouped around 2.45 GHz. The radiation produced at 2.45GHz strike with the metal cavity walls and reflect back and forth within the closed cavity structure. These high reflections create standing waves at different points inside the cavity leading to an uneven field distribution. It is very obvious that the hotspots appearing at the side walls of the cavity are unwanted because they cannot contribute in heating the food. As a result, a significant amount of microwave energy remains unused.

Conclusively, the magnetron as an individual component is an efficient microwave energy source but its integration with the commercial microwave heating system significantly degrades the overall system efficiency because of its large power consumption, the uneven electric field distribution and the fact that it can be matched only to a single load, typically represented by 1 litre of water.

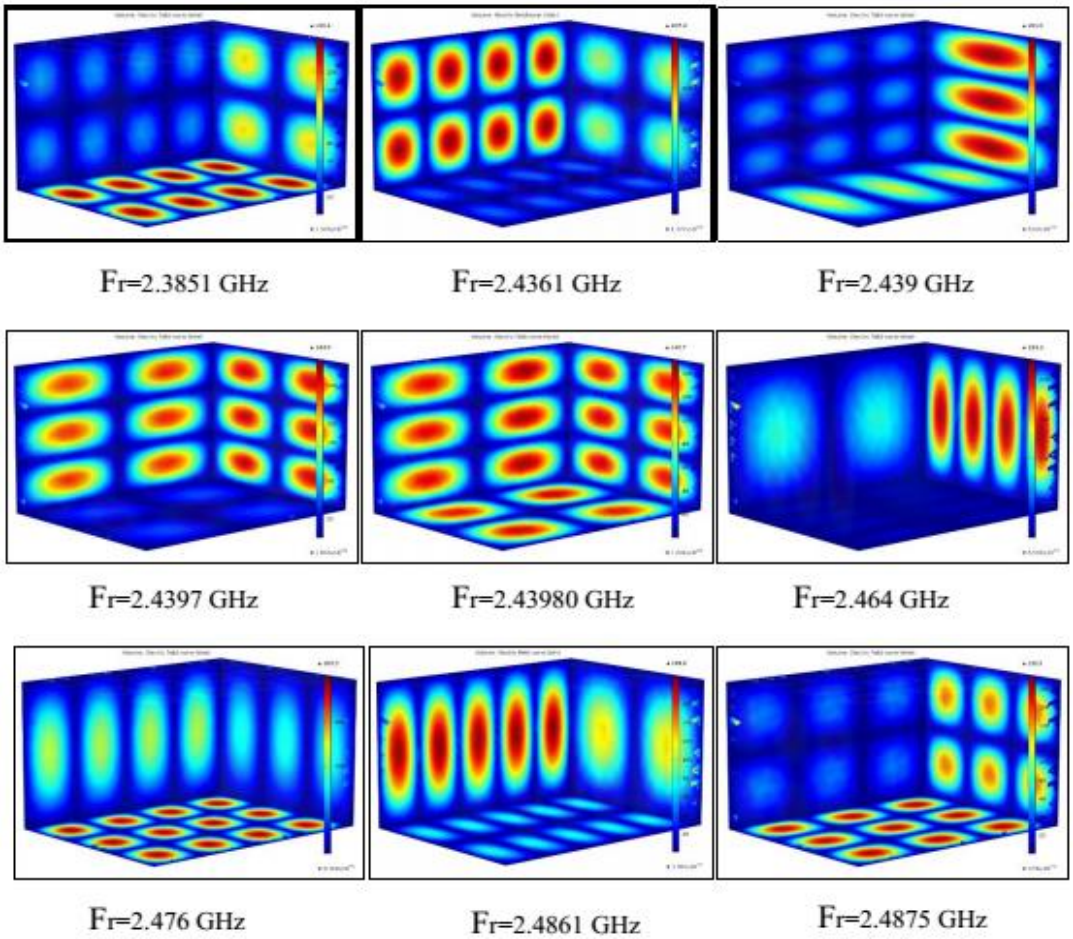

Figure 2.4: Eigen mode analysis (Comsol simulations) of the commercial microwave oven with fundamental frequency 2.45GHz, showing in 3D the different modes that can exist within the cavity.

2.3 Solid-State Microwave Heating

The solid-State microwave heating approaches that form the focus of this work significantly differ from the previously discussed, usually inefficient microwave heating approachs in which the heating is generated using a magnetron [7]. The heating principle in the solid-state approach is the same, but the working principle is entirely different. This approach is based on the initial generation and subsequent amplification of microwave power, using well-defined classes of microwave power amplifiers (*PAs*), systematically designed load environments (*Resonant Cavities*) and synthesized quasi-TEM wave guiding structure (*Microstrip Transmission Line*).

In such arrangements, the power amplifier can be designed to be highly efficient, and generates amplified RF signals which are guided by, in this case, microstrip transmission line structures into a single mode cavity resonator. The high amplitude

RF signals directed into the cavity are coupled into the cavity using a loop coupling structure and eventually used for sample heating. It is not remarkable that the high-amplitude microwave signals can be achieved using solid-state power amplifiers, but the real challenge is to maintain overall system efficiency when the loading conditions of the cavity can vary. The desirable objectives of the solid-state microwave heating apparatus can be defined as follows:

1- To couple to, and concentrate E-Field in the middle of the cavity for exposure to the sample under test.

2- To maintain a compact, portable and physically small apparatus for mobile, bedside, and potentially field-deployable equipment.

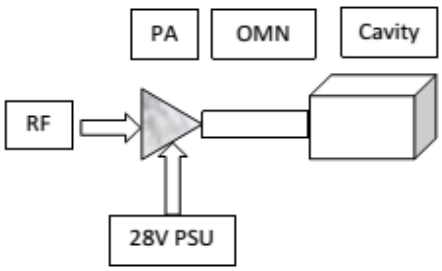

Figure 2.5: Solid-state microwave heating arrangement (proposed method), showing the power amplifier (PA) and the output matching network (OMN)

To differentiate the solid-state microwave heating arrangement from the magnetron-based microwave heating, it is important to understand the working principle of this flexible arrangement. In this section we will briefly discuss the constituents of the adopted solid-state microwave heating arrangement upon which the later work will be built and explained.

2.3.1 Microwave Cavity Resonator

Microwave cavity resonators are short circuited waveguides designed to resonate at a particular design frequency, where the resonance frequency depends upon their dimensions and the filling inside. Generally, for microwave heating applications (ISM-Band), rectangular cavities are designed to operate in TE_{011} mode whereas circular or cylindrical cavities to operate in TM_{010} mode because in both cases, the

resonant frequency is nearly 2.5GHz and high intensity microwave energy can be coupled through different coupling structures at the centre of the cavity.

To use the microwave heating arrangement for healthcare diagnostic applications, we have used single mode TE_{011} mode rectangular cavity designed at 2.45GHz [8] and a TM_{010} mode circular cavity designed at 2.5GHz [6]. Using a solid-state microwave heating arrangement in three different heating experiments, the electromagnetic energy has been coupled through loop antenna structure at the middle of the cavity to heat the sample. This will be explained in the coming chapters.

2.3.1.1 Coupling Mechanism

The feed-line is an important element of microwave cavity resonators that transfers the microwave energy from the external microwave source into the cavity resonator for its excitation. For maximum power transfer, the cavity and the feed-line should be matched or critially coupled.

The microwave energy coupling in typical microwave ovens is achieved by cutting a rectangular or circular hole in the side wall of the cavity. This coupling is called aperture coupling and it acts like a parallel plate capacitor, where the upper and the lower ends of the cut act as two metallic plates and the in between gap as air filled dielectric. Similarly, the cavities can be excited by probe coupling in which one end of the metallic probe is connected with the guiding structure and the other end terminates inside the cavity resonator such that when the probe is parallel to the E-field, the cavity resonates. However, in the application discussed here, achieving critical coupling always requires slight tuning of the coupling structure by adjusting the insertion length, planarity or physical size of the probe.

The most commonly used type of coupling structure in the single mode cavities discussed is the short circuited loop coupling of square or round shape. The loop is oriented parallel to the E-field allowing a maximum field passing through the current carrying loop. The more H-Field that passes through the loop area, the more microwave energy is coupled. Therefore, critical coupling can be achieved by increasing the loop area. However, if the loop area is increased above a certain limit, the cavity becomes over coupled and the *Q*-factor of the cavity decreases. Similarly, very small loop areas also degrades the *Q*-factor.

2.3.1.2 *Q*-Factor

Q-factor is a dimensionless parameter that describes the ability of a resonating structure to maintain its resonant properties. In different applications, the *Q*-factor has the same meaning but different definitions, for example, a pendulum swinging in air has a higher *Q*-factor than a pendulum swinging in oil. Similarly, a radio receiver with high *Q* filter can access a single channel within its narrow bandwidth but can deliver noise-free high quality output. In microwave resonating cavities, *Q*-factor is the ratio between the energy supplied to (dissipated in) the cavity, and the energy stored by the cavity. Cavities with a high *Q* have narrow bandwidths and excellent resonant properties while the cavities with lower *Q*-factor have wider bandwidth but poor resonant quality. Therefore, this dimensionless parameter defines the bandwidth and the resonant quality of a resonating structure.

$$Q = 2\pi \times \frac{Energy_Stored}{Eneregy_Dissipated_per_cycle} \tag{2.4}$$

The *Q Factor* of an empty, unloaded cavity is much higher than that of a loaded cavity holding a sample because the total value of *Q Factor* of a loaded cavity depends upon the quality of the conducting walls as well as the substance inside the cavity. Assuming a non-magnetic sample, the total *Q Factor* of a sample holding cavity can be calculated using set of equations (2.5-2.9) [7]

$$Q = \left(\frac{1}{Q_c} + \frac{1}{Q_d}\right)^{-1} \tag{2.5}$$

Where, Q_c and Q_d are the quality factors due to conductor loss of conducting walls and dielectric respectively.

$$Q_c = \frac{k^3 abd\eta}{4\pi^2 R_s} \times \left[\frac{1}{(l^2 ab/d^2) + (bd/a^2) + (l^2 a/2d) + (d/2a)}\right] \tag{2.6}$$

a, b, d are the *width, height, length* of the loaded resonating structure respectively and *l* represents the resonating mode.

Surface resistivity R_s and wave number k can be calculated using equations 2.7 and 2.8 respectively.

$$R_s = \sqrt{\frac{\omega\mu_0}{2\sigma}} \tag{2.7}$$

μ_o is the permeability and σ is the conductivity of the sample.

$$k = \frac{2\pi \cdot f\sqrt{\varepsilon_r}}{C} \tag{2.8}$$

$$Q_d = \frac{1}{\tan\delta} \tag{2.9}$$

Substituting these equations back in equation (2.5) will provide the total Q factor of a loaded cavity.

2.3.1.3 Rectangular Waveguide Cavity Resonators

Microwave cavity resonators are metallic hollow blocks of rectangular and circular shapes used in low power applications such as material characterization or in high power applications like microwave heating. Nevertheless, cavity resonators by no means look like the fundamental resonant RLC lumped circuits but in-fact they operate exactly like the RLC resonant circuits. Therefore, basic circuit theory laws are applicable on cavity resonators design and function. In series RLC circuits, the electromagnetic energy is inductively coupled through mutual induction prescribed as $'m'$

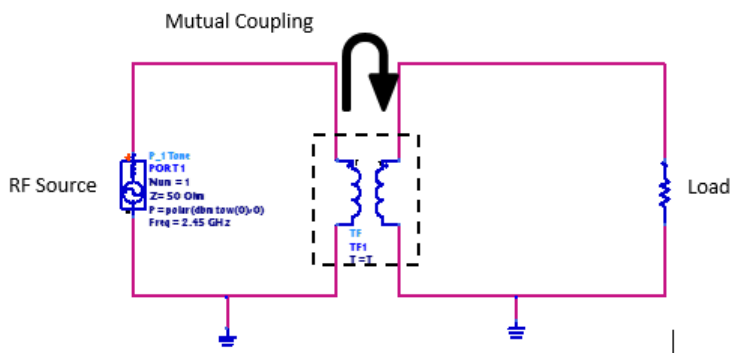

Figure 2.6 : Mutual coupling between the cavity resonator and the inductive coupling structure.

At resonance, the rectangular cavity resonators act like simple series resistor where the *L* and *C* cancel out the effect of each other and the power source sees the cavity as a simple resistive load. The basic equation to calculate the input impedance of one port mutually coupled short circuited rectangular cavity resonator is given by [5]

$$Z_{in} = R + j\omega L + (j\omega C)^{-1} \tag{2.10}$$

Where *R* is the resistance, *L* is the inductance and *C* is the capacitance.

The input power delivered to the cavity at resonance can be calculated by uesing equation(2.11)

$$P_{in} = \frac{1}{2} Z_{in} |I|^2 \tag{2.11}$$

Where I is the complex current flowing across the area of the inductive loop. Substituting equation (2.10) in equation (2.11) results in equation (2.12) which is a very important result describing a theotatical 100% power delivered to the cavity at resonance frequency.

$$P_{in} = \frac{1}{2} |I|^2 (R + j\omega L - \frac{j}{\omega C}) \tag{2.12}$$

In actuality this is not possible because some of the power dissipates in the sample and walls of the cavity. Therefore, the net input power delivered to the cavity is a sum of the dissipated power and the energies stored in the capacitor and inductor.

$$P_{diss} = 0.5 * |I|^2 * R \tag{2.13}$$

$$W_m = 0.25 * |I|^2 * L \tag{2.14}$$

$$W_e = 0.25 * |I|^2 * \frac{1}{\omega^2 C} \tag{2.15}$$

Therefore, the actual total power delivered to the cavity can be calculated using equation (2.16)

$$P_{in} = P_{loss} + 2 * j\omega(W_m - W_e) \tag{2.16}$$

Where P_{loss} is the total power loss due to the stored electric (W_e) and magnetic energies (W_m).

Finally, the input impedance of the cavity in terms of actual delivered power can be calculated by [5]

$$Z_{in} = \frac{P_{loss+} 2 * j\omega(W_m - W_e)}{0.5 * |I|^2} \tag{2.17}$$

From the mathematical analysis of the series resonant cavities, it is obvious that we need to properly account for the electric and magnetic energies stored in the cavity to ensure optimum impedance matching conditions between source and the cavity.

2.3.1.4 Circular Waveguide Cavity Resonator

Circular waveguide cavity resonators are short circuited circular waveguides that can radiate energy either in transverse electric or transverse magnetic modes at resonant frequency. Having cylindrical shape, the transverse-field components (E, H) of circular cavities can be calculated using the cylindrical co-ordinate system. Similar to rectangular cavity resonators, circular cavity resonators also have their lowest cut-off frequency defining their dominant mode. For example, the dominant mode of circular cavity working in its TE mode is TE_{111}. The TE modes of circular waveguides can be calculated using [5]. Since the cylindrical cavities already satisfy the boundary conditions necessary for the cylindrical waveguides therefore, the transverse-field components of the cylindrical cavity can be defined as

$$\overline{E_t}(\rho, \varphi, z) = \bar{e}(\rho, \varphi)\left[A^+ e^{-j\beta_{nm}z} + A^- e^{-j\beta_{nm}z}\right] \tag{2.18}$$

$\bar{e}(\rho, \varphi)$ Shows the transverse variation of the mode in ρ and φ directions, and A represents the arbitrary wave amplitudes. The mode propagation constants are defined by β in the direction of propagation, and the propagation constants of the TE_{nm} mode and TM_{nm} can be calculated using equation (2.19) and equation (2.20) respectively.

$$\beta_{TE_{nm}} = \sqrt{k^2 - \left(\frac{p'_{nm}}{a}\right)^2} \tag{2.19}$$

$$\beta_{TM_{nm}} = \sqrt{k^2 - \left(\frac{p_{nm}}{a}\right)^2} \tag{2.20}$$

Here K is the wave number and P'_{nm} is the mth root of the Bessel's function
In order for the cylindrical cavity resonators to resonate, the height of the cavity should be an integer multiple of half wavelength and the condition $\beta_{nm} \times d = l\pi$ must be satisfied.

where l=0, 1, 2, 3…..

Finally, the resonant frequency of the circular cavity can be calculated using equation (2.21).

$$f_{nml} = \frac{c}{2 * \pi\sqrt{\mu_r \varepsilon_r}} \sqrt{\left(\frac{p'_{nm}}{a}\right)^2 + \left(\frac{l\pi}{d}\right)^2} \tag{2.21}$$

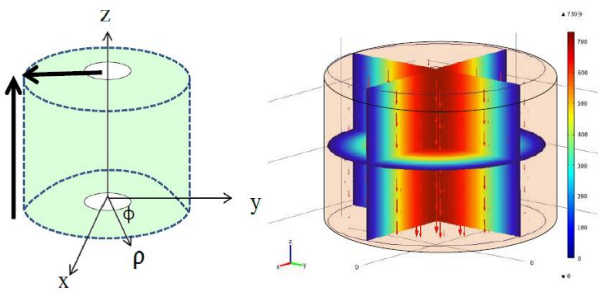

Figure 2.7: E-field distribution of a typical TM_{010} circular cavity resonator (at fr =2.5GHz)

2.3.1.5 TM Modes of Circular Waveguide cavity

E-Field in a TM mode circular cavity is perpendicular to the H-field where the H-field is in the radial direction and the E-field is maximum at the central point of the circular cavity and remains constant along its axial-direction. Therefore, the circular cavities are preferred for microwave heating applications because the sample placed in the middle of the cavity expereinces maximum E-Field. The detailed analysis of the

resonant properties and the field distribution of the TM_{010} mode circular cavity will be shown in chapter 5 and chapter 6.

The field distribution of some of the cylindrical TM_{nm0} modes can be seen in Fig.2.8.

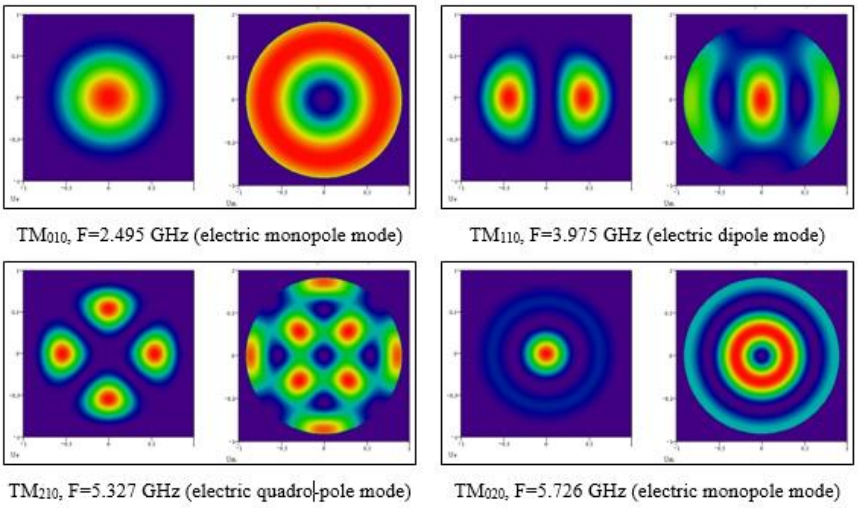

Figure 2.8: Field distribution of cylindrical TMmn0 modes for material characterization [2]

Microwave Heating using Solid-State source	**Microwave Heating using Magnetron.**
Operates at low DC power.	Operates at very high power
PA can be modified to operate under High efficiency modes.	Efficiency of magnetron cannot be improved after its design.
Clean and well-defined field distribution possible	Scattered field all over the cavity - unpredictable
Have high *Q* Factor at 2.45GHz	Have low *Q* Factor at 2.45GHz
Easy mode identification	Very difficult mode identification
Narrow band	Wide band
Compact, lightweight, flexible and energy efficient	Bulky, heavyweight, fixed and energy inefficient.

Table 2.3: Comparison of solid-state microwave heating system and magnetron based microwave heating system

2.3.2 Solid-State Microwave Source (Power Amplifier)

A compact and high efficiency power amplifier (PA) is an important part of the solid-state microwave heating arrangement that mainly defines the overall efficiency of the microwave heating structure. The efficiency depends upon the power amplifier mode of operation, DC power consumption and RF power generation. Since the PA converts the DC power into RF power therefore, the drain efficiency of a PA can be calculated by using equation (2.22)

$$Drain_Efficiency = \frac{RF_Power}{DC_Power} \times 100 \tag{2.22}$$

The magnetron, which is a fixed microwave passive device, is limited in terms of efficiency due to its dictated microwave design properties. In contrast, solid state power devices allow a significant performance improvement by changing the mode of operation.

The performance of a PA can be significantly compromised if it is not characterized properly. Therefore, in this work, transistor characterization through waveform engineering is a key tool in identifying optimal performance parameters [9]. Unlike the magnetron, PAs require low DC bias voltages for their efficient operation. The voltage applied at the gate terminal of a power transistor defines its fundamental class of operation and by adjusting its biasing conditions along with the harmonic impedance environment, a theoretical high performance can be achieved.

Both, classical and high efficiency modes of PAs are truly dependent upon their input biasing point. In classical modes of operation, the output harmonics of a PA are terminated to short circuits whereas, in high efficiency modes, these harmonic contents are controled in the output waveforms to modify voltage waveform shape and to improve performance.

Although, solid state PAs provide a good alternate to a magnetron, there are some limitations in their design. For example, power amplifiers are designed to match to fixed loads (generally 50Ω). This means that in addition to the harmonic tuning networks, additional 50Ω output matching networks are also required to minimize the reflections and to preserve amplifier's optimal operation. These networks are physically large and incur additional losses to the RF power that ultimately results in

a reduced system performance. Also, these harmonic matches are typically frequency sensitive therefore, it is very difficult to maintain their behavior at high frequencies.

In this thesis, we have introduced high efficiency integrated PA design techniques which are very simple, employing the natural impedance environments of the resonant cavities and eliminate the need for matching to a fixed 50Ω load. To differentiate between our proposed integrated PA design approach (for biomedical applications) and the traditional 50Ω PA design approach, it is necessary to understand the power amplifier modes of operation.

2.4 Power Amplifier Modes of Operation

The power amplifier is the last stage before propagation where the output amplified signal is either injected into the cavity resonator in heating applications or to the antenna in communication applications. The PAs in base stations are typically required to be linear, so are restricted to operate over the linear portions of their characteristics.

To keep the amplifier working in highly linear mode, the efficiency of the amplifier is greatly compromised. Typical average efficiency achieved within the base station setup is between 25-30% which means the amplifying unit is 70-75% inefficient [10]. This inefficiency has a serious impact on the overall running cost of the system. Contrary to that, in microwave heating applications the signal amplification and efficiency is more important than its linearity. In both cases however, the power amplifier is the key enabler for overall performance realization of a system.

At both industrial and academic levels, various techniques have been introduced regarding the efficiency enhancement of the power amplifier. For example, the efficiency enhancement over power dynamic range can be achieved by dynamically adapting the supply voltage applied to the drain terminal of the transistor. This approach is called envelope tracking (ET) and the amplifier only dissipates the instantaneous power it needs at the time, dynamically increasing the power and increasing overall efficiency [10].

An amplifier is a non-linear device that significantly distorts the fundamental current and voltage waveforms, generally by adding the unwanted harmonic components to the voltage waveform. This generally reduces fundamental energy contained in the waveform, and decreases the amplifier's efficiency and the output power. In classical

modes of operation such as class-AB, class-B or Class-C, the even and odd harmonic components are short circuited by deploying harmonic resonant tuning or 'tank' networks between traditional 50Ω load and the transistor. However, in terms of higher efficiency modes of operation, it is desirable to generate specific even and odd harmonics of precise phase, to boost the efficiency and the output power of the power amplifier.

Synder [11], discovered that it is possible to achieve 100% efficiency by the Fourier analysis of the output voltage and current waveforms, the operational mode in this case was given the name as class-F mode PA. Afterwards, this opened the way to analyse the PAs under different loading conditions by adding the harmonic components in both current and the voltage waveforms appearing at the output of the amplifier. In this regard, different high efficiency modes were discovered like Class-F, inverse class-F, continuous-class-F and continuous-inverse class-F. Traditional high efficiency PA approaches require deployment of lossy and physically large harmonic tuning networks within 50Ω environments [12] which sometimes make them less attractive in portable applications such as portable health-care applications.

The history of PAs goes back over four decades, where the very basic transistors were introduced. However, with the advent of the modern mobile communication technologies, these transistors were analysed and modified to operate more efficiently in an aggressive way. Further improvements to the transistor technologies allowed the users to operate them over wider frequency, higher drain efficiency and higher output power. These improvements were made by classifying the amplifier operation under different input biasing conditions whereas for each biasing condition a specific mode of amplifier operation was introduced. There is no point introducing the already well explained PA modes of operation in various textbooks and journal articles [13] but it is necessary to rephrase here because it will help reader to understand and easily differentiate the present from previous work.

When describing PA ideal modes of operation, the turn on characteristics of the transistor are often ignored which means the knee voltage of the transistor is often assumed to be zero. Therefore, the mathematically derived performance of the ideal operational modes tends to be higher than the measured performance. However, to start with the understanding of the PA modes of operation it is always a good choice to develop PA modes under ideal conditions. Gate biasing of a transistor is the starting

point of any class of amplifier design where classical modes of operation range from Class-A to Class-C.

2.4.1 Class-A

In this mode of operation the transistor conducts throughout its operation and continuously consumes the DC supply. The biasing point in this mode of operation is set where the output current is half of its maximum value. The PA in this class of operation is most linear but inefficient with respect to drain efficiency because the transistor consumes power even when it is not producing any RF power. The PA, in its class-A mode, outputs pure sinusoidal time domain voltage and current waveforms with their maximum and minimum alternating levels at different times. For example, when the voltage waveform is at its minimum level the current waveform is maximum and vice a versa. During the voltage waveform at its minimum, the output power is minimum; but due to the full time conduction, the DC power consumption remains constant. Therefore, theoretically we achieve 50% drain efficiency in Class-A mode of operation. However, due to its linear power gain, class-A mode of operation is a preferable choice in telecommunication applications.

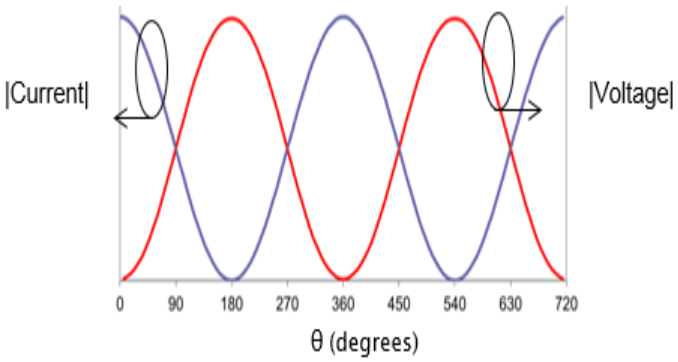

Figure 2.9: Typical class-A voltage and current waveforms

2.4.2 Class-AB

This mode of operation is obtained by biasing the transistor to its lower value compared to that in class-A. Generally in class-AB mode, $I_{d\text{-}Q}$ is set between 10-20% of $I_{d\text{-}max}$ due to which its conduction angle reduces and the maximum output power of the amplifier slightly increases compared to class-A [14]. In this mode, the transistor conducts for most of the positive half of the cycle and for the remaining negative part of the cycle it turns off. This mechanism allows more fundamental current to be

accomodated within the current waveform giving relatively linear power gain and drain efficiency greater than 50% (class-A) but less than 78.5% (class-B). The even and odd harmonic components are short circuited therefore they do not contribute to the output waveforms thus leaving them sinusoidal.

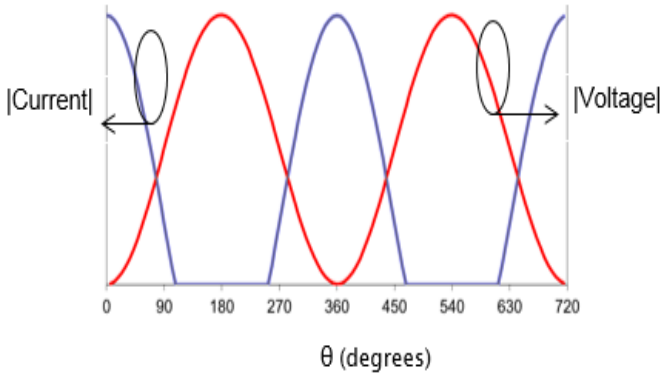

Figure 2.10: Class-AB voltage and current waveforms

2.4.3 Class-B

Class-B mode of operation is an extension of class-AB that is obtained by setting the biasing point to transistor's pinch-off voltage and again shorting the harmonic contents. This PA class is obtained by setting $I_{d\text{-}Q}=0$ that leads to a half rectified current waveform and a full rectified voltage waveform. In this class of operation, the transistor has a reduced conduction angle compared to class-AB with increased output power and drain efficiency. By adopting class-B, theoretically 78.5% drain efficiency can be achieved provided the knee voltage effect is ignored.

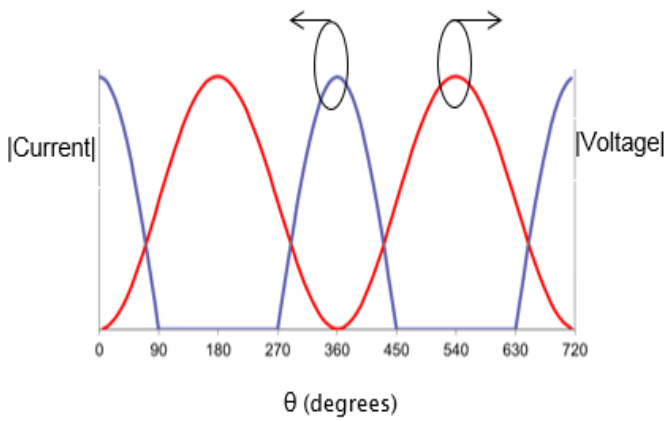

Figure 2.11: Class-B voltage and current waveforms

2.4.4 Class-C

In this mode of operation, the transistor is biased below its turn on voltage so that it conducts in the form of current pulses of very short duration. The conduction occures only during a small portion of the positive half cycle while during negative half of the cycle it remains off. The conduction angle in this class can be very small such that in the limit, it can be approximated to zero thus resulting in 100% theoretical drain efficiency. The harmonic contents in this mode are short circuited therefore, the voltage waveform remains sinusoidal. Though this class gives potentially 100% efficiency, it is not preferred because of very low output power and gain. In most of the practical applications this mode of PA is unfavourable.

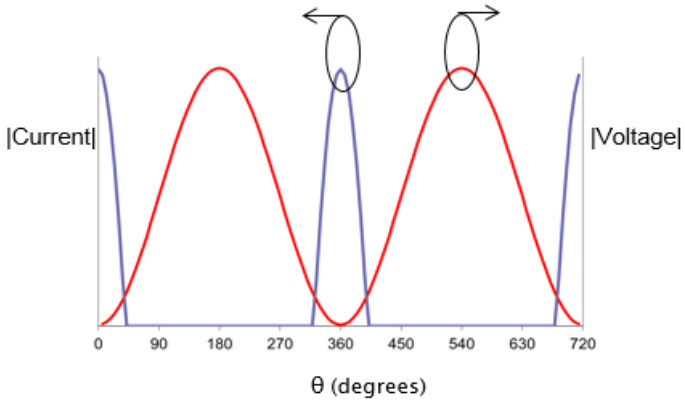

Figure 2.12: Class-C voltage and current waveforms

To ensure high efficiency and high output power, it is very important to reduce the output wave conduction angle by adjusting the biasing points and short circuiting the harmonic components as described earlier in classical modes of operation. However, the amplifier performance can be further improved by systematically utilizing the harmonic contents to the voltage or the current waveforms by the method called '*waveform engineering*'. This method will be explained in chapter 3 and will be applied in future chapters.

2.4.5 Class-F

The class-F mode of operation is achieved by biasing the transistor to its threshold gate voltage level and driving it into compression, where the transistor starts generating harmonics. This is a high efficiency class in which the voltage waveform is squared by adding odd harmonic voltage components and current waveform is shaped using even harmonics. This mode of operation requires an output harmonic trap to short circuit the even harmonics and to presents an open circuit to the odd

harmonics [12] as shown in Fig. 2.13. This in fact is an extension of the class-B PA in which the odd harmonic voltage components add to the fundamental voltage waveform and improve the efficiency from 78.5% to 90.7% [14]. The Fourier analysis shows that by adding infinite number of odd harmonics to the voltage waveform and even harmonics to the current waveform, 100% drain efficiency can be achieved. Thus ideally, class-F PA outputs perfect square voltage waveform by adding infinite number of odd harmonics and half rectified current waveform by short circuiting all the even harmonics. However, practically, it is sufficient to consider only upto 3 harmonics because the higher order harmonics above 3rd harmonic do not carry enough power to significantly improve the PA performance. With the contribution of the 3rd harmonic to the voltage waveform, the net amplitude of the output wave decreases therefore, the amplitude of the bifurcated voltage waveform can be increased by increasing the optimum resistive load value resulting in higher output power and efficiency.

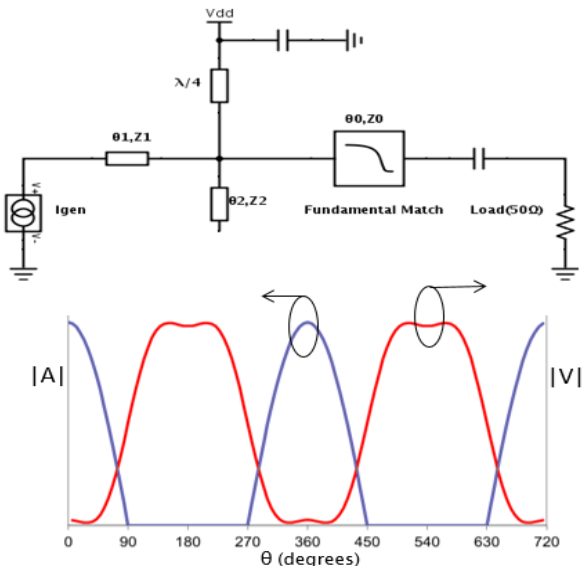

Figure 2.13: Traditional Class-F Network Topology and intrinsic voltage, current waveforms (limited to 3rd harmonic)

2.4.6 Class-F^{-1}

This mode of PA operation is obtained by generally reversing all the parameters required for engineering class-F mode of operation. The transistor is biased at its near class-A point to allow maximum output current flow from the tranistor such that the time domain current waveform has maximum allowable swing. The high efficiency inverse-F wave-shaping also requires the complicated and physically large harmonic traps between the transistor and the load to ideally short circuit the odd harmonics and

to present an open circuit to all the even harmonics. The square current waveform is shaped by slightly reducing the fundamental load resistance and driving the device hard into compression (typically 2-4 dB). The resulting, overdriven class-A 'square' current waveform still contains even order harminics, and presenting these with high-impedances allow a half-rectified voltage waveform to develop by short circuiting the odd harmonics. The voltage waveform in this mode demonstrates a higher fundamental voltage swing than other modes thus giving upto an extra 2 dB increased output power [14] .The squared current waveform has lower fundamental swing due to clipping which is increased by lowering the optimal load resistance and increasing the input drive level. This mode of operation is very useful for the transistors with higher drain to source capacitance because of short circuiting the higher harmonics. Care must be taken however as the elevated voltage swing can cause breakdown problems in the device. This phenomenon will be discussed further in chapter 4. The topology adopted in [15] can be used to obtain inverse-F waveforms.

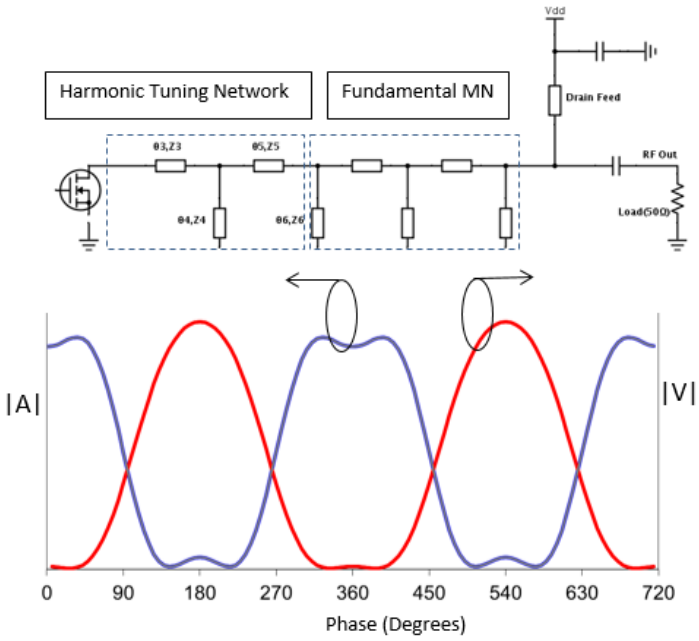

Figure 2.14: Traditional class-F^{-1} network topology and intrinsic voltage, current waveforms, limited to 3rd harmonic.

2.4.7 Continuous Modes

High efficiency modes of power amplifiers like class-F or inverse-F are narrow-band classes. These classes can be extended to operate over wider frequency range however

by replacing the fixed optimum load resistances of the fundamnetal and harmonic components with pairs of reactive fundamental and second harmonic impedances.

In these PA modes, the fundamental and harmonic optimum load requirements change systematically as function of frequency so that as the frequency-impedance (fundamental,2nd and 3rd) sequence remains true, the amplifier works efficiently over the targeted bandwidth. For example, the standard class-F mode of operation can be extended to continuous class-F by short circuiting the 3rd harmonic and providing specific reactive impedances to the fundamental and 2nd harmonic so that the fundamnetal voltage wave component can be extended by a factor of $(1-\gamma\sin\theta)$as given in equation (2.24) where $-1\leq\gamma\leq 1$. Basically the voltage waveform is raised above zero-crossing by adding the anti-phased 2nd harmonic voltage component. The optimum level of the 2nd harmonic is determined from the $-1\leq\gamma\leq 1$. The identified range of γ remains true as long as the output voltage waveform is non-zero-crossing and the amplifier is able to deliever the class-B mode performance.

$$I_{C.F} = \frac{1}{\pi} + \frac{1}{2}\cos\vartheta + \frac{2}{3\pi}\cos 2\vartheta \tag{2.23}$$

$$V_{C.F} = [1 - \frac{2}{\sqrt{3}}\cos\vartheta + \frac{1}{3\sqrt{3}}\cos 3\vartheta](1-\gamma\sin\vartheta) \tag{2.24}$$

Similiarly, the continuous-F^{-1} can be designed to work over wider frequency range by extending the inverse-F mode of operation [16]. This mode can be achieved by increasing the fundamental current wave component by factor $(1-\zeta\sin\theta)$ where $-1\leq\xi\leq 1$. In this mode the voltage waveform is second-harmonic peaking half-wave rectified sinusoidal voltage waveform and the amplitude of the current waveform is increased and phase shifted. At $\xi=0$ the continuous-Inverse-F mode reduces to simple inverse-F mode where the 3rd harmonic is fixed to short circuit and the 2nd harmonic to fixed open circuit. But as we anti-phase and vary the 2nd harmonic susceptive reactance and fundamental admittance, new family of phase shifted current waveforms emerge whilst the voltage waveforms remain half rectified due to 3rd short. This frequency-impedance variation results in constant output power and drain efficiency over extended bandwidth (the complete analysis of this PA mode will be shown in chapter.5). The complex matching network required to achive this mode typically

involves a physically large and lossy combination of lines and stubs as shown in Fig. 2.15 [17]

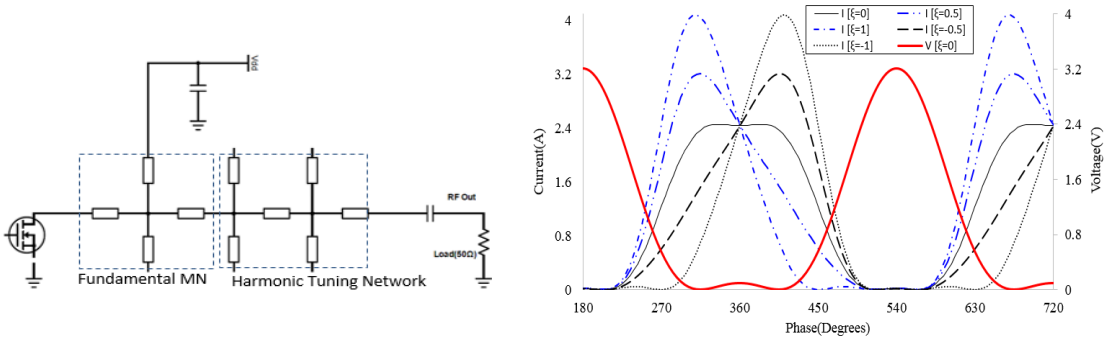

Figure 2.15: Traditional continuous class-F^{-1} Network Topology and intrinsic voltage, current Waveforms. Note the single, second-harmonic peaking half-wave rectified sinusoidal voltage waveform.

Class of operation	Conduction Angle	I_{dQ}	ηd (%)	ZFo	Z2Fo	Z3Fo
A	θ=2π	$I_{max}/2$	50	1	n/a	n/a
AB	π<θ<2π	0-$I_{max}/2$	50-78.5	1	0	0
B	θ=π	0	78.5	1	0	0
C	θ<π	<0	≈100	1	0	0
F	θ=π	0	100	>1	0	∞
F-1	θ=π	Imax/2	100	>1	∞	0
Cont-F^{-1}	θ=π	Imax/2	78.5	$\frac{R_{opt}}{\sqrt{2i_1 + j\sqrt{2i_{DC}} \times \zeta}}$	$j \times \frac{R_{opt}}{2(i_1 + i_3)\zeta}$	0

Table 2.4 : Summary of different power amplifier modes

2.5 Power Amplifier Design Limitations and Solutions

Efficiency, output power and gain are three main parameters that define the overall efficiency of a power amplifier depending upon the mode of operation. The PA modes can be achieved using properly designed output matching network so that the amplifier could function effectively according to the desired mode of operation. The output

matching networks designed for classical modes are much simpler compared to the high efficiency modes. For example, in case of class-B/AB the network synthesis is required to fit in over fundamental frequency only where the 2nd and 3rd harmonic loads are short circuited using quarter-wave short circuit stub [18]. The problem however arises when synthesizing the high efficiency mode output matching networks to work for fundamental and its integral frequency components. Although, these matching networks help shape the PA output waveforms, the introduced extra losses, difficult frequency synthesis and large physical size, result in a sub-optimal network response. At high frequencies, these networks become even more sensitive and their impedance response becomes unpredictable. Therefore, the solution to these limitations was found by adopting the '*direct integration approach'* where the application based PA design concept was introduced [19] that opened new doors to significantly simplifying the output matching network complexity and to make the PA designs simple and compact.

2.5.1 Direct Integrated PA Design Approaches

Low pass filtering approaches have their well-established grounds to provide desired output impedances to the transistors at fundamental and harmonic frequencies for achieving high efficiency PA modes of operation [20]. The synthesis of these harmonic tanks to properly fit in over desired frequency is very difficult because of the distibuted and quasi-TEM nature of the microstrip transmission lines. The losses and the bulk of the harmonic tuning networks can be dramatically eliminated by adopting the direct integration techniques. The first such technique was introduced in [21] in which the harmonically tuned (package plane) high efficiency PA was designed by direct integration into antenna-transmitter end. In this technique, the antenna was directly connected to the transistor and its parameters were tuned to present the optimal loading conditions to the transistor. Similarly in [22] another such direct integration technique was adopted to design a high efficiency power amplifier. In actuality, these were not fully integrated design approaches because the PAs and the antennas were designed and optimized separately with the input impedance of antenna closer to the optimum output impedance of the PA. Later on, another improved version of the integrated PA design was introduced in [23] where the fundamental, 2nd and 3rd harmonics were tuned simultaneously using only one open stub. Similarly in [24] by

using the inherent harmonic suppression nature of circular antenna, class-B (again at package plane) integrated PA was designed using PA-circular antenna integrated approach. Although, these new techniques offered compact PA designs using less complicated matching networks but still there were two limitations in these integrated designs.

The first limitation was the absence of the directional coupler at the output stage of the power amplifier i.e. between the load (antenna) and the source (transistor) to measure the transmitted and reflected power. Therefore, it was almost impossible to measure the actual output power delivered by the transistor except by only knowing the antenna radiated power through Friis free space equation [25]. Consequently, in all the direct integrated approaches, the drain efficiency measurements remained a question of interest. The second limitation was the lack of waveform visibility at the current generator plane of the transistor therefore, it was difficult to identify the actual mode of PA under active operation. Therefore, these two limitations questioned the actual system performance.

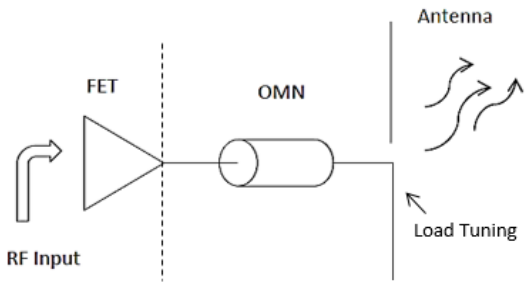

Figure 2.16: PA-Antenna Integrated Design

2.5.2 Proposed Integrated PA Design (Passive tuning approach)

Before designing any power amplifier, it is compulsory to consider optimum performance impedance points on a smith chart. Active and passive loadpull are two well-adopted techniques that follow a systematic method for synthesizing the load impedance environment for transistor characterization. This method allows the continuous monitoring of the PAE, output power and gain of the amplifier under test. Active harmonic loadpull technique is robust and fast where the passive loadpull technique is manual and slow where the magnitude and the phase of the load reflection

coefficient are adjusted manually by adjusting the stub position and the length between the device and the matched termination.

Although we have not used the passive loadpull approach for transistor characterization in our experiments but the direct integrated PA design approach follows the passive loadpull concept. Therefore, to fully understand the PA-Cavity integrated design procedure, it is important to understand the working principle of the passive loadpull tuning techniques.

The first automated passive loadpull measurement technique was introduced in early 1970, where the phase and the magnitude of the fundamental reflection coefficient was controlled by passive tuners [26]. In this tuning approach, two double slug tuners attached with servo motors were remotely controlled to change the phase and the magnitude of the reflection coefficient. This technique allowed the identification of fundamental reflection coefficient only for optimal behavior of the transistors where the 2nd and 3rd harmonics were terminated with 50Ω. This approach was later improved by Stancliff [27] who enabled the phase and magnitude control of the fundamental and 2nd harmonic reflection coefficients at a time. This technique allowed the utilization of fundamental and 2nd harmonic thus, resulted in further high efficiency achievable from transistors.

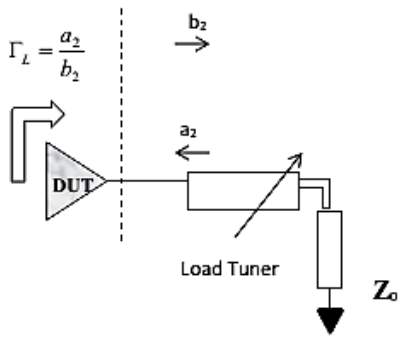

Figure 2.17: Block diagram: Passive loadpull measurement systems.

The approaches adopted in our experiments follow the same principle of controlling the phase and the magnitude of the reflection coefficients through passive tuners in typical passive loadpull measurement systems. The impedance environment of the cavity resonators together with simple series lines have been tuned to form high efficiency power amplifiers. The block diagram of the integrated setup can be seen in Fig.2.18 .The detailed passive tuning analysis of the cavity resonators for making true

integrated and physically small power amplifier structures will be explained in chapter 4, 5 and 6.

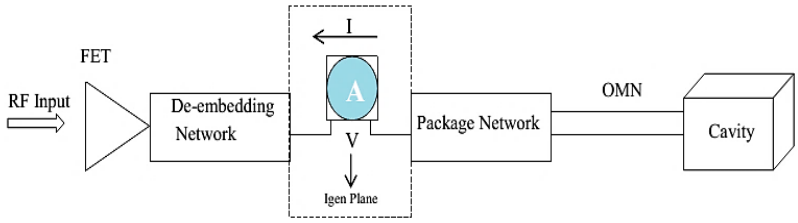

Figure 2.18: Block diagram: Waveform engineering enabled integrated PA structure for solid-state microwave heating applications (using simple delay line OMN)

2.6 Biomedical HealthCare Diagnostic Approaches

Almost all types of bacterial spores specifically *C-difficile* and anthrax when entered inside body get multiplied and spread so quickly that in two to three days severe infection get strict hold of the immunity system. These bacteria are primary cause of diarrhea in UK and USA where 8324 individuals died in UK in 2007 [28-29]. These bacteria produce dangerous toxins that at first instance affects the natural immune system. Therefore, it is highly recommended to use antitoxin with the consultation of medical professionals once anthrax has been diagnosed. The first phase for the treatment plan of bacterial attack is to diagnose the exact type of bacteria and once detected, the antibiotic treatment plan should be the second phase. Therefore, it is very important to know the exact type of bacteria using traditional diagnosis techniques [30]. In past, the decision on the presence of anthrax was made based on the exposure to animal products. However, with the advent in the biomedical diagnostic systems, the presence of anthrax in the human body is found by two largely adopted methods.

First method is to take different samples such as blood, spinal fluid, skin swab or other secretions in human body and make their culture analysis. Second method is to measure antibodies in blood.

Morton N.Swartz states in [30] that nasal-swab for diagnosis of inhalational exposure to B. Anthrax has yet not been confirmed for its accurate prediction of B.Anthrax bacteria therefore, this technique should be avoided until proved. Conclusively, serologic tests may not be sufficient enough to make a decision. Similarly, cell cytotoxin neutralization assay is the current gold standard capable of detecting only

B.Anthrax with 100% accuracy although taking 2 to 3 days for diagnostic results [31-32]

Similarly, microwave assisted healthcare diagnostic techniques have their recent origin, so the technology in this direction is still in its very early stages . However, some of the methods developed and tested so far have got significant encouragement from biomedical scientific community [33].

2.6.1 Microwave-Assisted Diagnostic Approaches

2.6.1.1 RT PCR (Real-Time Polymer Chain Reaction) Approach

In contrast to the diagnostic techniques stated above, detection techniques using RT PCR method have been reported in [34], which are sensitive and accurate. However, these diagnostic approaches use costly apparatus and produce results from 2 to 8 hours.

2.6.1.2 MAMEF (Microwave Accelerated Metal Enhanced Flourescence) Based System Approach

Similarly, one of the recently investigated MAMEF based system approach is to expose *C.difficile* to the high E-field so that with the microwave irradiation, the bacteria could release its Genomic DNA. The DNA information of the bacteria is detected and used to correctly diagnose the exact type of bacteria. In this diagnostic approach the apparatus consists of a glass sheet deposited with SiFs and coated with silicon isolators as a platform for *C.difficile* spore accumulation and the platform for bacteria DNA analysis. Two highly sensitive probes: anchor probe and fluorescent capture probes are used in this diagnostic setup to gather the genomic DNA information after microwave irradiation of the bacteria.

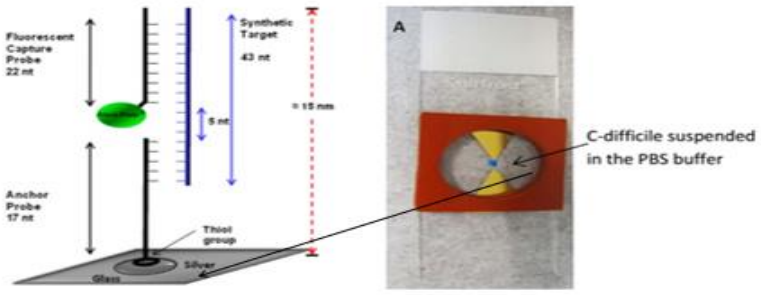

Figure 2.19: Configuration of 3 piece DNA detection assay [33]

To release the DNA of *C-difficile*, 500µl volume of spore is deposited into gold triangles and exposed to high power microwave pulse for 15 second. Microwave irradiations disrupt the sample properties and the bacteria release its DNA information which is collected for pharmaceutical analysis. However, the biggest disadvantage of this diagnostic technique is that it does not provide the accurate location and the intensity of the hot-spot. Therefore, sometimes this approach works but most of the time it does not, either boiling the sample and obliterating the bacteria, or not touching it at all. In conclusion, this approach was found no different than the magnetron based microwave heating approach with unpredictable E-field distribution. Therefore, an optimum solution for precisely exposing the sample to the focused E-field was found in the microwave enhanced portable diagnostic approach (adopted in this thesis).

2.6.1.3 Microwave Enhanced Portable Diagnostic approach

The microwave power delivery system used in this diagnostic technique is high precison, low power, highly efficient and much smaller in size than the magnetron based approach discussed above. Together with the novel and already patented DNA detection system [33], this solid state microwave power generation system can quickly diagnose and produce results in less than 5 minutes. With respect to Fig 2.20, at the source side of this system, a variable frequency synthesizer generates microwave power of approximately 10mW. After shaping into the required form, the pulse is amplified by the high power, high efficiency power amplifier and delivered to the sample holding microwave cavity resonator for sample disruption and sensing.

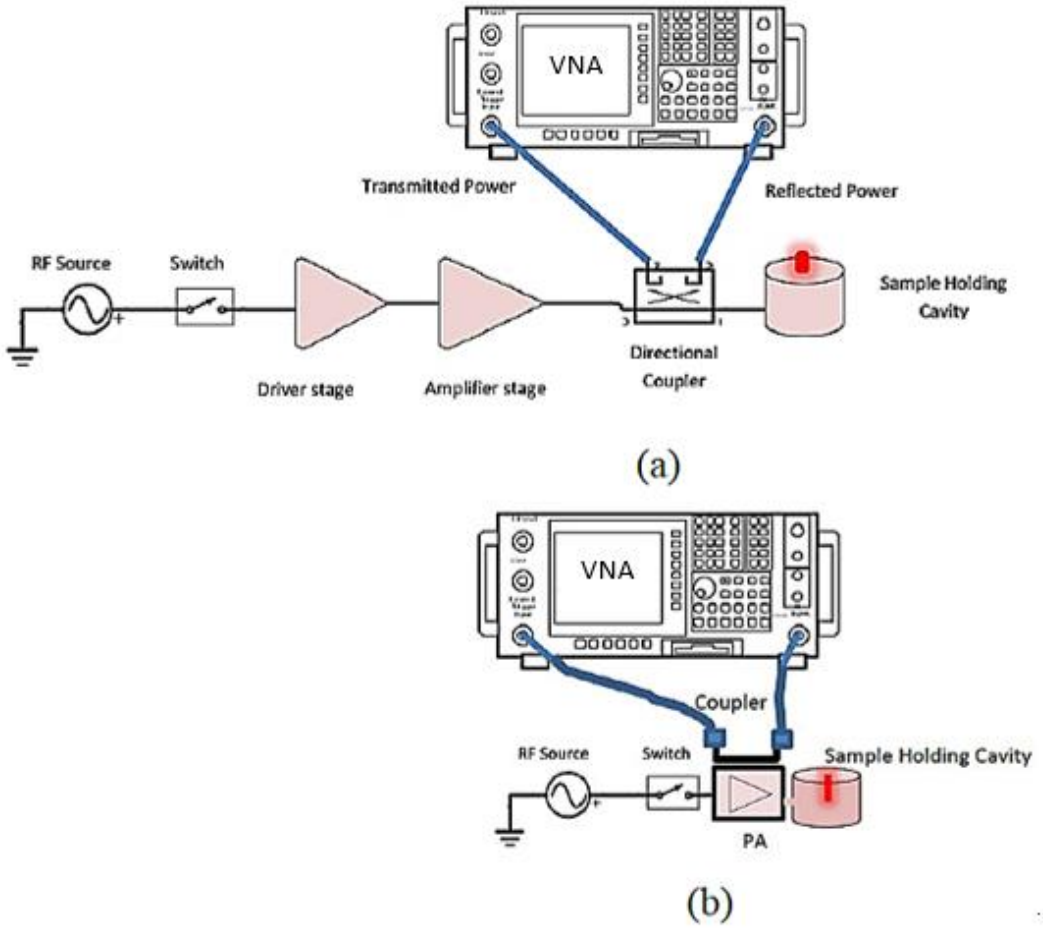

Figure 2.20: Microwave Enhanced heating systems for diagnostic applications
(a) Conventional (b) Proposed

Although, the microwave assisted biomedical diagnostic systems discussed here have proved their viability and efficiency but still the arrangements can be made for further improvement. The physical size of the system can be reduced by directly connecting the microwave source with the sample holding cavity resonator. Using the direct integration approach (discussed earlier) and waveform engineering techniques applied at the intrinsic plane of the solid state power amplifier can lead to a high RF power and low DC power consumption of the amplifier.

Traditional PA design Approaches	*Previous Integrated PA design Approaches*	*Proposed PA Design using Integrated Approaches*
Use physically large and complex matching networks.	Use comparatively small and less complex matching networks.	Use simple series microstrip lines to match fundamental 2nd and 3rd harmonic loads.
PA is matched to fixed 50Ω load.	Non-50Ω fixed Load is matched to PA.	Both Load and PA are matched with each other simultaneously
50Ω directional coupler in series with PA for performance analysis. Thus adds extra bulk.	N/A	Coupled line directional coupler printed parallel to the output stage. Thus assures the compactness.
Waveform engineering techniques allow realization of High efficiency PA modes.	N/A	Waveform engineering techniques allow realization of High efficiency PA modes.
Cannot be used for portable applications due to large size.	Can be used for portable applications due to compact and small size.	Can be used for portable and field deployable microwave heating applications due to compact and small size.

Table 2.5: Comparison of different power amplifier design techniques

2.7 Chapter Summary

This chapter provides the detailed literature review of the microwave heating using conventional approach (magnetron based) and using solid-state power amplifier. The first part of this chapter covers magnetron based microwave heating where the basic microwave oven working principle has been explained. Later on, the individual components forming the commercial microwave oven have been discussed in details. The multimode microwave cavities accommodating large number of resonating modes

have uneven field distribution therefore, the E-field analysis of the commercial size cavity has also been shown in this part through COMSOL simulations.

The second part of the this chapter starts with the microwave heating using a solid state power amplifier as a source. This section deals with the microwave cavity resonators used in the heating arrangement. Therefore we have discussed and explained two different cavity resonators i.e. single mode rectangular cavity resonator and circular cavity resonator. Later on, the important parameters of both the cavity resonators have been described in details. The field distributions of various TM_{mn0} modes have also been shown in this part. And finally, solid state microwave heating arrangement has been compared with the magnetron based microwave heating system.

Third part of this chapter begins with the power amplifier because, in solid state microwave heating, the power amplifier is the microwave energy source. This part starts with the modes of power amplifier operation with explanation to output wave-shaping using some of the referenced output matching network topologies. The limitations of the physically large harmonic tuning networks for wave-shaping have been discussed lastly in this part.

In the fourth part, the application based (wireless communication) integrated power amplifier design approaches have been referenced in the start where the harmonically tuned power amplifier has been designed by directly integrating with the microstrip patch antenna without deploying harmonic tuning networks between PA and antenna. Although this is a good power amplifier design approach, it has certain design implications which have been highlighted and discussed later in this section.

In the fifth part, the application based direct integrated PA design approach for microwave heating has been described and discussed. Basically this heating arrangement follows the working principle of the passive loadpull tuning mechanism in which the load is tuned to access the load reflection coefficient magnitude and phase. Therefore, this part starts off with the basic working principle of passive loadpull, which later on has been shown to be employed in the microwave heating arrangement. Using simplified series microstrip line, matching network together with cavity impedance, high power amplifier design completely eliminates the need for interstage matching to 50Ω.

Finally, different conventional and microwave assisted diagnostic techniques for the detection of dangerous *C-difficile* and Anthrax bacteria have been discussed very

briefly. In microwave detection techniques, the portable diagnostic approach will be adopted in the coming chapters where the focus will be made on the high efficiency power delivery stage of the diagnostic system.

References

[1] Fried,V,Hameka,H and Blukis,U. *Physical Chemistry 1st ed.London*:Macmillan, 1977.

[2] Porch, A. EN4806 *High Frequency Electronic Materials*. Course Documents. s.l. : Cardiff University.

[3] *The Magnetron*. Bournemouth University.

[4] Cavity magnetron inside view (wikipedia) Date Accessed Dece 28, 2014.

[5] Pozar,D.M, *Microwave Engineering (3rd edition)*. New York: John Wiley & Sons, 2005.

[6] Daniel Slocombe, *The Electrical Properties of Transparent Conducting Oxide Composites, PhD Thesis*, Schoolf of Engineering, Cardiff Uinversity UK, June 2012.

[7] Vollmer, Michael. 2004, *Physics of the Microwave Oven*, Physics Education, vol.39, no.1, pp. 74-81.

[8] Matthew Ayres, Robert Friedhoff Michael Gray, Owain Jones, *Microwave Heating in a Microfluidic Reactor, M.Eng thesis*, Schoolf of Engineering, Cardiff Uinversity UK, 2011.

[9] M.Demmler,P.J.tasker,and M.Schelecweg"A vector corrected high power on wafer measurement system with frequency range for higher harmonics up to 40GHz" *in proc. 24th EuMC.* ,1994, pp.1367-3172.

[10] Amir Sheikh, *High Power Waveform Engineering, PhD Thesis*, Schoolof Engineering, Cardiff Uinversity *UK*, June *2010.*.

[11] R. Snyder, "A theoretical analysis and experimental confirmation of the optimally loaded and overdriven RF power amplifier," *IEEE Trans. On Electron Devices*, vol. ED-14, no. 12, Dec. 1967, pp. 851-857,

[12] Andrei Grebennikov, "Load network design technique for class F and inv.F PAs,in *High Frequency Electronics*, May 2011, pp.58-76.

[13] S.Cripps, *RF Power Amplifiers for Wireless Communications*, 2nd Edn, Norwood, MA: Artech House, 2006

[14] R.M.Smith, *Broadband microwave push-pull amplifiers, PhD Thesis*, School of Engineering, Cardiff Uinversity UK, Sept 2013.

[15] Jingqi Wang , Yingjie Xu, and Xiaowei Zhu, "Digital Predistorted Inverse Class-F GaN PA with Novel PAPR Reduction Technique" *Microwave sysmposium Digest(MTT), 2011 IEEE MTTS-International*, June 2011.

[16] V.Carrubb, A.L.Clarke, M.Akmal, Z.Yusoff, J.Lees,J.Benedikt, S.C.Cripps, P.J.Tasker, "Exploring the design space for broadband Pas using the novel continuous inverse class-F mode" *IEEE EuMC*October 2011, ,pp.333-336.

[17] Kenle Chen and Dimitrios Peroulis "Design of Broadband Highly Effcient Harmonic-Tuned Power Amplifier Using In-Band Continuous Class-F/F^{-1} Mode Transferring" *IEEE MTT*, Vol.60 No.12, Dec 2012.

[18] John L.B.Walker, *Hand book of RF and Microwave Power Amplifiers*, Cambridge University Press 2012.

[19] J.Lin,T.Itoh,"Active integrated antennas,"*IEEE Trans.MTT*.,vol.42, ,Dec.1994, pp.2186-2194.

[20] Saad.P, et al, "An Inverse Class-F GaN HEMT Power Amplifier with 78% PAE at 3.5 GHz", *Proceedings of the 39th European Microwave Conference*, Oct 2009.

[21] Vensa Radisic et al, "Novel Architecture for High-Efficiency Amplifiers for Wireless Applications,"*IEEE Trans. MTT* , vol.46 , no.11,Nov 1998.

[22] W.R.Deal,V.Radisic,Y.Qian,T.Itoh, "A high efficiency slot antenna push-pull power amplifier," 1999 *IEEE MTT-S Symposium Digest*, Anaheim,CA,pp.659-662.

[23] P.Colanto, et al, "A method for PA-Patch Antenna Design optimization oriented to Maximum Efficiency", *12th GAAS Symposium-Amsterdam*, 2004

[24] Chung, Cynthia Y. Hang, Shujun Cai, et al, "Output Harmonic Termination Techniques for AlGaN/GaN HEMT Power Amplifiers Using Active Integrated Antenna Approach", *Microwave Symposium Digest IEEE MTTS-International*, June 2002.

[25] Balanis, Constantine A, *Antenna Theory: Analysis and Design (3rd edition), John Willey & Sons, Inc., Hoboken, New Jersey, 2005.*

[26] Cusack, J. M.; Perlow, S. M.; and Perlman, B. S.; "Automatic Load Contour Mapping for Microwave Power Transistors," *IEEE Transaction on Microwave Theory and Techniques,* vol.22, no.12, Dec 1974, pages: 1146-1152,.

[27] Stancliff, R. B.; Poulin, D. P.; "Harmonic Load-Pull," *IEEE MTT-S Symposium Digest*, 1979, pages: 185-187.

[28] Kuntz JL,Jhonson ES,et al. (2012), "Clostridium difficile Infection, Colorado and the Northwestern United States", 2007.*Emerging Infect Dis* 18(6):960.

[29] Office of National Statistics. www.statistics.gov.uk, Date accessed Dec 15, 2014.

[30] Morton N.Swartz,M.D, " Recognition and Management of Anthrax-An Update", *N Engl J Med*, vol.345,No.22. Nov 29, 2001.

[31] Poutanen SM, Simor AE (2004) "C-difficile associated diarrhea in adults", *Can Med Assoc J* 171:51-58.

[32] Goldenberg SD, Cliff PR,Smith S, Milner M, French GL (2009) "Two-step glutamate dehydrogenase antigen real-time polymerase chain reaction assay for detection of toxigenic Clostridium difficile", *Journal of Hospital Infection* 74(1):48-50.

[33] Lovleen Tina Joshi,Budha L.Mali, Chris D.Gddes, Les Baillie, "Extraction and Sensitive Detection of Toxin A and B from the Human Pathogen *C-difficile* in 40 Seconds Using Microwave Accelerated Metal Enhanced Flourescence"., vol 9, Issue 8, Aug (2014).

[34] Planche T, Wilcox M(2011) "Reference assays for Clostridium difficile infection: one or two gold standards?" *J Clin Pathol* 64:1-5.

Chapter.3 TRANSISTOR TECHNOLOGY AND CHARACTERIZATION

Time domain waveform measurement systems are an effective way of understanding and investigating the nonlinear behavior of the transistors at microwave frequencies. The modern, active multi harmonic loadpull measurement systems further facilitate the in-depth understanding of the transistor behavior at different measurement planes. But before we go deeper in discussion, analysis and measurements; it is important first to briefly discuss the transistor technologies used in this experiment.

3.1 Power Transistor

Silicon based bipolar junction transistor technology was the RF power technology of choice during the 1970s. Due to low power handling and low frequency requirements, bipolar junction transistor (BJT) technology was a perfect fit for that era with respect to sufficiently high efficiency and power >5W. However, poor gain, thermal runaway problems due to negative temperature coefficient and strict linearity requirements over higher microwave frequencies motivated the researchers to think of an improved transistor technology which could address these challenges.

After the struggle of almost a decade, double diffused metal oxide semiconductor power transistors gained interest in the RF community. These transistors were capable of delivering high power over relatively higher microwave frequencies. The high breakdown voltage operation without compromising the frequency, made it readily accepted by the RF industry. Further improvements in linearity over high efficiency, high power and S-Band microwave frequency operation made MOSFET the favorite technology of the mid1980s.

MOSFET power transistors are divided into two main classes, LDMOS-FET (Laterally Diffused Metal Oxide Semiconductor field-effect transistors) and VDMOS-FET (Vertically Diffused Metal Oxide Semiconductor field-effect transistors). In this chapter we will discuss the LDMOS transistor technology and will use 10W-LDMOS power transistor as RF power source in design and heating experiments.

3.1.1 LDMOS Power Transistor

N-channel enhancement mode laterally diffused metal oxide semiconductor field effect transistors (LDMOS-FET) contain n-type drift region lying laterally between the drain and the gate terminals of the transistor as shown in Fig. 3.1. The LDMOS transistors designed for mobile handsets have 0.5μm drift region length due to low power requirements, where the transistor's allowable drain supply voltage is 28-32V [1]. However, as the high power requirements increase, such as in industrial applications, the length of this region exceeds 5-6 μm. The breakdown voltage for 28V LDMOS power transistor is generally prescribed 65V in datasheets because of the twice drain voltage swing caused by the reactive elements present in the bare-die model. As the VDS increases, the n-drift region depletes until it reaches its critical E-field point after which the drain-source breakdown occurs. Therefore, complete depletion of the n-drift region should be avoided while applying the drain supply voltage. The doping of the p-type epitaxial layer plays an important role in achieving the high frequency operation of the transistor because, heavily doped epitaxy layer increases the drain-source capacitance. Hot carrier injection (HCI), on-state resistance and the drain-source breakdown voltage are the key parameters that allow high power and safe operation of the drain structure of the transistor.

The gate terminal of the LDMOS transistor consists of a metallic plate placed on a SiO_2 layer to prevent the diffusion of the electrons from source to gate. This shielding layer restricts the carrier flow through the channel (formed between drain and source) and assures a steady current flow. Gate resistance and the gate length are two very important parameters in determining the power gain and the high frequency response of the transistor. Shorter gate length and the thinner silicon-dioxide layer of Si-LDMOS transistor guarantees a high frequency response and vice versa. However, at the same time, thinner silicon dioxide layer increases gate-source capacitance and lowers the power gain which is a natural design tradeoff.

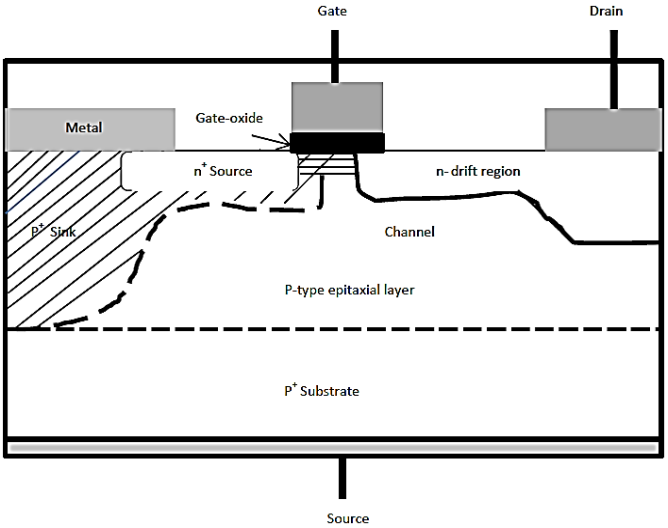

Figure 3.1: Cross-sectional view of a typical LDMOS power transistor

Having a leading role in the modern semiconductor industry, 10W Si-LDMOS transistors were found advantageous for this experiment. Therefore, an N-Channel BLF6G27-10G RF power transistor working from DC-2.7GHz was obtained from NXP Inc. This transistor model is very useful for microwave heating applications *firstly*, because of its specific design to work for base station applications (2500MHz-2700MHz). *Secondly*, its ruggedness, high power gain and high breakdown voltage (65V) make this transistor an ideal candidate for high power heating applications.

Breakdown V_{DS}(V)	Maximum V_{GS} (V)	Maximum output drain current I_d(A)	Design Frequency
65V	+13V	3.5A	2.3-2.5GHz

Table 3.1: Electrical properties of (BLF6G27-10G) transistor used in this experiment

3.2 Transistor De-embedding

To confirm the actual mode of operation, the analysis needs to be made inside the transistor, at the intrinsic plane often called the I_{GEN}-plane or the current generator plane. An accurate access to the I_{GEN}-plane of the transistor allows the desirable mode of operation by engineering the output voltage and current waveforms. This process is called Waveform Engineering. A fully waveform engineered class-B amplifier with zero knee voltage can give efficiency up to 70-78.5% with appreciable output power and gain. Traditional characterization techniques only provide a partial picture and

typically involve extracting linear small-signal S-parameters of the transistor extracted using a calibrated VNA and for large signal measurements, measuring harmonic behaviour using a spectrum analyser. In contrast, valuable information contained in the time domain output voltage and current waveforms can only be obtained through proper de-embedding the transistor package parasitic, and using a full non-linear wavform measurement system.

Transistors are placed inside plastic or ceramic packages to protect and prevent interaction with the outside world. These packages contain bonding wires and pad capacitors which, at microwave frequencies, transform impedance and disrupt the output waveforms. Similarly, manifold and the capacitor cells completely transform the output waveforms, thus making it difficult to analyse the exact behaviour of the transistor. Consequently, it is not possible to properly analyse the high efficiency modes at the package plane of the transistor. While performing waveform engineering, it is desirable to have access to the transistor intrinsic plane by nullifying the parasitic effects imposed by the package. The process of negating the effects of these parasitic elements, is called the de-embedding.

Power transistors do not contain the coaxial connectors, so a method must be provided to allow their connection with the outside measurement systems. A dedicated structure to accommodate the non coaxial devices is called the test fixture.

Figure 3.2: Transistor layout (BLF6G27-10G/10W-LDMOS)

3.2.1 Test Fixture

The test fixture provides a medium for connecting the non coaxial, non-insertable devices with the external measurement setup. Generally, the RF measurement devices and systems are developed to operate within fixed 50Ω characteristic impedance environments as standard. One type of system used for the characterization of power transistors is the active harmonic loadpull measurement system which will be described in detalis later in this chapter. The 10W-LDMOS power transistor was

placed in the test fixture structure for its non linear characterization through loadpull measurement system. To begin with, the dedicated test fixture was designed based on the physical dimensions of the 10W-LDMOS transistor. Using a metal-backed microwave laminate, a recess with dimensions equal to the base dimensions of the transistor was machined into the fixture to hold the transistor. Two 50Ω microstrip lines were milled on either sides of the center hole to establish a connection between the transistor and rest of the measurement system. Lines were printed on RTduroid/5880 substrate (ε_r=2.2, h=0.51mm, tanδ=0.0005) with each line 20mm long and 1.51mm wide giving a 50Ω system impedance. The LDMOS transistor provided by NXP Inc. was available in a ceramic package attached with two wider flanges (3.5mm). Therefore, the two 50Ω test fixture lines were extended by additional pieces of microstrip line (W=3.5mm, L=1.7mm) to accommodate the wider flanges as shown in Fig. 3.3. Similarly, the outer dimensions of the drilled square were fixed to 10x10 mm^2 and the depth to 1mm to hold the transistor. Through this dedicated arragement, the transistor was now ready for its connection to the measurement system. However, for proper transistor characterization, it was necessary to de-embed the test fixture lines and the transistor's package network, and this was achieved using TRL-calibration technique. [2].

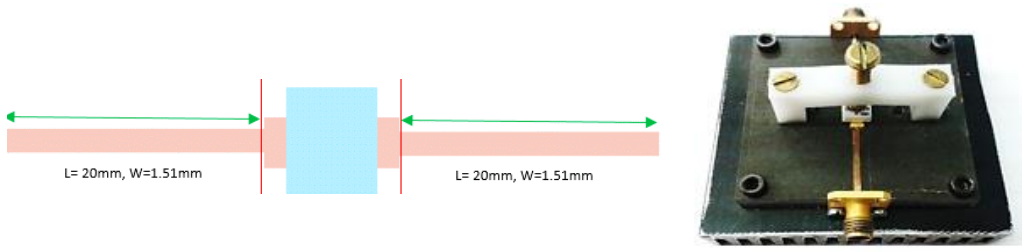

(a) (b)

Figure 3.3: (a) Test fixture layout (b) Test fixture prototype fabricated on RTDuroid5880 substrate

3.2.2 TRL calibration and calibration kit design

Calibration is a measurement enhancement technique that allows a true characterization of an RF device under test. Commonly known and used calibration techniques include amongst others S-O-L-T (Short-Open-Load-Thru) and T-R-L (Thru-Reflect-Line).

The S-O-L-T calibration uses one transmission standard and three reflect standards to solve the 12 term error model. This calibration technique is generally only applicable to coaxial connector or RF probe compatible devices for their characterization analysis. The RF devices with coaxial connectors can be physically connected to instrumentation through co-axial cables for their electrical analysis. True S-parameters of these devices can be mesaured by negating the effect of extra co-axial cables and shifting the mesaurement reference plane to the ports of the actual device under test. For this work, Keysight Inc. calibration standards were adopted for the characterization of the RF devices because of their accuracy and higher frequency range. For example, the keysight calibration kit (85052D) with the S-O-L-T standards can be used to characterize the coxial connector RF devices from DC-26.5 GHz. These 'cal-kits' are very expensive and the electrical information of each of its standards is already stored in the measuring instrument, or is available via the calibration kit user manual.

Similarly, another calibration technique used to measure the S-parameters of non-coaxial or non-insertable device is the TRL (*Thru-Reflect-Line*) calibration technique. It is also a useful calibration technique to accurately solve 2-port 12 term error coefficients. The accuracy of this claibration technique is defined by the quality and the repeatability of its standards. To achieve the best performance of a TRL calibration, the discontinuities and the bends should be avoided in the connecting caoxial cables. TRL kit contains three calibration standards, *Thru*, *Reflect* and *Lines*, which need to be verified over a wide frequency range. Therefore, the TRL kit was designed and verified using the procedure outlined in [3]. The design procedeur and step by step analysis of each of the three standards is described below.

1. Decide a reasonable frequency range with a definite start and stop.

2. Calculate the number of frequency break points required to cover the complete frequency range and then decide the number of line standards according to each break point.

   The number of line standards required is always one more than the number of frequency break points in a reliable TRL kit. For decreasing frequencies, the physical length of a line standard increases. Therefore, depending upon the frequency range, the number of line standards should be decided. For example, to

design a calibration kit working over a very wide frequency range (few MHz to several GHz), more than one line standards will be required because; one line standard will not be able to cover such a large frequency range. At the point where first frequency break point occurs, a second line standard is required to fill that frequency break. Similarly, for the second frequency break point, a third line standard is required and so on. The process follows until the complete frequency range has been covered. However, to avoid missing any frequency segment, the frequencies of lines must overlap at breakpoints as shown in Fig 3.4.

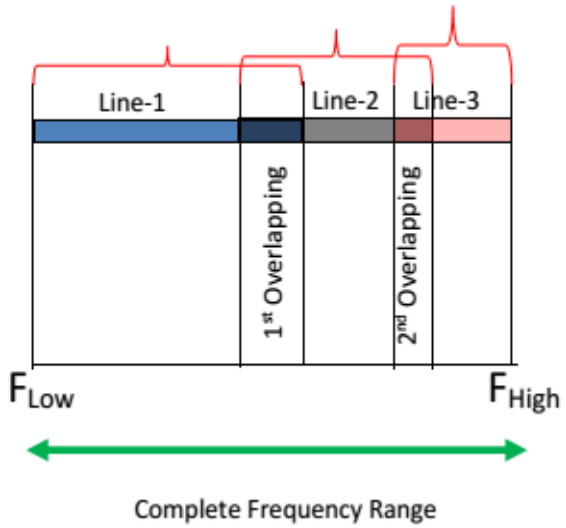

Figure 3.4: Block diagram for specifying the line standards

As a rule of thumb, the electrical length of each *Line* standard should not be less than 20° and greater than 160°. However, for the best accuracy the length of the *Line* should be 90° [3].

3.2.2.1 THRU Standard

Ideally, a *Thru* has zero phase length and zero insertion loss such that the incident signal propagates without any delay and loss. There is no difference between the S-O-L-T and T-R-L calibration except an additional *Line* to provide the necessary propagation delay. This phase delay is necessary to differentiate between the *Line* and the *Thru* standards. The phase difference between *Thru* and *Line* and between *Line* and *Reflect* is maintained according to the mathematical equations explained very well in [3]. The reference impedance of the measurement system is defined by the characteristic impedance of the *Thru* and *Reflect* standards. As we are are going to

characterize the transistor in a 50Ω impedance environment , we need to calculate the width of the *Thru*, *Reflect* and *Line* standards with 50Ω characteristic impedance. To establish a 50Ω *Thru*, the length and the width of the microstrip line was calculated in ADS software using RTduroid/5880 substrate. The physical parameters of *Thru* standard were calculated at θ=160∘, Z=50Ω, which are the standard dimensions at fundamental frequency (2.45GHz). Thus a microstrip line of 40mm length and 1.51mm width was printed on the RTDuroid/5880 substrate and the insertion loss was simulated using ADS momentum from 700MHz to 15GHz. As shown in Fig. 3.5, the *Thru* standard experiences a 0.12 dB loss over 15GHz which can be due to the distributed nature of the microstrip lines or the fabrication tolerance. However, the maximum cutoff frequency of the components used in loadpull measurement system is up to 18GHz thus, -0.12dB loss at 15GHz can be easily considered.

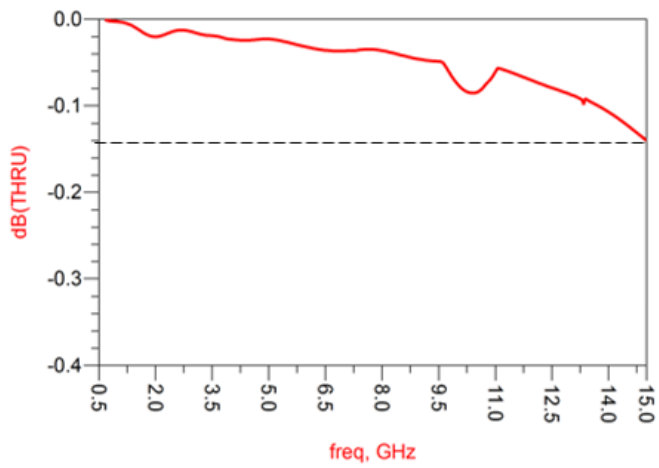

Figure 3.5: Insertion loss of the Thru standard (Simulated) (0.7GHz-15GHz)

3.2.2.2 Delay Line Standards

Frequency selection is a critical starting point before developing the *Line* standards in a TRL calibration design. A very broad or a very narrow frequency range can result in an unrealistic dimensions of *Line* standards in a calibration kit. The length of a *Line* standard is directly related to the frequency of operation therefore, a very high frequency can result in a very small physical *Line* length which may not be suitable for coaxial connections. Similarly, if the selected frequency is very small, the length of the *Line* standard can be extremely large which may not be suitable for its placement in the measurement setup. Therefore, according to the frequency requirements, a reasonably broad frequency range was selected. This frequency range is

advantageous because, it easily covers the fundamental (2.45GHz) and its 6 harmonic components necessary for waveform engineering. Also, the upper cutoff frequency of the loadpull measurement system is 15GHz. The targeted frequency range of the TRL-Kit is given below.

$$F_{Low} = 700MHz \qquad F_{High} = 15GHz$$

$$F_{Geometric_mean} = \sqrt{\left(F_{Low} \times F_{High}\right)}$$

Above equation results in the geometric mean of the upper and lower frequency limits which is finally used in equation (3.1) to calculate the length of the Line standard under restricted phase conditions.

3.2.2.3 Delay *Line-1* (for upper frequency band)

After making a resaonable frequency selection, the next step was to establish the *Line* standards. *Line* standard has a direct relation with the *Thru* standard because, a *Line* is formulated by adding a precise phase delay to a zero length *Thru* standard. To differentiate the *Line* from *Thru*, the basic phase difference between two standards should be strictly maintained between 20° and 160° degrees. This phase arrangement preserves the separate definitions of the two standards and avoids any phase overlap. Thus, the *Thru* standard can be confidently setup as a calibration reference point. A phase overlap between *Line* and *Thru* standards can give rise to an uncertainty in the exact definition of a *Thru* standard, the worst case occurs when the phase difference between these two standards is either 0 or 180 degrees.

Another important consideration while defining *Line* standard is to maintain the phase difference over a wide frequency range. If it is not possible, the *Line* standard should be divided into two or multiple parts to cover the whole frequency range. For example, in our case one *Line* is not sufficient to cover the targeted frequency range (700M Hz to 15 GHz). Therefore, we must have to divide this frequency range into two or multiple segments so that the *Lines* should be able to satisfy the phase requirements (20° and 160° degrees) over their designated frequency band . The frequency mid-point

is used to calculate the physical length of the *Line*-1 and can be calculated using equation (3.1)

$$F_{m.p} = \frac{F_{low} + F_G}{2} \tag{3.1}$$

Substituting equation 3.1 in 3.2 will result in the physical lengthg of *Line*-1.

$$L_1 = \left[\frac{90^\circ}{360^\circ}\right] \times \left[\frac{c}{F_{m.p}\sqrt{\varepsilon_{eff}}}\right] \tag{3.2}$$

Where ε_{eff} is the effective permittivity of the substrate used in the design process and *c* is the speed of light.

The *Line* was simulated (using ADS momentum simulator) up to the highest frequency 15GHz. It was discovered that the phase 20° to 160° is only true from 2GHz-15GHz. As the intention is to intially characterize the transistor at 900MHz therefore, we must need to design another *Line* which should be able to maintain with the phase requirements for the lower frequency range. To observe the phase response of the *Lines*, following equations were used.

$$PhaseLine_1 = \left(\frac{SP_Thru}{SP_Line1}\right) \tag{3.3}$$

$$PhaseLine_2 = \left(\frac{SP_Thru}{SP_Line2}\right) \tag{3.4}$$

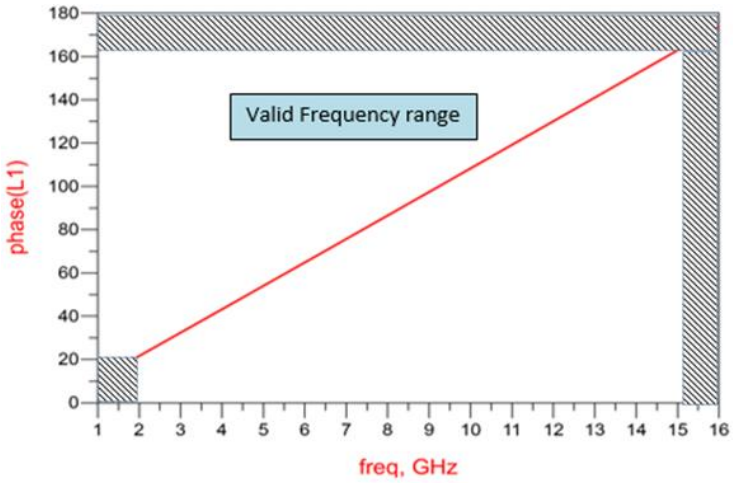

(a)

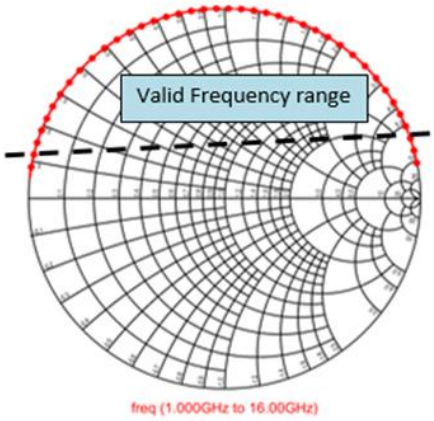

(b)

Figure 3.6: Phase length of Line2: 20° ≤ Line1≤160° (2GHz-15GHz) (2-D plot) (a), smith chart mapping (b) (Simulated)

3.2.2.4 Delay *Line-2* (for lower frequency band)

As we can see in the Fig. 3.6, the *Line*-1 is suitable for 2GHz-15GHz and cannot cover the lower frequency therefore, another *Line* is required to cover the lower frequency limit. Similarly, delay *Line*-2 was designed to cover the lower frequency range where the new limiting values of the lower frequency and higher frequency were adjusted as follows:

$$F_{Low} = 700MHz \qquad F_{High} > 2GHz$$

$$F_G = \sqrt{\left(F_{Low} \times F_{High}\right)} \tag{3.5}$$

$$F_{m.p} = \frac{F_{low} + F_G}{2} \tag{3.6}$$

The new frequency mid-point value was substituted in equation (3.2) and the length of *Line*-2 was calculated. The *Line* was simulated in ADS momentum using 50Ω terminations and the phase versus frequency plot is shown in Fig.3.7. It is evident that this *Line* covers 0.7GHz-6.3GHz frequency range where again the phase difference is maintained between 20 and 160 degrees. Also, the two *Line*s make a frequency overlap which avoids missing any frequency segement. Thus in conclusion, by using pair of phase delay *Line*s the frequency range from 700MHz to 15 GHz can be covered which contains 6 harmonic multiples of 2.45GHz for *Line*-1 and 6 harmonic multiples of 900MHz for *Line* 2.

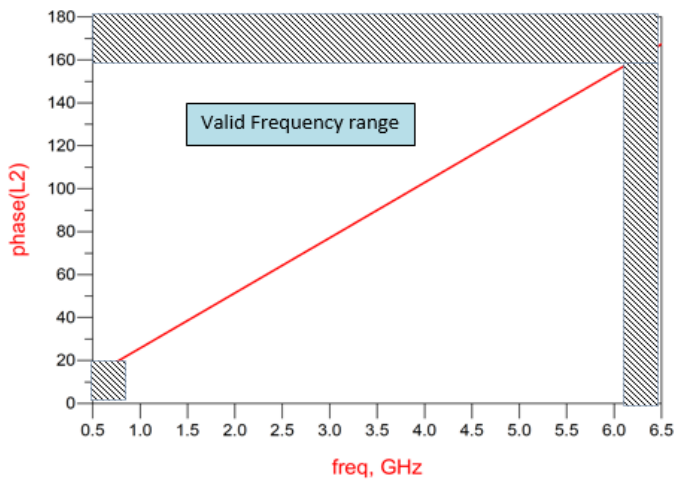

(a)

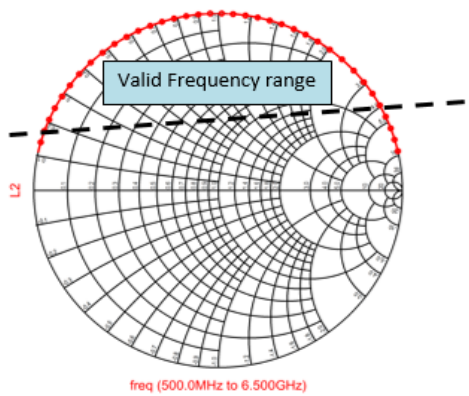

(b)

Figure 3.7: Phase length of Line2: 20° ≤ Line1≤160° (700MHz-6.3GHz) (2-D plot) (a), smith chart mapping(b) (Simulated).

3.2.2.5 Reflect (Open)

Reflect standard is exactly the half the length of the *Thru* standard. Therefore, the phase of the *Reflect* must be within $\lambda/4$ or 90°. Once the correct phase information is known, the *Reflect* standard can also be used to setup the reference plane. It is not necessary to know about the magnitude of the *Reflect* standard because it is obvious that any signal incident upon an open circuit will not be transmitted. The *Reflect* (open) was simulated in ADS momentum and its phase response was observed.

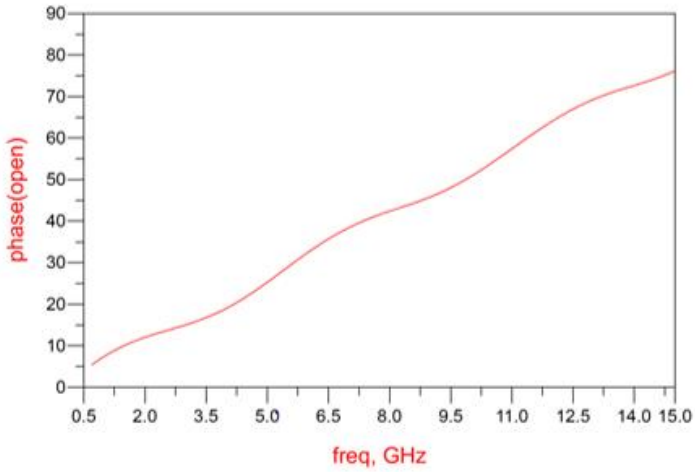

(a)

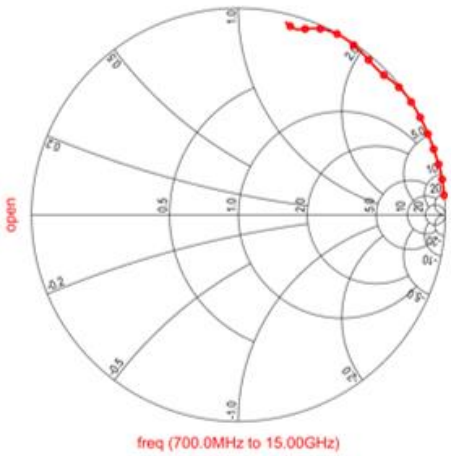

(b)

Figure 3.8: Phase of the open standard over the targtede frequency range (700MHz-15GHz) (2-D plot) (a), smith chart mapping(b) (Simulated).

The momentum simulations of microstrip standard *Reflect* were conducted over specified wide frequency range. It can be seen in Fig.3.8 that the *Reflect* standard fufills the phase requirements and exists between 90°.

3.2.2.6 Beatty Line

A Beatty line is a standard for verifying the completed calibration [4] in case there is no mathematically established TRL calibration program using matlab or ADS etc. However, the verification process becomes much simpler by comparing the mesaured beatty line response with the mathematically derived simulated response. Therefore, to verify the TRL kit standards, a Beatty line was fabricated on the same substrate with a simple impedance configuration of 50-25-50Ω. The verification process includes measuring the S-parameters of the beatty line then comparing with S-parameters taken through the TRL calibration. A good comparison between two measurements can assure the validity of the calibration. The response of the beatty line after S-O-L-T cal and TRL cal should be alike.

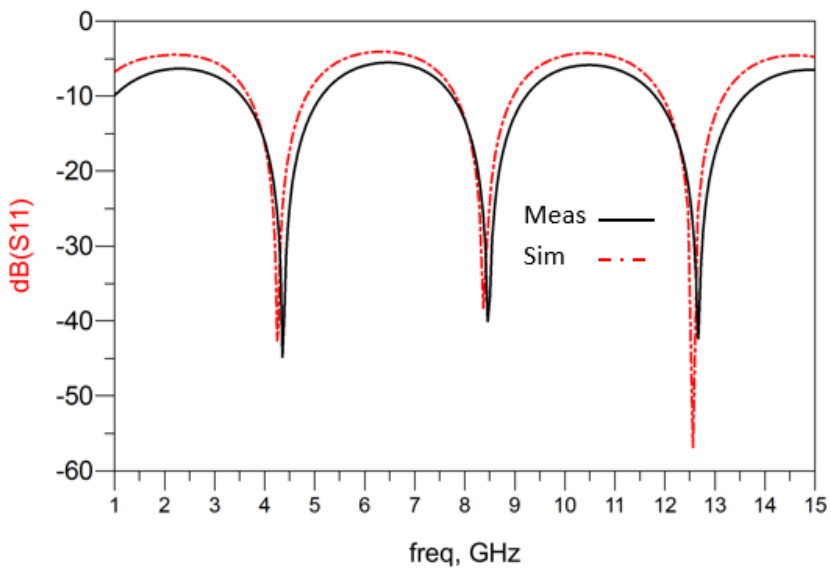

Figure 3.9: Simulated vs Measured S11(dB) Response of Beatty Line for calibration accuracy.

After a mathematical analysis, all the standards were mapped on the RTDuroid 5880 substrate and the Kit was finalized as shown in Fig 3.9.

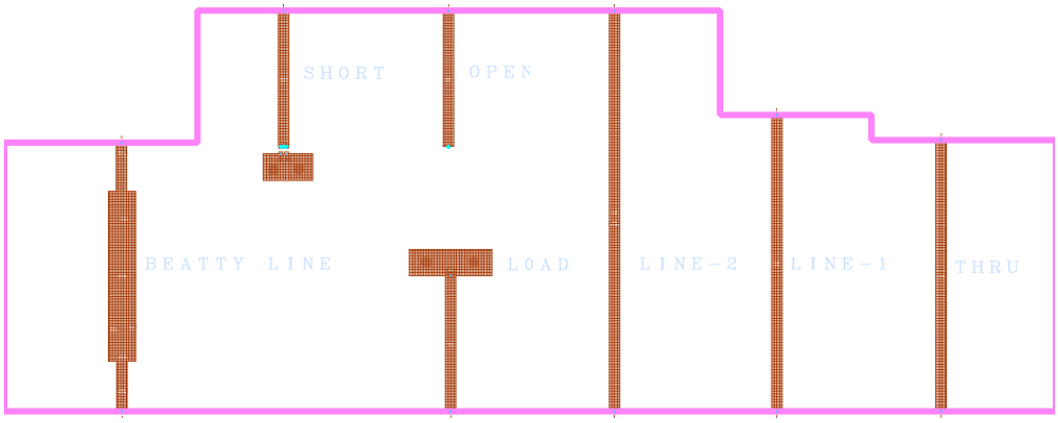

Figure 3.10: 50Ω TRL-Kit containing Thru-Reflect-Line standards and BEATTY Line (useful for calibration from 700MHz-15GHz)

3.2.2.7 Test and Measurement

The TRL kit was manufactured and the S-parameters of the *Thru*, *Reflect*, *Line-1* and *Line-2* standards were measured using S-O-L-T calibration kit. To verify the accuracy of the manufactured Kit, the measured S-parameter files of the standards were imported into a 12 error term methematical model (developed at Cardiff University) in ADS. After reading the files, the program automatically maps their 2 port response against the ideal standards. Also, the program generates the measured S-parameter files describing each half of the test fixture, which can then be used in loadpull measurement systems for fixture deembedding. The mathematical model was simulated two times,once for each of the two *Line* standards. During first simulation, the mesaured S-parameter data of *Line-2* was imported into the model and the fixture port S-parameter files (for low frequency limit) were extracted. Similarly, during second simulation, the mesaured S-parameter data of *Line-1* was used to extract the fixture port S_{2P} data file covering high frequency band upto 15GHz. It is important to mention here that the upper frequency limit was restricted to 15GHz because of the SMA connectors maximum frequency limiting factor. For 2.45GHz fundamental frequency, the 3rd harmonic is equal to 7.5GHz and the maximum cutoff frequency of DSA8200 sampling scope is 12.5GHz. Therefore, in both cases we have great freedom to use this TRL-kit for transistor characterization at 900MHz and 2450MHz.

The measured S-parameters of the test fixture were compared with the extracted standard fixture S-parameters as shown in Figures 3.11.

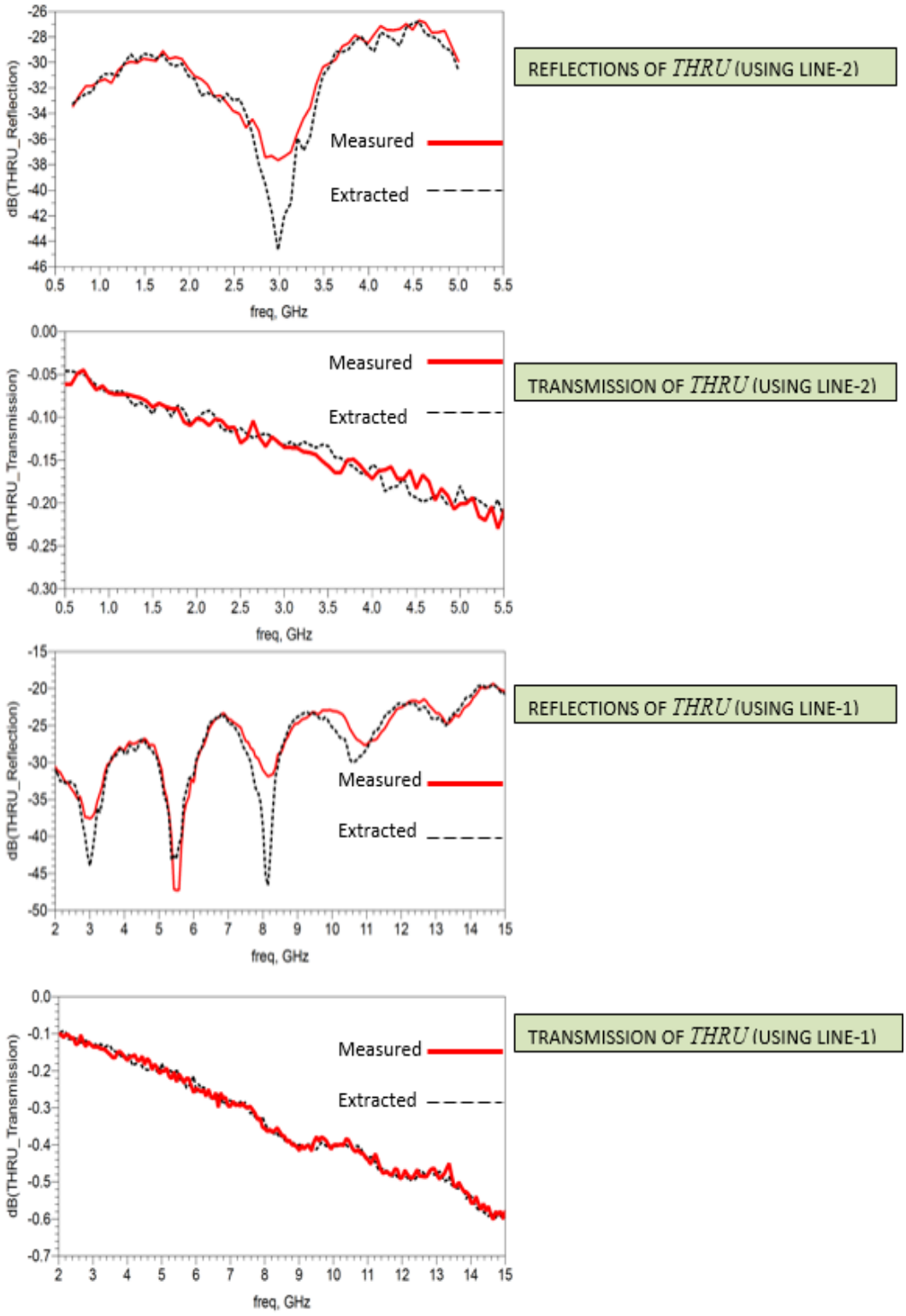

Figure 3.11: Measured vs simulated Thru-standard using two separate delay Line standards.

The measured S-parameters of the 50Ω test fixture *Lines* show an excellent agreement with the mathematical model from 0.7GHz to 15GHz. Therefore, de-embedding the

input and output test fixture ports will give an accurate access to the transistor package plane both for 900MHz and 2.45GHz.

3.3 Transistor Characterization and Load Line

Transistor characterization is the first step before designing a power amplifier. As the transistor is a nonlinear device, its behaviour changes with respect to the biasing voltage and input RF signal. The impact of these two parameters can be observed through well known loadline analysis. The loadline and the DC-IV curves provide the correct information of the transistor operating point. The position of the loadline relative to the DC-IV defines the dynamic operating points of the transistor. The operating point of a transistor can be adjusted by adjusting the load line. During the RF analaysis, the reactive components associated with the transistor can play a significant role and transform a real load line into a complex load line. As a result, we observe the time domain output voltage and current waveforms.

DC load line analysis is an easy and quick way of determining the optimal parameters of a transistor and it allows a true performance realization of a transistor. Under optimal load resistance, the device operates in its maximum output current, and the loadline hits the knee region of the DC-IV curves. At this point, the output voltage and current waveforms have their maximum swing resulting in a maximum output power. The current waveform swings within [0, I_{max}] and voltage waveform swings within [V_{Knee}, $2(V_{dc}-V_{Knee})$] range. This special situation occurs when an optimum impedance is presented to the transistor i.e. $R_L=R_{opt}$. However, when the output load resistance is less than its optimum value, the loadline moves away from the knee region and the output voltage swing reduces which results in a reduced output power and efficiency. The reduced efficiency is due to the transistor's operation in its deep saturation region because, in this region the dissipation power is maximum. Therefore, the DC power consumption is more than RF power generation and the transistor becomes less efficient. For $R_L>R_{opt}$, the load line kneels down more and displaces off the knee bend curve. Under this condition, the reduced effect of the knee voltage on the output voltage waveform results in an increased output voltage swing. Also, as the loadline goes away from the deep saturation region, the reduced DC consumption of the transistor results in an increasesed drain efficiency but at the cost of lower output power due to a lower drain current. However, the output power can be increased by

shaping the output waveforms through a logical addition of harmonic content to maintain both high efficiency and output power. This method is called waveform engineering which will be explained later in this chapter. Three load conditions can be seen in Fig 3.12.

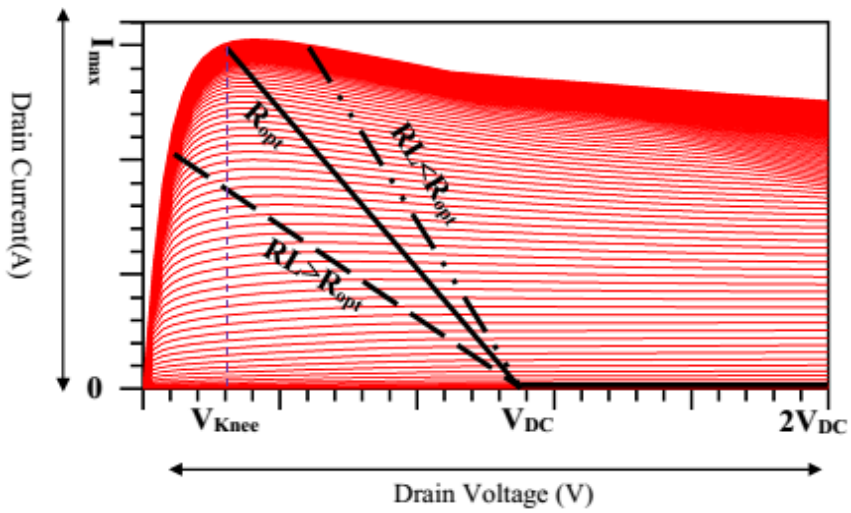

Figure 3.12: Simulated DC-IV curves and Load-Line analysis.

3.3.1 DC Behaviour

DC-IV characteristic curves are gate voltage dependent nonlinear drain currents that provide an understanding of the limiting values of a transistor under measurement conditions. These nonlinear curves hold information of the saturation current, knee voltage and transfer characteristics of a transistor. These curves also facilitate the biasing point selection of the transistor which then helps in defining the specific class of transistor operation.

To start with, the device was simply turned on by supplying DC current at its gate and drain terminals. The gate voltage at which the transistor starts drawing current is called its turn-on point. At this gate voltage, first drain voltage sweep was conducted (from 0 to 8V) to determine the maximum drain current of the device. For each gate voltage, a separate drain voltage sweep was conducted and nonlinear current curves were generated. The data was plotted and the measured drain current was found to be approximately 1A less than the simulated current and the measured knee-voltage was higher than the simulated one. The possible reason for this increased output voltage was likely due to the unaccounted resistance of the cable. Therefore, the resistance of the DC supply cable was separately measured using simple multimeter which was

found to be 2 Ω. This resistance value was substituted in equation (3.7) and the actual voltage and current supplied to the transistor was recalculated.

$$I_d = \frac{V_{\sup} - V_{Transistor}}{R_{cable}} \tag{3.7}$$

Finally, the measured drain current and knee voltage were found in a close agreement with the simulated one as shown in Fig.3.13.

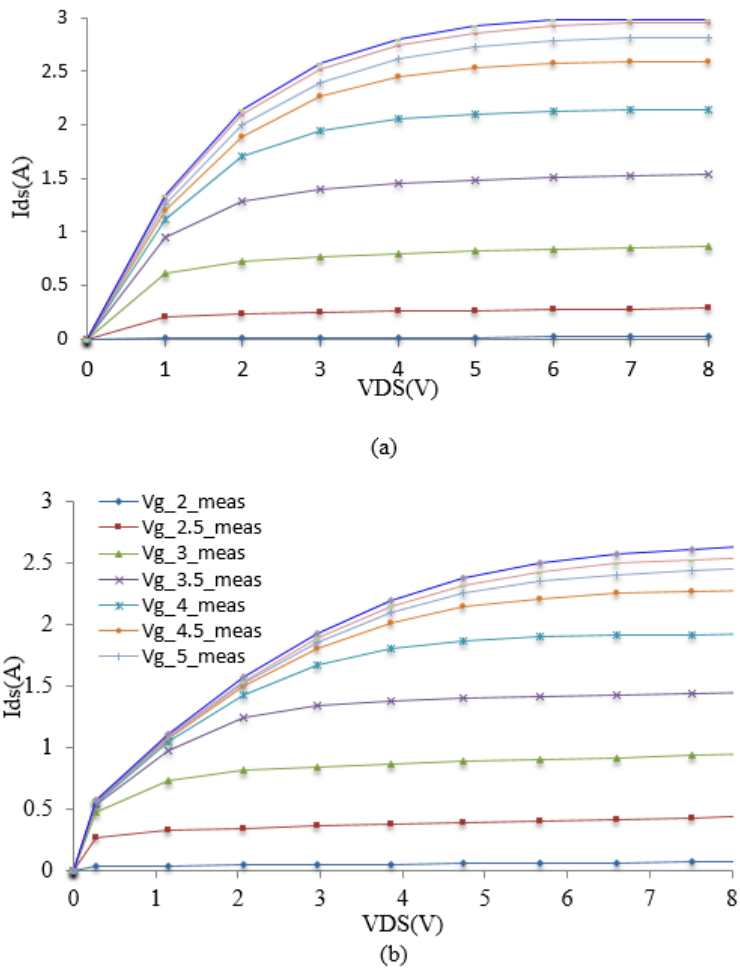

Figure 3.13: DC-IV analysis with including cable resistance. (a) Simulated (b) Measured.

3.3.2 RF behavior and De-embedding

Scattering parameters or S-parameters is a relative term that defines the ratio between an incident and reflected normalised wave amplitudes. These parameters are used in the linear characterization of an electrical network. In modern electrical engineering,

S-parameters can be measured by simply connecting a coaxial RF network with the ports of a clibrated network analyser. These parameters are used to define the electrical response of the microwave devices. Small signal sacttering parameters are sufficient to characterize the passive RF devices because of their independent linear voltage ratios and passive response. However, the active devices cannot be fully characterized by small signal S-parameters alone because of their bias dependency and active response. In these devices, the voltage ratios (reflected, incident) change with the application of external DC voltage supply. Thus, the transistor's complex impedance environment changes significantly with frequency and biasing due to its transfer-resistance nature.

As we know that the transistors are housed in the plastic or ceramic packages for their practical use. These packages contain a set of inductive bond-wires and pad capacitors which transform the ideal real resistive load at the I_{gen}-plane to a complex impedance at the package plane. consequently, it becomes very difficult to gain knowledge of the transistor's optimum impedance environment. For an accurate transistor characterization, it is important to negate the effects of its parasitics to get access to the current generator plane because, at this plane the transistor usually wants to see a pure resistive fundamental load. The process of negating the parasitic is called de-embedding and it is key to waveform engineering. Therefore, it is very important to get the right information of the de-embedding network to gain access to the transistor's current generator plane for accurate waveform engineering. The output current waveform is affected by the built-in parasitic capacitors that generate displacement current as a function of the time varying voltage across the capacitor. [5]

$$I_{disp} = C\left(\frac{dv}{dt}\right) \tag{3.8}$$

This extra current is out of phase with and adds to the output current wave appearing at the transistor intrinsic plane. Thus the final time domain current waveform becomes the sum of the actual current and the displacement current as shown in equation (3.9)

$$I_{Meas} = I_{disp} + I_{current_gen} \tag{3.9}$$

From these two equations, it is obvious that leaving the capacitive effect unaccounted for leads to the lower output power due to the relative phase-offset at the current generator plane. Similarly, the inductors attached with the bare die as bonding wires disrupt the output voltage waveforms by adding displacement voltage. This displacement voltage is a time derivative of the output current.

$$V_{disp} = L\left(\frac{dI}{dt}\right) \tag{3.10}$$

$$V_{meas} = V_{disp} + V_{Current_gen} \tag{3.11}$$

As is the case for displacement current, displacement voltage adds to the time domain voltage waveform appearing at the intrinsic plane of the transistor. These parasitic elements start getting more reactive at higher frequencies due to their inherent reactive properties. Therefore, the estimated de-embedding network needs more refinement when moving on to S-Band or higher. The de-embedding techniques presented in [6-7] allow access to the current generator of the transistor, but in our case, the intrinsic and extrinsic parasitic network of the 10W-LDMOS power transistor was provided by the manufacturing company NXP Inc. with the small signal network topology shown in Fig 3.14 and the component values provided in table 3.2.

C_{ds}	L_{Bond}	C_{Pad}
≈ 3.9pF	≈ 93nH	≈ 0.9pF

Table 3.2: Estimated values of parastic components

3.3.3 Large Signal Analysis (Simulations)

After obtaining the de-embedding network, the next step was to verify with the device package model. As the S-parameters of the transistor depends upon biasing and frequency therefore, the de-embedding network needs proper evaluation under biasing conditions. In the ADS simulation environment, two design schematics were created, firstly for the die-model of 10W-LDMOS power transistor and then for the die with its package model. In first design, the obtained de-embedding network was placed in

series with transistor current generator, which was biased in class-A because of intention to characterize it for F^{-1} later on. In the second design, the packag model was biased and simulated under the same biasing conditions. In both cases, the transistor was driven to its 1dB compression point (26dBm input drive power) for verification of the de-embedding network. The voltage and current waveforms were obtained at the package plane of the transistor as shown in Fig.3.14.

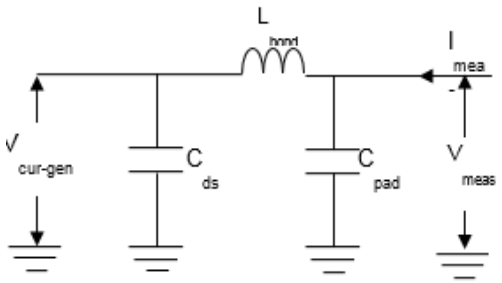

Figure 3.14: Small signal parasitic network of BLF6G27-10G 10W-LDMOS power transistor

In both cases, the simulated voltage and current waveforms were compared side by side, as shown in Fig.3.15. The comparison of the time domain waveforms show a good level of agreement and validated the de-embedding network for its further utilization in the measurement setup.

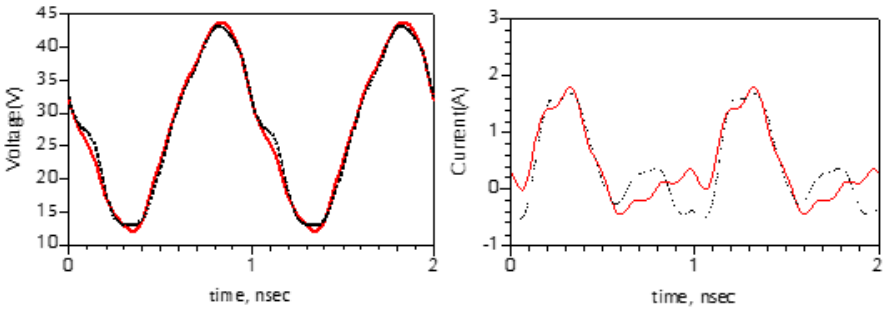

Figure 3.15: Simulated time domain waveforms of 10W-LDMOS power transistor at 1GHz (left) voltage waveforms (right) current waveforms, for both die+package network (Solid) and package models (Dotted).

3.3.4 Waveform Engineering

Waveform engineering is a systematic process in which the output voltage and current waveforms are shaped for optimum performance. During active characterization of the transistor operation, a time domain output current wave is controlled mostly by adjusting the gate biasing and input CW drive signal. Similarly, the time domain

output voltage wave is controlled by adjusting the fundamental load impedance and drain voltage. In modern automated multiharmonic active load-pull measurement systems, the output voltage and to a lesser degree the current waveforms are shaped by controlling the phase and magnitudes of the fundamental and harmonic load impedances under predefined biasing and drive conditions. Therefore, waveform engineering is the first step before designing a high performance power amplifier.

With the evolution of the high-efficiency PAs, different operational modes of the power amplifiers have been introduced. These modes range from linear waveforms (Class-A) to non-linear waveforms (Class-F etc.). The output fundamental voltage and current waveforms possess certain lower amplitude under their classical modes like Class-A, Class-B or Class-C. However, these amplitudes can be increased by an in-phase addition of the integral harmonic components. Transistors driven with input RF signal, produce number of harmonic signals along with the fundamental. These harmonic signals can guarantee optimal performance of the device if used correctly. For example, in a class-F PA mode, the voltage waveform is squared by the contribution of odd harmonics and the current waveform is half rectified by virtue of bias, resulting in 100% drain efficiency [8]. Similarly, in the F^{-1} mode of operation, the even harmonic voltage components are combined with the fundamental voltage waveforms and all the odd harmonic currents are short circuited. In this mode of operation, the amplitude of the fundamental voltage wave is increased by adding suitably phased 2nd harmonic voltage components, leading to high output power and efficiency. This mode of operation is suitable for high breakdown voltage transistor techonolgies such as silicon LDMOS and GaN. Large drain-source capacitance present in Silicon LDMOS devices short circuits the higher harmonic current components thus only 2nd harmonic voltage component can be added to the fundamental voltage wave to increase its amplitude for higher output power and efficiency.

3.4 Active Harmonic Load-pull Measurement Setup

A multiharmonic active load-pull measurement system is an arrangement of RF and DC equipment used for transistor characterization. In a load-pull measurement system, the transistor is presented with different load terminations and its active performance is monitored. This is achieved by controlling the magnitude and phase of signals

incident upon and reflected from the drain terminal of transistor. The block diagram depicted in Fig.3.17 best describes the working principle of the active loadpull system. High power amplifiers installed at the output side of the transistor present the amplitude and phase variant fundamental, 2nd and 3rd harmonic CW signals to the transistor. The active injection of these load signals is provided by the passive low-pass filter network called a tri-plexer. Tri-plexer has the ability to combine these signals whilst providing a high level of isolation between the inputs and maintaining a low insertion loss.

Incident and reflected voltage travelling wave signals measured in the time domain possess all of the required phase and the magnitude information, which is collected by the sampling scope through a set of highly sensitive, sub-sampling receivers for active time domain wave sampling. High directivity directional couplers are very important part of the loadpull measurement system because, they provide an accurate information of the incident and reflected signals to the four channels of the sampling scope. The incident and reflected signals at both input and output of the DUT are accessed through a 20dB directional coupler and presented to the four channels of the sampling oscilloscope. Channel-1 and Channel-4, collect the information of the incident signals at input and output ports whereas, channel 2 and channel 3 collect the information of the reflected signals at input and output ports of the transistor respectively. For a proper transistor characterization, these incident and reflected signals should have sufficiently high amplitude observable well above the noise floor of the sampling scope. This can be achieved by decreasing the channel attenuations however, care should be taken because any signal (incident, reflected) higher than 23dBm will damage the low power reciver channels.

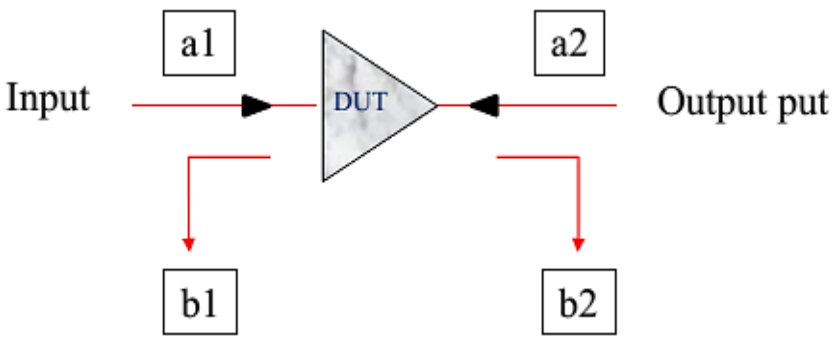

Figure 3.16: Block diagram of incident and reflected signals upon transistor

The complex incident and reflected waves carry the phase and amplitude information of the signals which is then translated into complex reflection coefficient for impedance calculations. By actively varying the magnitude and the phase of complex load reflections, the performance of the transistor is monitored and the best optimum loads are impirically identified.

$$\Gamma_{in} = \frac{b_1}{a_1} \tag{3.12}$$

$$\Gamma_L = \frac{a_2}{b_2} \tag{3.13}$$

In equation (3.12), b_1 and a_1 are the reflected and incident signals at input port of the transistor respectively and their ratio gives the information of input reflection co-efficient. Similarly, in equation (3.13), a_2 and b_2 are the reflected and incident signals at output port of the transistor and their ratio gives information of the load reflection coefficients used in the loadpull measurements.

For a successful loadpull analysis of the transistor, it is very important to negate the effects of all the cables and interconnects between the signal sources and the transistor. This allows a true behaviour of the transistor under different loading conditions and determines its actual high performance optimum load. To do that, two types of the calibrations are performed. The first involves a conventional small signal S-O-L-T-calibration, but the second involves an indirect calibration also known as the large signal calibration that allows the measurement of absolute travelling wave powers, as well as the S-parameter ratios. An accurate calibration guarantees accurate waveform engineering provided that the transistor de-embedding network is correct.

All of the singal sources including fundamental trigger and sampling scope are phase synchronized to a 10MHz CW signal and their port addresses are intercommunicated through GPIB (General Purpose Interface Bus) cables. Finally, the complete system is communicated with a remote PC. The software used in this measurement activity accesses the instruments through GPIB cables and instructs them to perform the directed tasks. In this measurement system, loads can be presented directly at the intrinsic plane of a transistor by importing the package de-embedding network and the resulting output waveforms can be monitored on the remote PC.

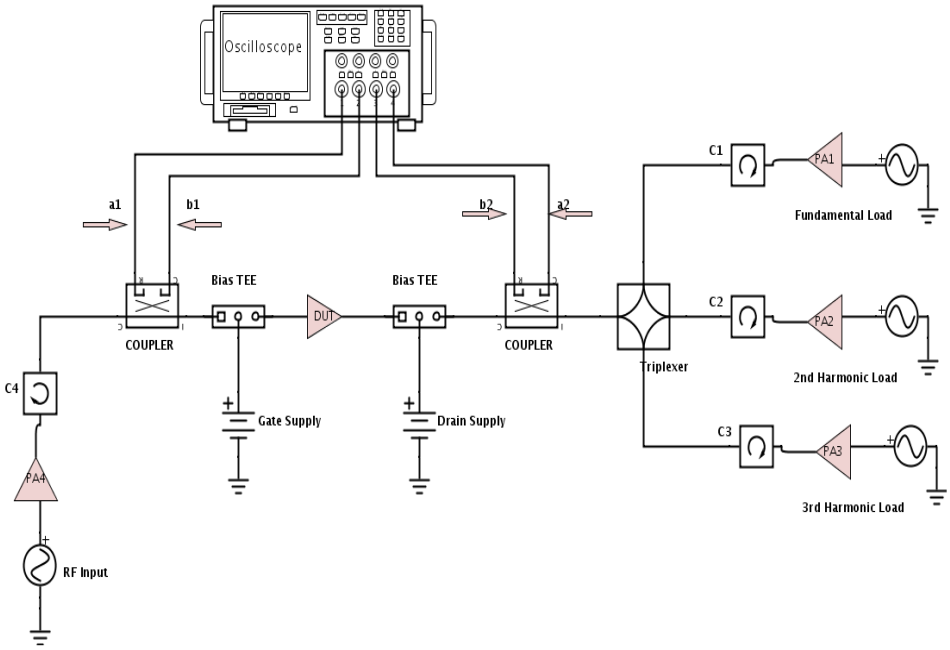

Figure 3.17: Typical Block diagram of a CW active harmonic loadpull measurement system.

3.4.1 Tri-plexer Network Design

Triplexer is a passive filtering device consisting of three input ports and one output port. It is a systematic combination of four low pass filters used to accept three different RF signals and transmit them from the fourth common output port. For a reliable and purposeful operation, the triplexer maintains the integrity of the incident signals by keeping a high level of isolation between them. Presently, high frequency and compact but expensive triplexers are available in the RF markets for simultaneous three signals transmission with high isolation. For this experiment however, the triplexer was manually designed by the combination of low pass filters and 90° hybrid couplers. A single hybrid coupler divides an input signal into two *half power* and *90°out-of-phase* signals that appear at its two output ports; the second input port of the hybrid coupler is terminated with 50Ω load. However, the original signal with the same power and phase information can be recovered back by combining two back-back quadrature hybrid couplers. This natural attribute of the hybrid couplers can be utilized to formulate a triplexer network capable of sustaining the amplitude and phase information of the incident signals. This network accepts three input signals and transmits them from a common port as shown in Fig.3.18. However, this arrangement has an added advantage of providing an extra input port for the DC signal injection as

well, thus eliminating the need for an additional biase-tee and resulting in four isolated transmitted signals from the common port. The left half of the triplexer accommodates the 2nd and 3rd harmonics with high isolation and the right half accommodates the DC and fundamental signals. The triplexer network was designed by systematically arranging the low pass filters to avoid the mixing of three different signals and its output signal response was verified before its placement in the load pull measurement setup.

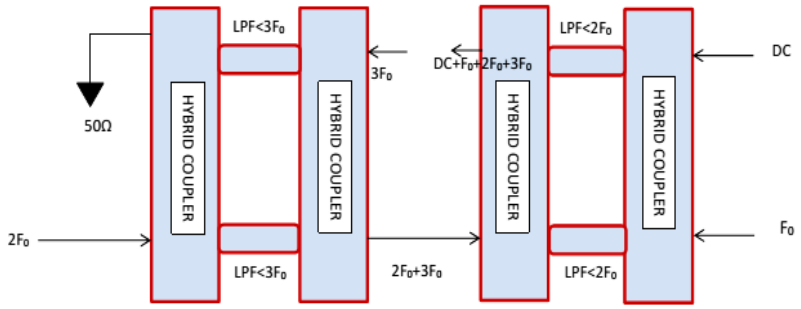

(a)

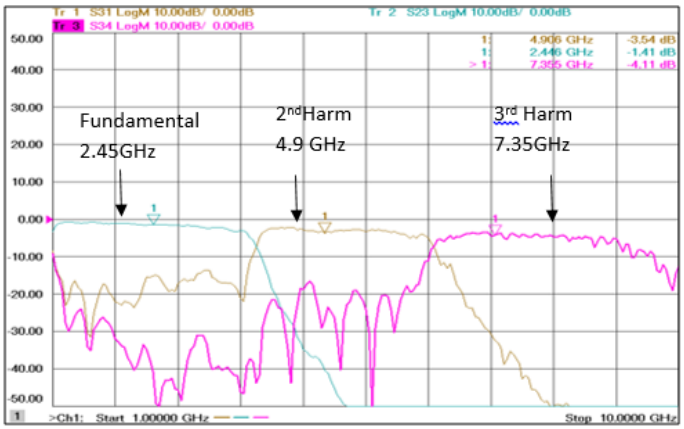

(b)

Figure 3.18: (a) Triplexer working principle (b)measured response for three injected signals.

The results depicted in Fig.3.18 clearly show the phase and magnitude recovery of the input signals with an average -20dB isolation. This level of isolation is high enough to accurately present three different loads to the transistor during its characterization. However, the insertion loss for 2nd and 3rd harmonic frequencies is much higher than it was expected. The reason for this loss is due to the dielectric loss of the physically large hybrid couplers. However, this loss can be compensated by using high power amplifiers within loadpull mesaurement system which will then be able to create high magnitude load reflection coefficients to the transistor during its characterization.

3.4.2 System validation in 50Ω environment

A properly calibrated loadpull measurement system is an important step in transistor characterization. A similar response of the transistor in the physical loadpull measurement setup and in a CAD environment can validate the calibration accuracy of the loadpull measurement system. After verification, the nonlinear loadpull simulations can be set as a reference for loadpull measurements. Therefore, in both real and simulation environment, the 10W LDMOS power transistor was biased to its class-AB point (Vg=2.3V) and its output port was terminated with a 50Ω passive load. The transistor was then driven with an arbitrary input CW signal to generate and compare the load lines in both cases as shown in Fig.3.19.

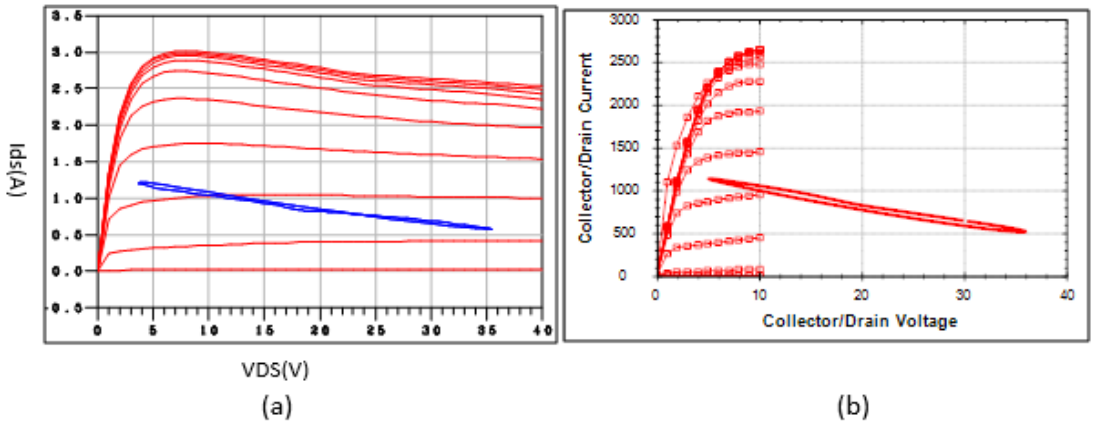

Figure 3.19: Dynamic load line after system calibration (a) simulated (b) measured

It can be seen that the amlitudes of the voltage and current waveforms in both cases are exactly the same where the transistor outputs 1.2A drain current and 36V drain voltage. Thus, at first hand it shows the calibration accuracy of the loadpull measurement system and on the other hand it shows a great resemblance of the 10W-LDMOS power transistor with its package model(BLF6G27-10G). Therefore, the loadpull measurements can be confidently followed by the loadpull simulations.

3.5 Inverted Class-F Waveform Engineering (at 900MHz)

Optimum performance of a transistor can be easily determined by calculating its optimum load resistance (R_{opt}) through simple DC-IV measurements [9].

$$R_{opt} = \frac{(V_{dc} - V_{Knee})}{I_{dc}} \tag{3.14}$$

Load-line matching is a quick way of calculating transistor's optimum load resistance, but unfortunately it does not provide the large signal behaviour of a transistor. Under large signal operation, the intrinsic and extrinsic parameters of a transistor can play a dominating role and alter the optimum load resistance to a suboptimal impedance at the package plane. Also, the output harmonics further complicate the load impedance envrionment and if this is not understood, this can make the transistor a difficult active device to control. Loadpull measurement is a cumbersome but an effective way of truly characterizing a transistor under large signal conditions for its optimum operation. By adopting an accurate loadpull measurement process, the safe and optimal operation of a transistor can be guaranteed.

To begin the loadpull process, a passive load termination (50Ω) was replaced with the multiharmonic active injection system described earlier. High-power amplifiers with circulators were used to compensate the filtering network losses which were further reduced by using short lengths coaxial cables. Nonlinear power transistors driven with a CW signals produce number of current carrying harmonic signals which are integral multiples of the fundamental signal frequency. These signals are generally out of phase with the fundamental wave due to the intrinsic and extrinsic reactive elements. This phenomenon becomes more evident when the device is biased to its pinch off point and driven into its compression region. Generally, these hard drive conditions are required during high efficiency mode waveform engineering where the loadline interacts with the knee voltage and the transistor can generate a significant number of harmonics.

In performing inverse class-F waveform engineering, the 2nd, 3rd and higher harmonics are systematically controlled to engineer the fundamental voltage waveform. The 2nd harmonic is terminated with an open circuit, so its in-phase voltage component contributes to increase the peak amplitude of the fundamental voltage waveform. Similarly, 3rd harmonic is terminated with a short circuit and its current component together with the boundary conditions squares the current waveform. LDMOS power transistors due to their lower cut off frequency, possess less number of harmonics, so it is easier to see their high efficiency response at lower frequencies [5]. Therefore,

900MHz fundamental frequency was seleceted as a starter before moving on to higher frequencies such as 2.45GHz. To start with, the ADS loadpull simulation environment was prepared and the package model of 10W-LDMOS was employed to apply waveform engineering techniques. The device was biased at its class-AB point (I_d=1.2A, V_d=20V, V_g=2.2V) for an initial safe operation. The de-embedding network verified in the previous section was used to negate the effects of the extrinsic and intrinsic parasitic of the transistor to access its I_{gen}-plane. This is a pure resistive plane where there are no reactive elements to interfere with the complex output waveforms. Therefore, the resulting waveforms are purely sinuosoidal and amplified. The loads seen by the transistor at its current generator plane are purely resistive therefore, simple loadline theory can be applied at this plane. However, C_{DS} is a function of drain voltage therefore, it slightly interacts with the output current waveforms even if the transistor is de-embedded upto its intrinsic plane [5]. The loadpull process was started to identify the best optimum fundamental and harmonic load impedance values for 10W-LDMOS transistor at 900MHz.

3.5.1 Load Optimization

Load optimization is an iterative process in which different complex loads are presented to the transistor and its optimum impedance design space is determined and updated after each iteration. The systematic iterations are followed by continuously observing the output performance of the transistor during the loadpull process. Using the automated multharmonic loadpull measurement system, different complex loads are presented to the transistor by electronically spreading them at different locations of the smith chart. The iterative load sweeps identify a certain area of the smith chart, where the transistor exhibits the highest output power and drain efficiency. That specific area holds the optimum impedance of the transistor. By following this process, fundamental, and harmonic loads are identified which will be discussed in the next section in details.

3.5.1.1 Fundamental Load Optimization

To begin the fundamenal load characterization, the 2nd and 3rd harmonics were terminated with passive 50Ω loads. High density fundamental load impedance points were spread over full smith chart to roughly locate the initial optimum area. After

performing a large load sweep, the specific area where the transistor showed a relatively high power and efficiency was locked. During the second iteration, the fundamental load sweep was conducted by populating the load points only in the area identified after first iteration. In the second iteration it was discovered that the fundamental optimum impedance points lie near 50Ω where the transistor shows near 75% drain efficiency at 38dBm output power as given in Table 3.3 .

$Z_{Fo\,(opt)}$ (Ω)	Z_{2Fo} (Ω)	Z_{3Fo} (Ω)	η_{Drain} (%)	$P_{out(dBm)}$
44	50	50	75	39.055
40+j*10	50	50	67	40

Table 3.3: Measured output performance of 10W LDMOS transistor at 900MHz with (Zfo=Zopt, Z2fo=50Ω, Z3fo=50Ω)

3.5.1.2 Harmonics Load Optimization

To achieve best performance of the transistor, the harmonic contents play a major role because these components contribute to increase the output voltage and current swings that result in increased transistor performance. To begin with, the fundamental load was fixed to its optimum impedance point and the 3rd harmonic was passively terminated with 50Ω. The 2nd harmonic load was swept across the smith chart and the loadpull iterative process was conducted to find out the 2nd harmonic optimum impedance. After several iterations, the optimum 2nd harmonic load point was identified as shown in Fig.3.20(a). It is obvious that the drain efficiency increases from 67% to 77% as the impedance of 2nd harmonic load increases and the pattern shows that the efficiency improves as the 2nd harmonic load moves towards higher impedance. This shows the contribution of the 2nd harmonic voltage component to increases the output voltage wave swing. It is however a fact that the large C_{DS} of the transistor presents a low impedance to the 2nd harmonic therefore, to create a reflection coefficient of unity magnitude, a very high level RF signal is required. In this case, the power was insufficient to present a high impedance load to the 2nd harmonic. The reason was high insertion loss incured in the triplexer network causing significant amount of power attenuation. Therefore, the magnitude of the 2nd harmonic load reflection coefficient could not be increased further thus fixed at this location.

As the intention is to engineer F^{-1} mode therefore, the 3rd harmonic was presented with a short circuit as shown in Fig.3.20(b). Similar iterative loadpull process was adopted to locate 3rd harmonic optimum load around the low impedance area of the smith chart whilst the fundamental and 2nd harmonic loads were fixed to their optimum values.

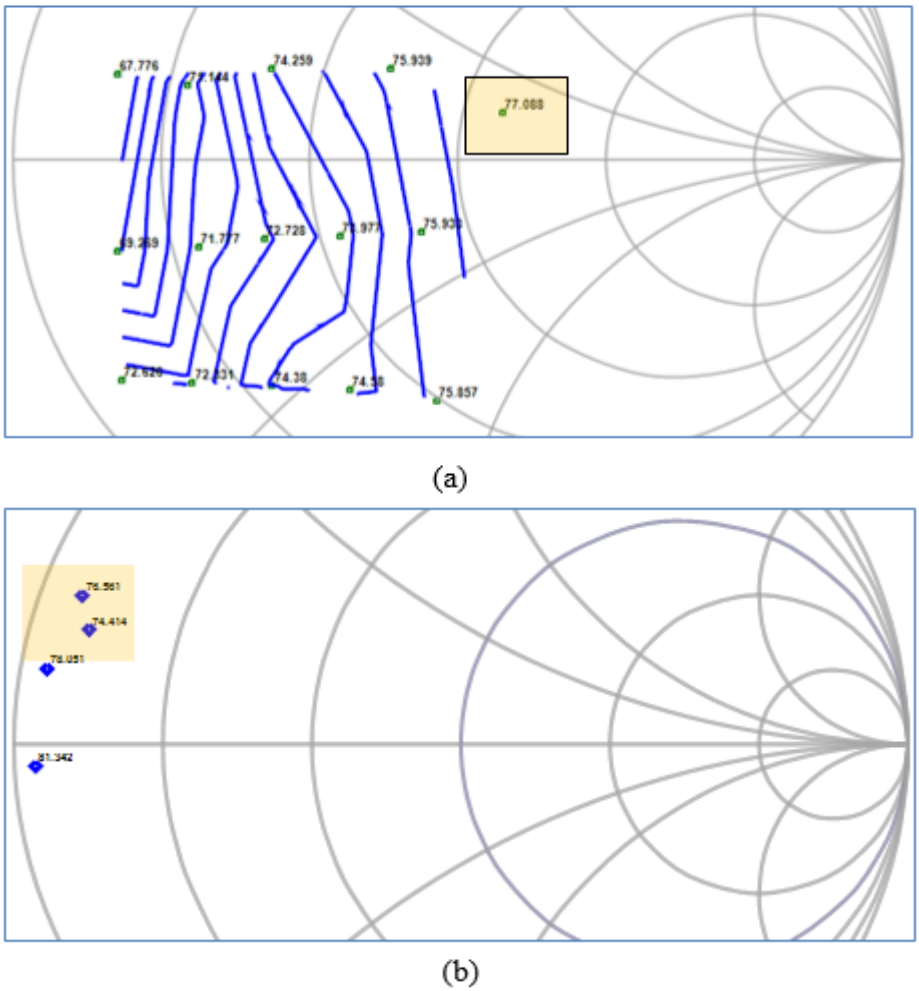

Figure 3.20: Measured load points for 10W LDMOS power transistor at 900MHz: (a) 2nd harmonic drain efficiency contours (b) 3rd harmonic drain efficiency spot measurements.

After locating the optimum impedance points of the fundamental, 2nd and 3rd harmonics, another fundamental load sweep was conducted around the optimum fundamental area of the smith chart. This is necessary because, after adding the harmonic contents to the fundamental waveforms, the fundamental optimum impedance of the transistor is changed. Therefore, the dynamic loadline needs a slight tuning to fit in over its optimal position in the nonlinear current curves. The contours generated with the fundamental load points clearly show a further 6% increment to the

drain efficiency of the transistor. The new optimum fundamental load now is 48Ω and the efficiency is 83% at 40dBm output power

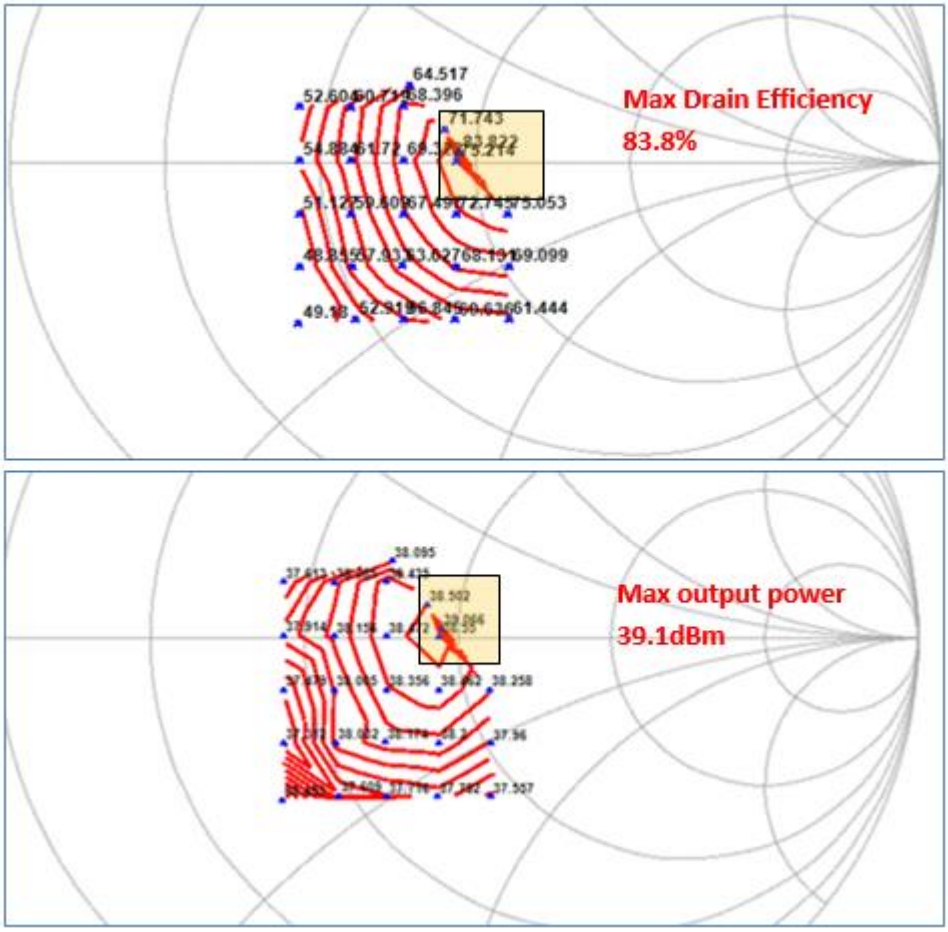

Figure 3.21: Tuned optimum load points for 10W LDMOS power transistor at 900MHz.

3.5.2 Gate Voltage Optimization

Gate voltage is a key parameter in defining the transistor mode of operation. For example, in F^{-1} mode of operation the device is biased at its class-A point to allow a squaring of the current waveform and maximum current swing for higher output power. Having a direct impact on the performance of a transistor, it is also very important to determine the optimum gate bias voltage. After terminating the transistor to its optimum loads, gate voltage sweep was conducted from its pinch off point (Vgs=1.5V) to near saturation level (Vgs=4V). Measured results showed that within the deep Class-AB biasing region, the device exhibits a uniform performance but as we move towards Class-AB, the performance degrades significantly. To investigate this phenomenon, the transistor was biased within this gate voltage range and

fundamental load was varied that immediately resulted in the device damage due to a huge gate leakage current. Different parameters such as fundamental load impedance, input power and drain voltage were varied one by one to determine the root cause but any apparent reason for this strange behaviour of the transistor couldn't be determined. However, such phenomenon have been reported previously in [10]. It was believed that, the sub optimal behaviour of the transistor within this range could be due to the instability and oscillations at the gate terminal. Therefore, this input voltage was avoided and the transistor characterization was finalized.

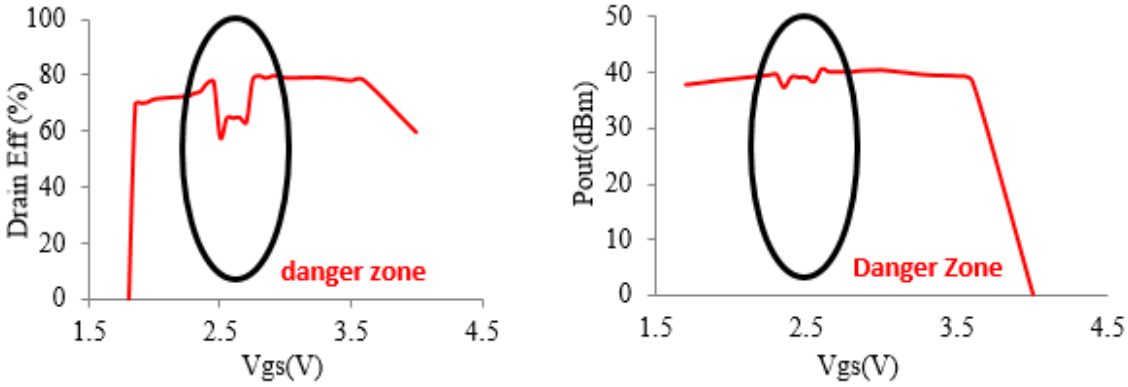

Figure 3.22: Measured drain efficiency and output power as function of gate voltage of 10W LDMOS transistor at 900MHz.

To avoid further damaging of the devices and maintain the already identified improved performance, the gate voltage was selected from within deep class-AB range and the transistor was driven upto its 1dB compression (26dBm). The final output voltage and current waveforms were obtained resulting in 83% drain efficiency at 40dBm output power. The comparison between mesaured and simulated waveforms showed an excellent agreement.

V_{gs}(V)		V_{ds}(V)		RF_{input} (dBm)	
2.2		25		26	
Γ_{Fo}		Γ_{2Fo}		Γ_{3Fo}	
Intrinsic	Package	Intrinsic	Package	Intrinsic	Package
0.1<116	0.693<139.76	0.1<146	0.853<157.7	0.95<-177	0.493<-93
MAG(dB)		Drain-Efficiency (%)		RF-output(dBm)	
16		>80%		40	

Table 3.4: Finally Optimized performance parameters of 10W LDMOS PA in inverse-F mode of operation at 900MHZ

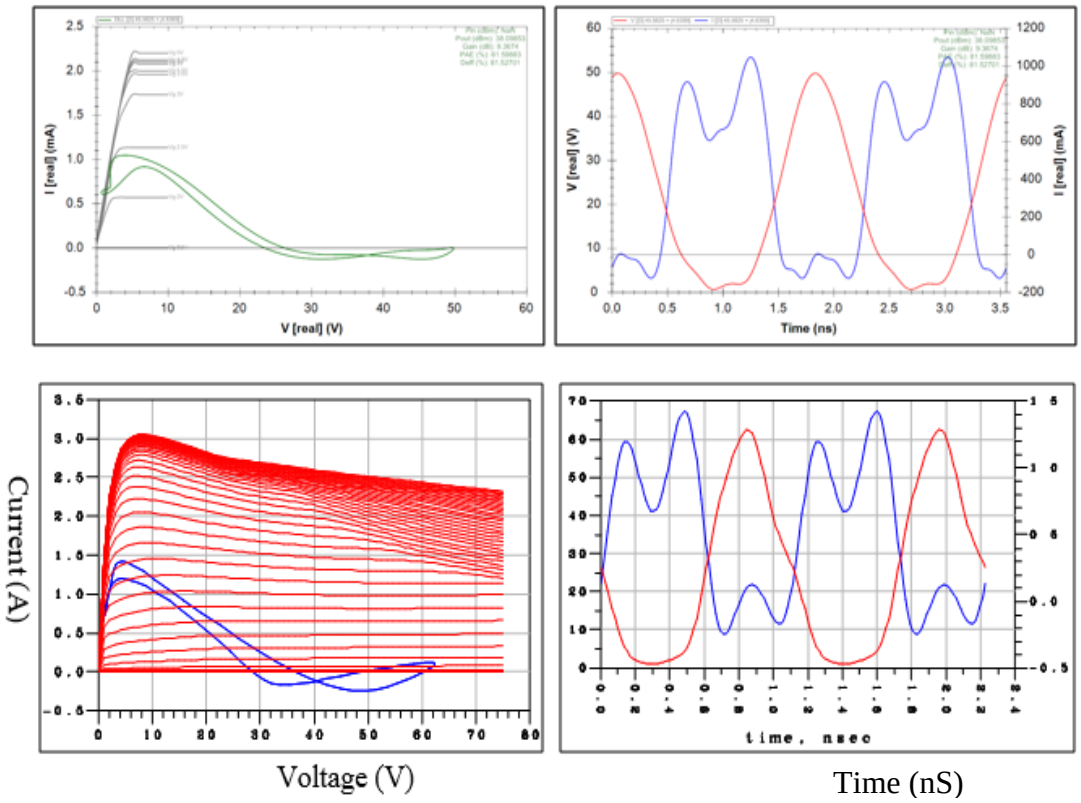

Figure 3.23: 10W-LDMOS inverse-F analsysis at 900MHz: (top) measured (bottom) simulated.

3.6 Summary

Before practically designing any power amplifier, it is very important to select a right transistor technology and to carefully identify its optimal and safe design parameters. Silicon LDMOS power transistors, because of their shorter gate length are ideal to work at microwave frequenies. Also their high voltage handling capability makes them suitable for microwave heating applications. The LDMOS power transistor characterized in this chapter is a 10W Si-LDMOS field effect transistor designed to work at DC-2.7 GHz.

Unlike most of the microwave components, transistors are non-coaxial devices which require dedicated test fixtures for their interaction with RF systems. As a starting point, a test fixture was designed using two 50Ω microstrip lines printed on aluminium backed RTduroid 5880 substrate. Transistor characterization needs complete access to its input and output flanges by negating the pair of test fixture transmission lines which is only possible through TRL calibration process. A step by step procedure for designing a TRL-kit was prescribed and verified in the first half of this chapter.

The second half of the chapter began with the transistor DC analysis in which the measured DC behaviour of the transistor was compared with its equivalent software package model. After making the DC analysis, the frequency sensitive package parasitic and their influence on the output waveforms was briefly highlighted. De-embedding and its benefits for high efficiency mode characterization of the transistor were also briefly discussed.

Later, half way through this chapter, the loadpull measurement system, its working principle and its constituent components were explained in detail.

The last part of this chapter started with the concept of waveform engineering and its procedural details for obtaining high efficiency F^{-1} PA mode of operation. Minor details of waveform engineering were furnished with the experimental demonstrations in details. To gain a deeper knowledge of the transistor's non-linear behaviour, characterization process was conducted at 900MHz where the identification of fundamental, 2nd and 3rd harmonic optimum loads and their impact on the performance of the transistor were shown experimentally. Similarly, the gate voltage and its influence on the amplifier performance and reliability were also probed during the waveform engineering process.

In conclusion, this chapter gives a deeper insight of the 10W Si-LDMOS solid state power amplifier. Higher efficiency (>80%), 10W output power , more than 15dB gain and lower price (33$/Piece) claims its utilization as an efficient microwave source in microwave heating applications which will be presented in the next chapter.

References

[1] John L.B.Walker, *Hand book of RF and Microwave Power Amplifiers*, Cambridge University Press 2012.

[2] Valentin Niculae and Umberto Pisani, " TFU Calibration Kit for characterizing waveguide embedded microstrip circuits at millimeter-wave frequencies", *IEEE Instrumentation and Measurement Technology Conference*, Anchorage,AK,USA, 21-23 May 2002.

[3] California Eastern Laboratories, *Designing and characterizing TRL fixture calibration standards for device modeling*, AN1041 Application Note.

[4] Wong,K.Pollard,R.Shoulders,et al, "Using a mismatch transmission line to verify accuracy of a high performance noise figure measurement system", *ARFTG Conference*, June 2007, pp.1-5.

[5] Amir Sheikh, *High Power Waveform Engineering, PhD Thesis*, Schoolf of Engineering, Cardiff Uinversity UK, June 2010.

[6] P.H.Aen, J.A.Pla, Blanis, "Modeling techniques suitable for CAD-based design of internal matching networks for high-power RF/Microwave transistors", *IEEE MTT*., vol.54,no.7, , July 2006, pp.3052-3059.

[7] R.Gaddi,P.J.Tasker,J.A.Pla, "Direct extraction of LDMOS small signal parameters from off-state measurements", *IET Electronic Letters*,vol.36, Nov.2000, pp.1964-1966.

[8] Paul J.Tasker, "Practical Waveform Engineering", *IEEE Microwave Magazine*, pp.1527-3342, December 2009.

[9] S.Cripps, *RF Power Amplifiers for Wireless Communications*, 2nd Edn, Norwood, MA: Artech House, 2006.

[10] Peter H.Aaen, Jaime A.Pla, Jhon Wood, *Modeling and Characterization of RF and Microwave Power FETs*, 1st ed. Cambridge University Press 2007.

Chapter.4 INTEGRATED INVERSE-F POWER AMPLIFIER FOR MICROWAVE HEATING

4.1 Introduction

It is a fact that biomedical research centers at both industrial and academic levels are becoming aware of the benefits of enhancing current diagnostic healthcare equipment with the microwave exposure [1]. As highlighted in the literature review chapter, compact, portable and field deployable diagnistic solutions will be valuable additions to modern age medical technology where there is a pressing need to operate the medical equipment at point-of-care, and a patients bedside for example [2]. For the application targeted for this research, the rapid and accurate detection of dangerous pathogens including *C-difficile* and anthrax, the sample is precisely exposed to the high E-field causing DNA release and allowing subsequent detection. Using this approach, detection is possible within a few minutes [1], and compared to at least 24 hours for current detection solutions, this represents a transformational step forward. The accuracy of the medical equipment is of prime importance because any degree of inaccuracy can ultimately be harmful to the patient. Ease of use and the cost effectiveness are the other important parameters of efficient biomedical equipment that define the overall efficiency of the system under operation.

The traditional diagnostic methods contain physically large structures which due to their larger size cannot be placed within medical wards for continuous sample monitoring and analysis. Such larger systems therefore are confined to the separate laboratories where the samples are examined and then the diagnosis results are returned to the hospitals. Normal sample analysis and response time in UK hospitals vary from 2 to 7 days depending upon the type of analysis.

In this chapter the solid state microwave heating apparatus suitable for biomedical applications has been introduced and the limitations (outlined in literature review) in the conventional microwave heating systems have been addressed. The design process has been followed by aiming to improve the existing microwave heating systems to efficient, portable and compact microwave heating systems. In this novel approach the purpose built TE_{011} mode rectangular cavity coupled using a stepper motor controlled

loop antenna has been used to concentrate E-Field at the middle of the cavity where the sample is exposed.

In this approach, the need for transitional 50Ω interconnect has been removed by directly presenting the cavity resonator to the RF source (LDMOS Transistor) and the physical size of the heating structure has been reduced significantly. In this design method, the natural impedance environment of the cavity resonator has been exploited and used to present high-efficiency loads directly to 10W-LDMOS power transistor for F^{-1} wave-shaping at 2.45GHz.

The achievable cavity impedances have been emulated using the waveform engineering and harmonic load-pull measurement system capabilities, and presented at the current generator plane of 10W-LDMOS power transistor. This has been achieved by de-embedding the package parasitics and using only simple series microstrip lines for the necessary tranformations. Measurement results have shown 69% drain efficiency and more than 40dBm output power whereas, with 7dB return loss recorded in this arrangement. Finally, the measured and simulated results have been compared and found in excellent agreement.

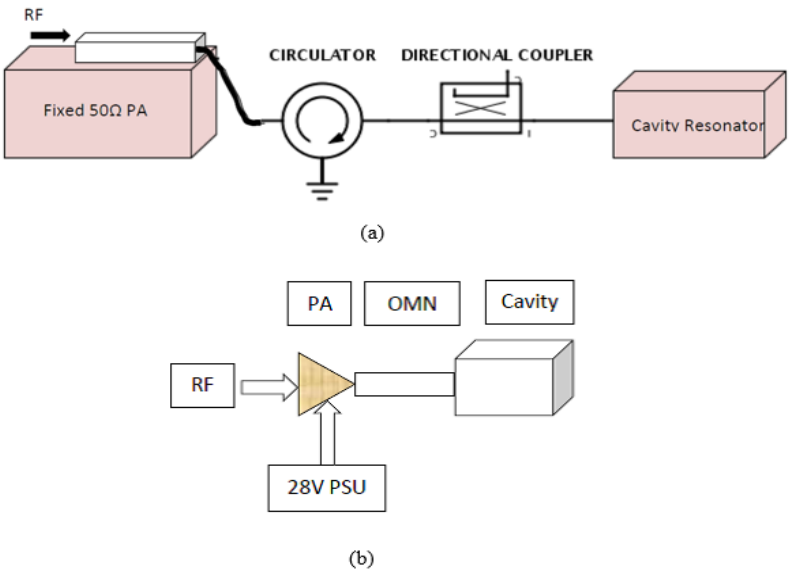

Figure 4.1: Block diagram: Solid-state microwave heating system (a) Conventional 50Ω approach (b)Proposed direct integration approach

4.2 Design Process

In many RF applications, power amplifiers play a significant role in defining the overall system efficiency. Efficiency of PAs can be increased by utilizing the

harmonic content in the current waveform, generating required voltage waveforms through synthesized harmonic matching networks. Such harmonic control networks are universal and effectively control the harmonic impedance according to the design requirements. However, due to extra bulk of the series and shunt stubs, these control networks require extra board space and matching complexity. Also, these harmonic matching networks contribute significant loss to the RF output power thus resulting in the reduced efficiency. A unique solution to these problems has been presented by passively tuning the cavity resonator, and using it as a direct load to the transistor. The fundamental, 2nd and 3rd harmonic impedances selected from the cavity impedance design space together with simple series delay lines have been transferred to the transistor's intrinsic plane. The block diagram of the proposed solid-state microwave heating apparatus depicted in Fig.4.1 clearly shows the physical size reduction compared to the conventional approach. To properly understand the importance of each design part of the integrated structure, the process has been simplified in discrete steps where each step expresses the deeper analysis of each integral part supported by the findings, mathematical analysis, simulations and measurements. The design process has been summarized in following five steps:

- Characterize the transistor using a state-of-the-art time-domain waveform based load-pull measurement system and obtain its optimum performance points both at package and intrinsic plane at 2.45GHz (cavity design frequency).
- Characterize the cavity by systematically rotating the motor controlled inductive loop antenna over a cycle of 360° in discrete steps and for each step record the cavity S-parameters, while critically coupled into a representative sample.
- Design as simple as possible harmonic transformation network between transistor and cavity to transfer the already identified cavity fundamental and harmonic optimum load points to the transistor optimum points (obtained through loadpull measurements).
- Perform the non-linear and EM simulations to estimate the overall performance of the integrated structure offline in CAD environment.

- Fabricate and measure the complete setup and compare measurement results with simulation.

4.3 Transistor Characterization (at 2.45GHz)

The amount of DC power consumed by an amplifier during RF power generation process partly defines its performance, with the conversion from DC to RF power is always being less than 100%. High efficiency modes of PA can be adopted to enhance the drain efficiency and output power to achieve better amplifier performance. Among high efficiency PA modes, F^{-1} mode carries a leading role in which the 2nd harmonic is terminated with very high impedance and 3rd harmonic is short circuited. In this mode, the amplitude and shape of the output voltage waveform is effected by the contribution of the 2nd harmonic voltage component and current waveform is squared by 3rd harmonic current component and the boundary conditions. Thus the PA design requires logical utilization of harmonic components to shape the fundamental voltage and current waveforms according to the required class of operation.

As described earlier in detail, transistor characterization is the ideal initial step before any PA because this allows an in-depth understanding of the DUT both at DC and RF levels necessary for meeting the design goals. Although the literature provided with the transistor model allows a deeper insight of its operation, both at DC and RF levels, it is still recommended to verify the transistors limiting operation through simulation and measurements. As the microwave heating apparatus is required to operate at ISM (Industrial Scientific and Medical) frequency band, therefore this section of the thesis explores the transistor RF behavior at 2.45GHz.

At low frequencies the parasitic elements embedded inside the transistor package are less reactive and their influence on the output waveforms is minimal. However, with the increase in frequency, these parasitic elements become more reactive and disrupt both output voltage and current waveforms. The first and the most influential reactive element seen by the transistor current generator is the drain-source capacitor (C_{DS}) which largely disrupts the output current waveform. Similarly the bond wires attached with the built-in MOS capacitors and the transistor flanges act like inductors and disrupt the voltage waveform. Therefore, the waveform engineering at high frequencies becomes a real challenge and it becomes quite difficult to obtain the intended performance for a specific mode of amplifier. For example, at S-band, all the

higher order harmonic current components get short circuited by the large C_{DS} (≈3.99pF) value in Si-LDMOS thus only 2nd and limited amounts of 3rd harmonics make it through the device to appear at the device's output terminal, resulting in difficult waveform engineering. Another, related factor is the lower cut off frequency of the Si-material (≈7.5GHz) such that all the higher order harmonics above certain limiting frequency are naturally attenuated [3]. Thus the contribution of the 3rd harmonic for current wave shaping is negligible. In the F^{-1} mode, the second harmonic is the main component of interest, so this is in fact why this mode is of interest in this application. Similarly, the sampling scope DSA8200 used for transistor characterization in this experiment has cut-off frequency 12.25GHz which equals nearly 5 Harmonics with fundamental 2.45GHz. Therefore this frequency limiting factor also makes the waveform engineering a difficult task. To achieve high efficiency at 2.45GHz while using Si-LDMOS as microwave energy source, F^{-1} mode of operation is a right choice because of low power of 3rd harmonic. This fact will be further explored by the harmonic phase sweep plot in the coming part.

As shown earlier in chapter 3, the software package model of 10W-LDMOS power transistor has great resemblance with the actual transistor and the well calibrated measurement setup resembles greatly with the ideally calibrated ADS environmen thus the simulations can reliably be setup as a basis for real performance estimation of the device. Therefore, the measurements were followed by conducting nonlinear simulations and the final performance analysis was made at 2.45GHz.

Test-fixture assisted transistors contain three reference planes,

1. Calibration Plane (50Ω coaxial environnement)
2. Package Plane (contains the extrinsic and intrinsic parasitic)
3. Intrinsic Plane (contains current generator I_{dS} and the C_{DS}).

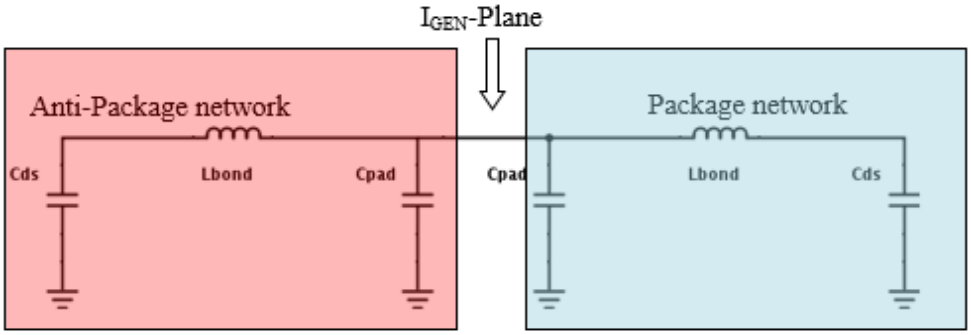

Figure 4.2: Technique for accessing the I_{GEN}-Plane of packaged transistor.

The dedicated de-embedding network provided by NXP, already verified in chapter-3 was applied in series with the transistor package network in the actual measurement system to get access to the current generator of the transistor. The waveforms appearing at this plane are free from any influence of the reactive elements and can be related directly to the boundary conditions (knee, pinch-off, breakdown and saturation current) identified on the transistors DC_IV measurement plane.

Dedicated software (Mesuro) used in automated active loadpull measurement setup supports the run time on screen analysis of the waveforms appearing as a result of the presented harmonic load at both the current generator and the package planes of the transistor. The process was started with the gate voltage sweeps.

4.3.1 Gate Voltage Characterization

Gate voltage sweep is the starting point to engineer the high efficiency modes because in these modes the harmonic components play a vital role in output voltage and current wave shaping. Transistor is voltage controlled current device, so the harmonic current components produced at the drain terminal largely depend upon the gate bias voltage in combination with the drive level. At some specific voltage levels, the even harmonic are dominant and at some other voltage levels the odd harmonics are more obvious. This is of course due to the changing conduction angle of the device operation. Therefore, before shaping the F^{-1} waveforms it is necessary to know the gate voltage levels and their impacts on the harmonic current components.

To start with, the device was driven up to 1dB compression point (≈26dBm) while fundamental frequency component was presented with a real optimum load and the harmonics were short circuited at the current generator plane of the transistor. The gate voltage sweeps were conducted from turn-on point (V_g≈2V) to saturation point

(V_g≈4V) and the resulting output currents were recorded as shown in Fig.4.3. It is evident that the 2nd harmonic carries the majority of the current compared to the 3rd harmonic because of the large C_{DS} value that short circuits the higher harmonics. To shape the output current waveform for inverse-F mode of operation, it is very important to identify the gate voltage and drive level resulting in a squaring of the current waveform where the 3rd harmonic current is maximum. It can be seen that the 3rd harmonic carries a peak current of nearly 100mA at 2.9V. This current is 3.7% of the maximum available current from the transistor and is sufficient to contribute to properly shape the current waveform. The 2nd harmonic carries about peak 550mA which is equal to the 20.37% of the peak obtainable current from the transistor. Therefore the influence of 2nd harmonic on the output power and the efficiency of the transistor is higher. From the Fig.4.3 it is clear that for Vgs 2.8V to 3.4V (which is the class-A biasing range of the transistor) the 2nd harmonic possesses the lower amplitude whilst the 3rd harmonic current being increased. To progress with, 2.9V gate voltage was adopted and used for further waveform engineering analysis.

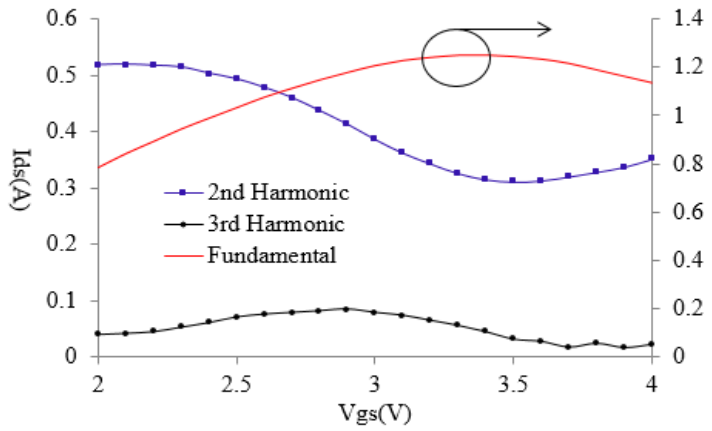

Figure 4.3: Measured harmonic currents of 10W LDMOS PA as a result of gate voltage sweep at 2.45GHz.

4.3.2 Fundamental Load characterization

Systematic loadpull process is an important step in power amplifier designs because it helps optimizing the output power, gain and efficiency by dynamically locating the optimum fundamental and harmonic loads. In an active harmonic loadpull process, initially the 2nd and 3rd harmonic loads were terminated to 50Ω and the transistor was driven by a conastant input power CW signal. A high density mesh grid of fundamental

points was spread over the Smith chart to figure out the fundamental optimum impedance design space. Active harmonic loadpull is an iterative process which automatically targets and narrows down the high performance impedance area on the smith chart (as shown earlier in chapter.3). After first iteration, the high performance area was identified and another grid of fundamental load points was spread in that specific area. Again, the remotely controled automated loadpull process was repeated and the further optimized high performance area was located. The process was iterated several times and finally the high performance fundamental load points were discovered as shown in Fig.4.4.

After locating the optimum fundamental impedance points the same process was iterated to locate the optimum 2nd harmonic impedance.

The process was started by sweeping the 2nd harmonic load around the smith chart whilst the fundamental load was set to its optimum point and 3rd harmonic to 50Ω. The process was repeated several times until the point at which the amplified half rectified voltage waveform was obeserved on the remotely attached computer. it was also observed that at that point the transistor wass delivering high power and drain efficiency as it is obvious through the grid points.

Finally, the fundamental and 2nd harmonic loads were fixed to their optimum locations on the smith chart and the 3rd harmonic load was swept around edges of the smith chart. The same process was iterated until the output current waveform was squared and the transistor was capable of showing highest drain efficiency (≈65%) and the (≈43dBm) output power and above 12dB gain. It is obvious in Fig.4.4 that the optimum fundamental load point exist on the real axis which shows the correct deembedding of the parasitic network . To further optimize the fundamental load resistance, the harmonic loads were fixed to their optimum points and a real load sweep was conducted to see the impact of the resistive load on the drain efficiency and output power of the transistor as shown in Fig.4.5.

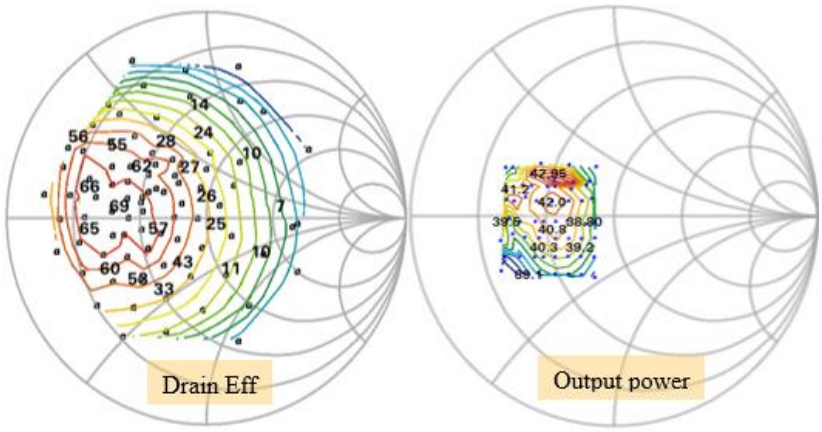

Figure 4.4: Measured high performance impedances obtained at the current generator plane of the transistor BLF6G27-10G LDMOS transistor at 2.45GHz.

$$R_{opt} = \frac{2*(V_{dc} - V_{Knee})}{I_{dc}} \tag{4.1}$$

In this case R_{opt}= 17 Ω, V_{dc}= 25 V, V_{knee}=3.5 V, I_{dc}= 2.5 A

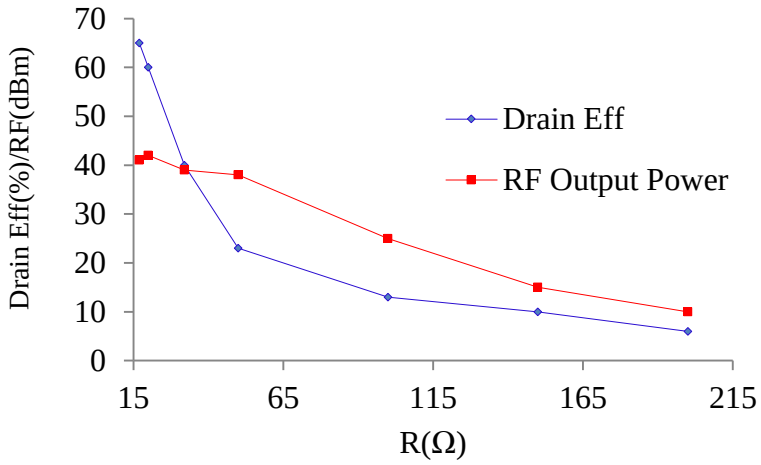

Figure 4.5: Fundamental load resistance swept at IGEN-Plane of 10W-LDMOS power transistor.

Figure 4.5 shows that the optimum real load resistance for maximum power lies near to 17Ω which is the theoratical optimum resistance of this transistor according to equation (4.1).

4.3.3 Harmonic Load Optimization

As seen in the above section, 2nd harmonic carries nearly 20% of the maximum transistor current whereas 3rd contains only 3.7% of the maximum obtainable current from the transistor. However it is necessary to see the impact of both the 2nd and 3rd harmonics on the output waveforms of the transistor. To start with, the fundamental and 3rd harmonic loads were fixed to their optimum points and the phase of 2nd harmonic load was swept around outside the smith chart to see its impact on the drain efficiency. It was observed that the 2nd harmonic is a strong function of transistor performance because the drain efficiency increased from 35% to 66% with the phase variation of the 2nd harmonic load. This means that the amplitude of the fundamental voltage waveform can be increased by adding the in-phase 2nd harmonic voltage component to increase the efficiency and output power.

Similarly, the fundamental and 2nd harmonic loads were fixed to their optimum positions and the phase of the 3rd harmonic load was varied with fixed magnitude set to one. It was observed that the 3rd harmonic contributes only 1% to the drain efficiency of the transistor as shown in Fig.4.6. The reason for lower 3rd harmonic contribution is the large drain to source capacitance in LDMOS power transistor which presents a low, reflective impedance to the higher harmonic contents. The power required to pull the 3rd harmonic load was found to be nearly 70W while the power amplifiers available in the lab were narrowband and capable of delivering maximum 25W power at 7.35GHz.

From this analysis, it is easy to conclude that F^{-1} mode of operation (at 2.45GHz) is the right choice for 10W-LDMOS power transistor because of the natural 3rd harmonic low impedance due to larger C_{DS} and lower cut-off frequency of this device technology. Thus the 2nd harmonic is the main contributor to the amplifier's performance, which suits class-F^{-1} of course.

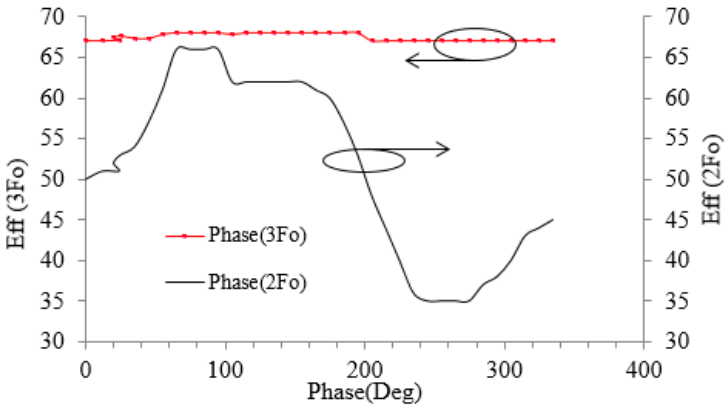

Figure 4.6: Measured harmonic load impact on the drain efficiency of 10W LDMOS transistor at 2.45GHz.

4.3.4 Input Power Optimization

The input RF signal injected to the input terminal of the transistor, generates the output current and this, in combination with the harmonic impedance environment, the voltage waveforms. When driving into a proper load, the higher level of the input RF signal generally leads to the higher voltage and current waveform swing to further efficiency and power enhancement. In high-efficiency modes, it is important to understand how the input drive level impacts on the harmonic currents, because these harmonic current components are key in achieving higher efficiency modes, by shaping the waveforms. An input power sweep was conducted driving the transistor upto its 3dB compression point and the optimum drive levels were discovered.

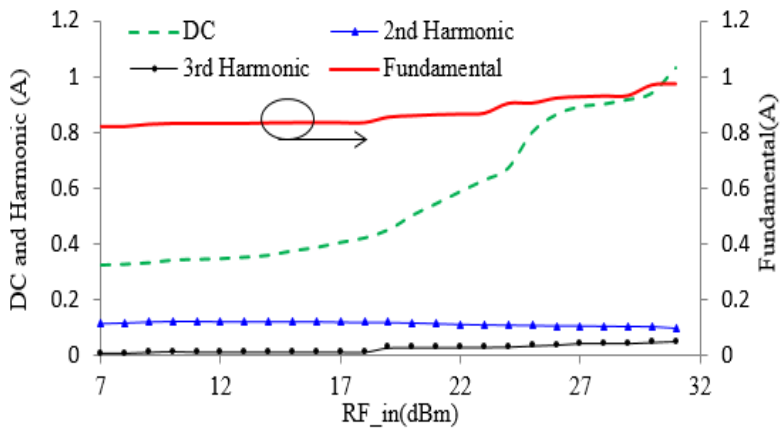

Figure 4.7: Output harmonic currents(peak) as function of input drive

Fig.4.7 shows that the DC and fundamental components grow at a constant rate with the input drive where the harmonic contents remain almost at their fixed levels. This shows the dominating effect of C_{DS} at high frequency currents which is more prominent in 3rd harmonic. Therefore, it is very important to properly de-embed the intrinsic and extrinsic parasitics because small part of the unaccounted C_{DS} can make a huge difference to all the harmonic currents by short circuiting them [4]. Thus the RF drive at which the fundamental, 3rd harmonic currents are maximum and 2nd is minimum, can be chosen for the inverse class of operation.

In case of F^{-1} mode of operation it is customary to biase the transistor at its class-A point and keep the load value up-to its optimum level ideally where it should hit the knee bend region where the maximum current can be obtained from the transistor. Finally the transistor under its optimum conditions was driven by the RF CW signal sweep and drain efficiency, maximum available gain and output power were measured. the plots are shown in Fig.4.8.

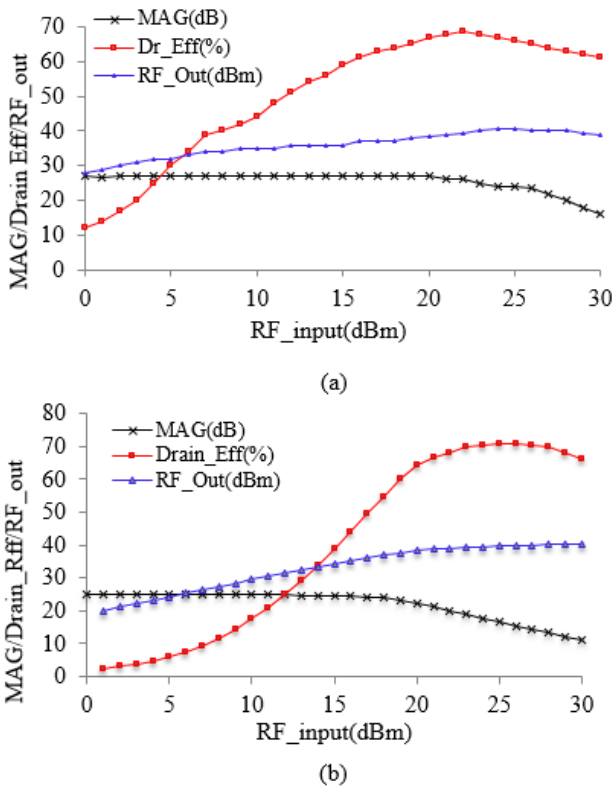

Figure 4.8: BLF6G27-10G 10W-LDMOS power transistor performance at 2.45GHz- (a) Measured, (b) Simulated

The finally engineered F^{-1} current and voltage waveforms were obtained at the transistor intrinsic plane by employing the de-embedding network as shown in the Fig.4.9. The final waveforms can be tuned further if we have access to the more harmonics, in that case it becomes easier to add the mutiples of even and odd harmonics to shape the fundamental voltage and current waveforms and thus the performance can be further improved.

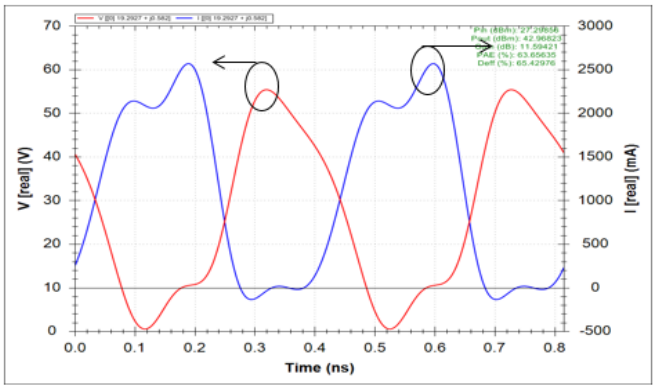

(a)

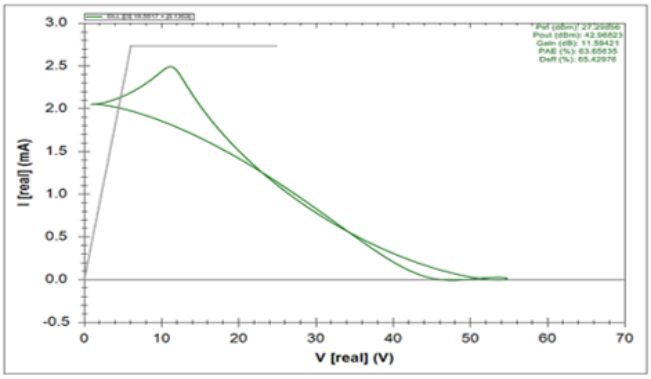

(b)

Figure 4.9: (a) Measured intrinsic inverse-F waveforms (b) load line at 2450MHz

Reference Plane	$Z_{Fo}\,\Omega$	$Z_{2Fo}\,\Omega$	$Z_{3Fo}\,\Omega$
Package Plane	8+j0.65	3+j*30	2-j*15
Current Genenerator Plane	20+j*0.55	0+j*42	0-j*5

Table 4.1: Optimum Impedance Points at Package and I_{GEN}-Plane

Pinput (dBm)	MAG (dB)	Drain-Eff (%)	RF Output dBm	Vgs (V)	Vds (V)	Freq (GHz)
27	20	67	41.5	2.1	28	2.45

Table 4.2: Transistor Performance at Optimum Points

The RF power generated by the 10W LDMOS power transistor was needed for microwave heating applications. Therefore a high efficiency, compact and flexible arrangement is required to constitute the solid-state microwave heating arrangement. Thus TE_{011} mode rectangular cavity available in the lab was chosen for this experiment.

4.4 Rectangular Cavity Resonator

Single mode rectangular waveguide cavities are narrow band resonating structures capable of handling high power and developing very narrow band resonances. These cavities are purpose built and designed for specific applications. Rectangular microwave cavities are in fact short circuited rectangular waveguides and their cut-off frequency depends upon their length, width and height according to the mode of operation. Similar to rectangular waveguides, these microwave cavities also either work in transverse electric (TE) or transverse magnetic (TM) modes and the field components exist within three dimensional space. The microwave energy is coupled into the cavity using structures such as aperture coupling, loop coupling, monopole antenna coupling etc. The field components of the electromagnetic energy are stored in the cavity where the power is dissipated in the cavity walls (due to metal boundary conditions) and/or the filling inside the cavity. Rectangular cavity resonators resonate depending upon the boundary conditions and so the frequency of resonance can be calculated using [5]

$$f_r = \frac{c}{2\times\pi\sqrt{\mu_r\varepsilon_r}}\sqrt{\left(\frac{m\pi}{a}\right)^2+\left(\frac{n\pi}{b}\right)^2+\left(\frac{l\pi}{d}\right)^2} \tag{4.2}$$

Where *a, b, d* are the width, height and length of the cavity respectively. The indices *m,n,l* refer to the number of standing wave variations along *x,y,z* directions

respectively. Thus For TE_{011} mode, the resonant frequency depends upon length, height and the dielectric material filling the cavity.

To begin the cavity analysis, the empty, air filled cavity was critically coupled through inductive loop adjustment and the S-parameter data was captured through calibrated VNA during first measurement. However, in the second measurement, the cavity was loaded with 100µL water-filled Eppindorph tubes and the S-parameter data of this 'loaded' cavity was recorded without inductive loop adjustment. The reason for this step was to observe the impact of 100µL water on the resonant properties of the empty rectangular cavity. Water, due to its high dielectric permittivity, has a significant affect on the resonance properties of the cavity, thus the resonant frequency of the air filled cavity drops from 2.45GHz to 2.4GHz as shown in Fig.4.10.

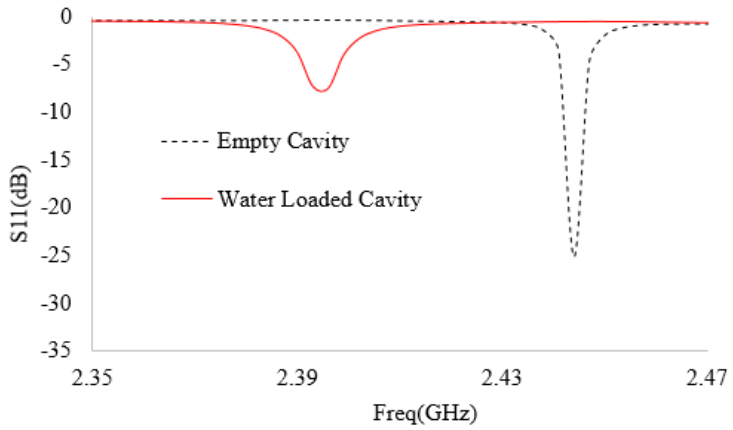

Figure 4.10: Measured reflection loss of the TE_{011} mode rectangular cavity resonator

However, to allow critical coupling of the cavity and to achieve the same as that at 2.45GHz, it is necessary to adjust the angular position of the internal coupling loop. The detailed systematic analysis of the loop adjustment will be explained later in this chapter.

Field distribution is a very impotant parameter in a single mode rectangular cavity resonator because it gives a deeper insight of how a single-mode rectangular cavity can be more efficient than commercial multimode microwave oven in microwave heating. The rectangular cavity with following dimensions was designed to resonate at 2.45GHz (a=5cm, b=7.3cm and d=13cm) and the 3-D model was simulated in COMSOL multiphysics to observe the E-field analysis.

To analyze the electromagnetic field distribution inside the air filled cavity, the cavity was excited by feeding-through a coaxial cable and a small, short-circuited metallic loop was used to couple the electromagnetic energy into the H-field concentrated at the centre of the side of the cavity. A high density meshing was conducted to best solve the electromagnetic field components and the microwave radiator was simulated at 2.45GHz. Simulated results depicted in Fig.4.11 clearly show a focused E-Field of the magnetically coupled resonant cavity resonator. Therefore, any sample inserted into the center of the cavity will experience maximum focused electric field, which is very important in microwave heating because the E-field is directly proportional to the power conversion into heat per unit volume [6].

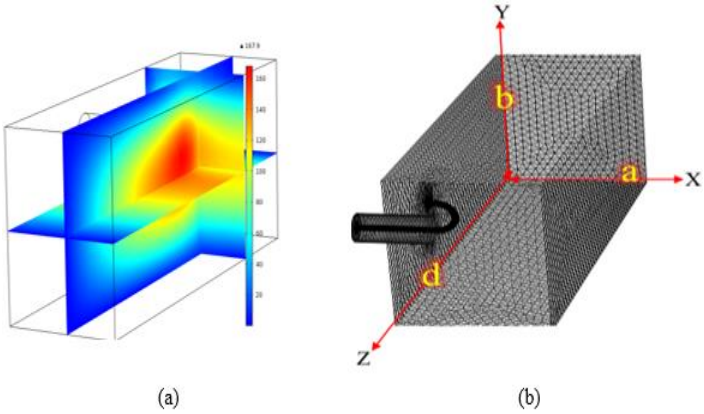

Figure 4.11: (a) E-Field distribution (V/m) inside empty loop coupled TE_{011} mode rectangular cavity at 2.55GHz (side view) (b) Extra-fine meshing of the loop coupled cavity (perspective view)

$$P_V = 2\pi \times f \times \varepsilon_o \varepsilon'' \times E^2 \tag{4.3}$$

$$P_V = 5.56 \times 10^{-11} \times f \times \varepsilon'' \times E^2 \tag{4.4}$$

Where,

P_V= power converted to heat per unit volume

F= operating frequency

ε'' = dielectric loss factor

E= Electric Field Strength

From equation (4.4) it is evident that the E-Field strength has direct relation with heating. The comparison of the field distribution inside the single mode cavity and the

commercial size microwave oven in discussed in the literature review chapter readily provides a quick analysis for the energy efficient load in microwave heating apparatus. Therefore, in our first experiment, we have used the TE_{011} mode rectangular cavity with short circuited magnetic loop coupling for the microwave heating experiment.

4.4.1 Loop-Coupled Rectangular Cavity (TE_{011}) Used in The Design

The one port rectangular cavity used in this experiment was previously designed by a group of students at Cardiff University [7]. The rectangular cavity operates in its TE_{011} mode which is its dominant mode. TE supported cavities have lower attenuation, narrow bandwidth and can accommodate high power. The narrow band operation of the single mode rectangular cavity is due to its single mode resonant nature which allows a focused area of concentrated E-field for intense microwave exposure. For first compact solid state microwave heating experiment, this cavity was used to hold a 100μL water sample.

As already observed in Fig.4.11, Electromagnetic energy in an air filled rectangular cavity can be concentrated in the center of the single mode rectangular cavity resonator using short circuited loop coupling antenna. However, different coupling structures can be launched inside the cavity to allow maximum transfer of RF energy. Short circuited circular loop coupling structure is the well adopted method of coupling the microwave energy in the center of the cavity resonator, where the intenisty of the microwave energy depends upon the positioning of the inductive loop. The maximum power transfers when, ideally the loop is perpendicular to the magnetic-Field and parallel to E-field, because the magnetic lines of force passing through the loop area are maximum and the Q factor of the cavity is highest. The point at which the cavity has the highest Q factor, is called critical coupling point of the cavity and the maximum power transfer occures at this point. At critical coupling, the cavity acts like a resistor and the load reflection point stays at 50Ω.

The dynamic coupling mechanism consisted of the inductive loop antenna attached to the movable pulley, a rubber belt and a stepper motor which was used to control the loop orientation. The coupling strength was tracked electronically using Lab-View and the adaptive coupling was applied to keep the cavity critically coupled under all loading conditions. The low DC supply voltage (12V) stepper motor controlled the

orientation of the coupling antenna within the one port rectangular cavity depicted in Fig.4.12 which was purposely designed for microfluidic heating using adaptive coupling mechnism.

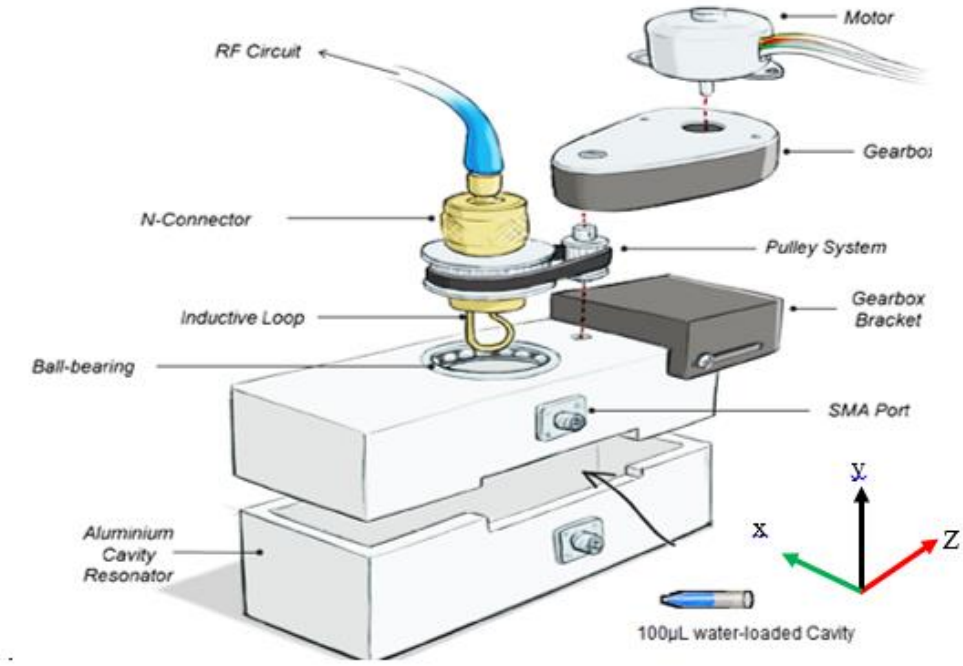

Figure 4.12: Motor controlled loop coupled cavity used in the design [7]

In TE mode, rectangular waveguide cavity the microwave energy flows along its length (Z-axis) so the E-Field being perpendicular to the direction of motion concentrates in the middle of the cavity. Therefore, a test sample inserted in the middle of the cavity experiences maximum electric field intensity and can quickly get hot if exposed to continuous microwave.

Initially, within COMSOL multiphysics simulation environment, the cavity was loaded with 100µL water (contained in an Eppendorf tube), and the E-Field exposure in the water carrying tube was observed. The harmonic propagation method was adopted in COMSOL for an accurate field distribution analysis whilst extremely fine mesh grid was chosen to obtain the fine tuned results. The design frequency range was selected from 2.3GHz to 2.5GHz with 10MHz frequency resolution to capture the new resonant frequency of the water filled cavity. Resonance frequency of a resonator is a strong function of the dielectric filling the cavity. Therefore, with the insertion of a dielectric material the resonant frequency of the cavity decreases. However, with a slight loop adjustment the cavity can be critically coupled again at new frequency.

Therefore, the magnetic loop was adjusted using a built in 'rotate' function and the E-field was concentrated back to 2.45GHz as shown in Fig.4.13.

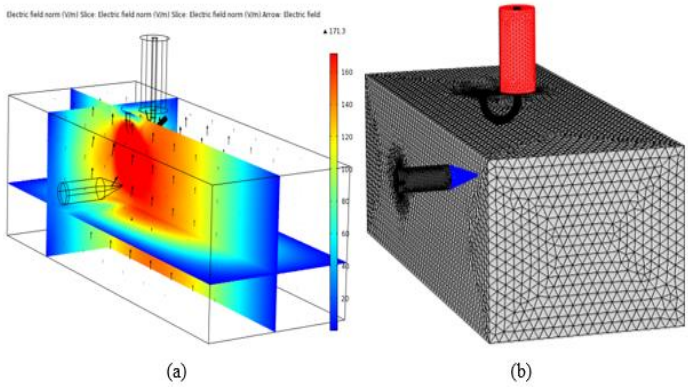

Figure 4.13: (a) E-Field distribution (V/m) inside water filled loop coupled TE_{011} mode rectangular cavity at 2.45GHz (front view) (b) Extra-fine meshing of the loop coupled cavity (perspective view)

It is worth pointing out here that the mutual coupling is directly proportional to the short circuited inductive loop area due to the magnetic flux density phenomenon. However, if we keep on increasing the loop area further, the *Q* Factor starts decreasing as the cavity gets overcoupled. However, In some particular situations, over coupling is desirable because it allows the radiator to operate over more than one frequency within its narrow band but at the cost of poor matching. In our case however, the loop area 2.4cm (adopted in [7]) was maintained after verifying the cavity resonance response on VNA as already shown in Fig.4.10.

Resonant cavities possess quite complex wideband impedance environments which become more complex in case of multimode cavities. The cavity used in this research however, is a single mode microwave reactor cavity which makes life easier because of its well-defined realizable impedance environment. Precise control of the loop positioning allows the exploration of wide band reflection coefficients change over smith chart for different loading conditions. The natural impedance loads of the cavity resonator can be used for direct emulation at the current generator plane of the transistor during microwave heating arrangement. Therefore, it is very important to properly understand and characterize the cavity resonator for its actual impedance measurements.

4.4.2 Cavity Characterization (Through Loop Rotation)

To start the loaded cavity mesaurements, the motor controlled moveable loop antenna was attached to a modified inner conductor of the N-type connector with the other end connected to the wall of the connector. The loop assisted N-Type connector was then connected to the moving rubber belt to reposition the metallic loop with the stepper motor. This would lead to a change in the magnetic flux density passing through the loop area according to its physical angle with the H-Field, and effectively allow tuning of the structure.

It is worth remembering that the purpose of this experiment is to track and with a view to exploiting the cavity input impedance as function of the loop orientation to see if the cavity impedance under specific loop angle can be used as a direct match to the microwave source (transistor) for microwave hetaing. This is necessary because this can result in significant reduction in transistor output matching network by simply transferring the cavity loads through simplest matching network. Also, it may not be necessarily required to employ extra harmonic tanks for harmonic impedance controls. It is worth mentioning here that a small interruption in the field environment of the cavity resonator results in a significant change in its resonance behaviour which is due to the field perturbation. Field perturbation is an important phenomenon which is sometimes used to characterize different material properties. However, in terms of impedance analysis, fundamental frequency load is the most affected frequency component which is due to the single mode nature of the cavity resonator. For 50Ω source and under critical coupling, the fundamental load impedance exists at the center point of smith chart (at 50Ω) whilst the harmonic loads can be existent anywhere on the chart. Thus with the cavity field perturbation, frequency load points move dramatically over different locations of smith chart. One way to exploit this impedance phenomenon was to electronically rotate the built-in loop coupling antenna using defined discrete steps and record the resulting S-parameters using a network analyzer over a full cycle of 360 degrees. To start with, the vector network analyzer was calibrated from 2 GHz to 7.5GHz to accommodate the fundamental, 2nd and 3rd harmonic impedances of the cavity. The 100µL water filled rectangular cavity resonator was connected to the network analyzer and rest of the electronically controlled measurment setup was arranged as shown in Fig.4.14

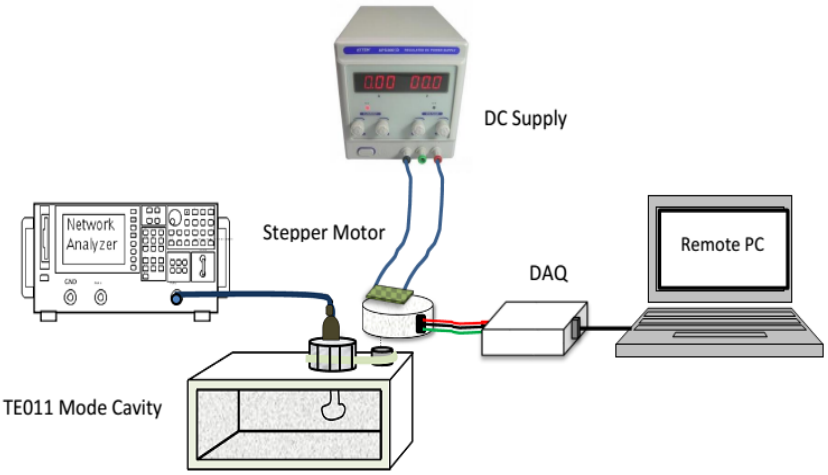

Figure 4.14: Electronically controlled setup for the measurements of the TE_{011} mode loaded rectangular cavity.

Before starting the measurements, the loop position was fixed parallel to the H-Field as a reference point to track the full loop cycle. This indicated that there was no power delivery into the cavity and the S_{11} observed on the analyzer was close to zero.

To be able to capture and model the complex impedance environment of the cavity; an approach introduced in [8] was adopted where the S-parameters were recorded as function of loop angle (φ).

$$S_{11} = \left[\frac{K\cos(\phi)^2 - 1}{K\cos(\phi)^2 + 1} \right]^2 \tag{4.5}$$

$$\phi = arcCos\left(\frac{1}{\sqrt{K}} \right) \tag{4.6}$$

Where 'φ' is the angle of coupling loop, and 'K' is the coupling factor related to the loop angle. A deeper analysis of equation (4.5) reveals that the loop angle directly affects the matching conditions of the cavity resonator. This means that the impedance environment of the cavity can be plotted against loop positioning. Therefore, an arrangement was made to acquire the fully controlled S-parameters of the water loaded cavity with defined loop orientations.

4.4.3 Coupling Control Technique

To accurately understand and capture the cavity impedance behavior as a function of the loop positioning, it was important to get an accurate control of the loop positioning.

Therefore, National Instruments Labview code was written to control the discrete motion of the loop and allowed it to move according to the desired discrete step. The purpose of this step control mechanism was to see the cavity response under different loop angles starting from the 'no-coupling point' i.e. when the loop is parallel to the H-filed and perpendicular to the E-Field. As a starting point, the loop was rotated using the motor and the time for the loop to complete one cycle was noted down which was recorded to be 56.2 Sec. The information of the loop complete cycle as a function of time was used to calculate the motor step as given in equation (4.7). Based on this formula, a Labview code was developed to control the loop angle through stepper motor. The time required by the loop to complete one cycle was divided by 360 degrees to find out the time of one degree motion. Finally, using the logical *'controls'* in the Lab-view, the accurate angle marking was labeled on the N-Type connector and the apparatus was setup to take the cavity measurements.

$$Motor_Step = \left(\frac{T_{cycle}}{360}\right) \times \phi_{angle_to_move} \tag{4.7}$$

Where T_{cycle}: is the time required for loop to complete one complete cycle and $\Phi_{angle\ to\ move}$: is the angle of desire

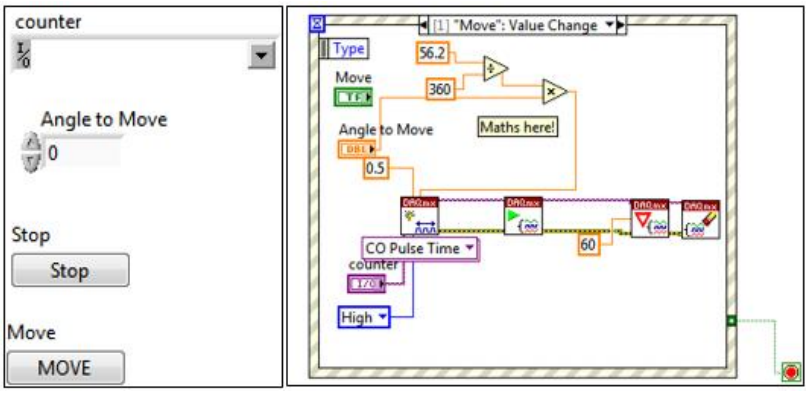

Figure 4.15: Labview diagram to control loop motion and electronically set the angle [Labview code written by Nicholas Clark]

4.4.4 S-parameter Measurements

To allow further PA – cavity integration analysis offline in a CAD simulation environment; The frequency span on the VNA was setup from 2-8GHz over 210000 frequency points which can easily cover the fundamental, 2nd and 3rd harmonic

reflection coefficients information. This extra fine frequency resolution is very important because it allows a true frequency impedance characterization of a narrowband resonator such as the single mode rectangular cavity in this case. The stepper motor was switched on with 12V DC supply and using a remote Labview control, the motor was rotated in discrete angular steps by simply inputting the angle of loop rotation. The S-parameter data for each specific angle was collected. This resulted in discrete S-parameter data related to various loop positions for 360 degrees rotation. Ideally, the angle resolution of the inductive loop should be very small to see the actual cavity response but this would result in extremely large unmanageable S_{1P} data set. Therefore, to avoid the extremely large data collection, the angle resolution was decreased and each step was fixed to 10 degrees each giving 36 touch stone data files with each file containing 21000 frequency points. Although it is still quite large data pertaining to long non-linear simulation time but at the same time it is precise enough to provide a good cavity impedance information as function of loop angle. These 36 S-parameter files collectively possess the microwave properties of the cavity and provide the definite information of the fundamental, 2nd and 3rd harmonic impedance load points under different loop angles

4.4.5 Measured Data Processing (Step-1)

To merge the measured discrete S-parameter files to a single file, a code was written in ADS nonlinear circuit simulator. This was necessary to access that single file into SNP1 component in ADS schematic and formulate a single passive load which can finally be presented to the transistor during simulations. A built-in data access component (DAC) has the ability to read through different data file formats in the ADS schematic window and to use them for linear or non-linear simulations. The passive load formation process can be understood in Fig.4.16.

ADS circuit simulator has a great facility of data extrapolation through various algorithms such as LMS, Newton Raphson, and Random Error etc. to best estimate and generate estimated data plots. Therefore, by using any of the suitable extrapolation algorithm the measured cavity data captured over 10 degree loop angle step can easily be scaled down to very small steps but again at the cost of large simulation time.

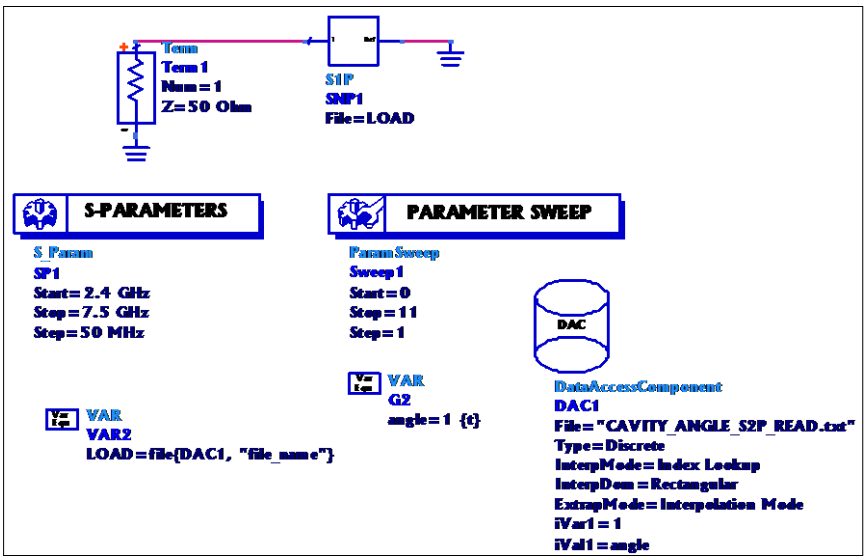

Figure 4.16: ADS schematic for accessing measured cavity S1P files as a function of loop angle.(using single discrete data file format)

The schematic shown in Fig.4.16 represents the exact behavior of the cavity over varying loop angles. Therefore, in ADS schematic we defined a continuous variable *'angle'* which is linked with the index number of a specific data file. Now, as we change the value of the variable angle, the corresponding data file is accessed from the data base and we are able to see the cavity measured response offline in CAD environment. The gap between each angle step can be minimized through extrapolation facility as described earlier. The variable *'angle'* possesses a continuous range from 0-360 degrees so that if the value of angle is set to an integral multiple of 10, the actual measured file is accessed and the actual measured response of the cavity is displayed otherwise for any other *angle*, the data will be extrapolated. This arrangement not only presents the S_{11} response of the cavity but also allows the fundamental, 2nd and 3rd harmonic load mapping on the smith chart for impedance emulation. The data accessing technique can be seen in table 4.3.

ANGLE	INDEX	DATA FILE
0	0	1
10	1	2
20	2	3
30	3	4
.....	.....	.....
.....	.....	.....
350	35	36

Table 4.3: Data accessing technique in CAD environment

4.4.6 Measured Data Processing (Step-2)

After loading the measured discrete S-parameter data and forming a static passive load in ADS schematic environment, the next step was to convert the static discrete data load to a dynamic multi-dimensional-data *mdif* format with an independent and tunable variable *angle*. This was necessary to access of the angle resolution and adjust the simulation time as outlined earlier. This was achieved by sweeping the variable *angle* in the previous step and a resulting data set was generated. The data was containing the frequency information, measured S-parameters of the cavity and the corresponding loop angle. With this information, it was possible to convert this data into *mdif* format. ADS has another built-in functionality to convert one file format to another file format in its display dataset environment. Therefore, the simulated dataset was converted into a single multi-dimensional-data format (MDIF) file with each block of data referring to the measured S_{11} at a specific loop orientation over full frequency range (2GHz to 7.5GHz).

To access the single multi-dimensional-index-file into ADS schematic window, another code was implemented in ADS and a dynamic load was formed. This load component was an accurate replica of the physical rectangular cavity and the term component used with this dynamic load was referring to VNA as shown in Fig.4.17.

This simulation design setup enabled us to present this load to the 10W-LDMOS power amplifier during nonlinear simulations whilst the angle tuning could be used to dynamically monitor the power amplifier's performance. In conclusion, this setup was representing the passive loadpull approach where *angle* being the tunable variable.

However, before integrating the 10W-LDMOS power transistor with the cavity load, the measurement based cavity model was compared with the corresponding extrapolated data. A single cavity measurement was taken (at angle=229°) and the same was simulated in ADS. ADS extrapolated and measured data for a loop angle 229 were plotted and found to be in excellent agreement as shown in Fig.4.18. The broadband loads obtained after extrapolation (at angle=229°) were mapped on smith chart over the broad frequency range (2-7.5GHz). Three Smith charts depicted in Fig.4.19 show the variation in fundamental, 2nd and 3rd harmonic impedances as a function of φ. The challenge was to understand how these loads can be used as optimum loads to the 10W-LDMOS transistor and to engineer a high-efficiency mode of PA operation.

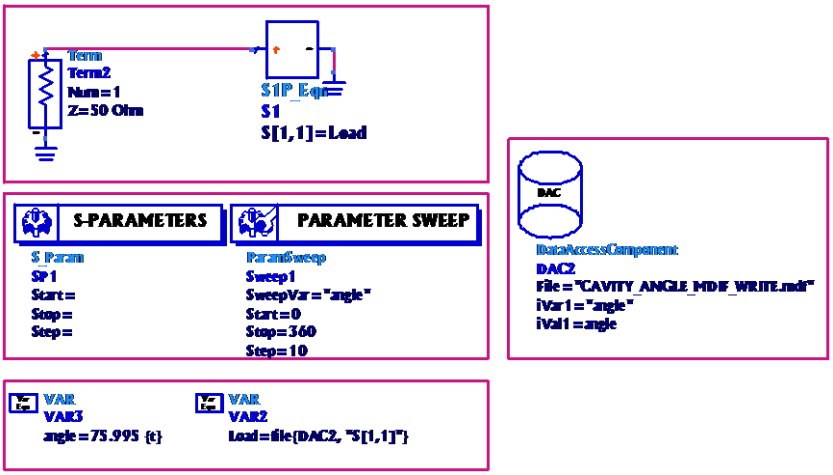

Figure 4.17: ADS schematic for converting 36 S2P measured data files to angle dependent single MDIF.

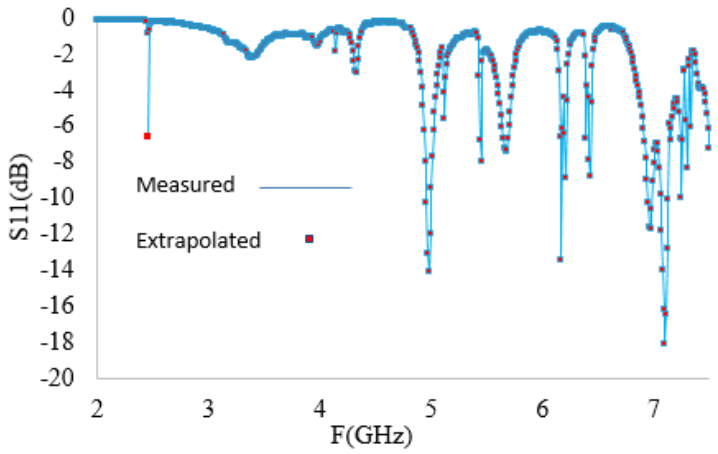

Figure 4.18: Cavity S11 measured response at loop angle=229°

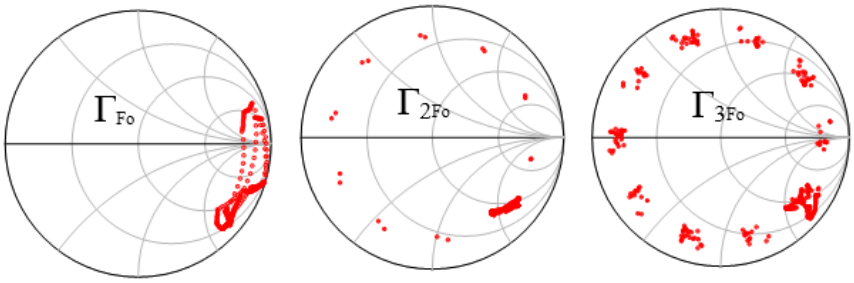

Figure 4.19: Measured cavity reflection coefficients for 360° loop rotation at (2.45GHz, 4.9GHz, 7.35GHz).

4.5 Integrated F^{-1} Power Amplifier Design

The stepped series impedance matching techniques have been presented in detail in [9] where the OMN is designed to match at single frequency for 50 Ω without having a need for extra matching stubs. As the objective of this experiment is to establish a portable and compact microwave heating arrangement for biomedical applications, it is necessary to reduce the physical size of the structure as much as possible. Therefore, the stepped impedance load transformation technique was adopted to transfer the already identified cavity non-50Ω loads to the transistor's optimum impedance design location. Because of the phase delaying and impedance transforming nature of the series transmission lines, an arrangement of lines can be established to match the fundamental and its integral harmonic loads to the points of interest on smith chart.

It is important to highlight here that the power delivery into the cavity resonators is an important figure of merit for a high efficiency microwave heating system. Therefore a two-way matching network enabling high efficiency waveform engineering of the transistor as well as preserving cavity resonance properties is very important in such applications. Having this in mind, the loop was rotated and return loss (-7dB) was observed at 2.45GHz at a loop angle ∠229° as shown earlier in Fig 4.18.

2.45GHz is an important frequency because it relates to the design frequency of the microwave source (10W-LDMOS) and the transistor has been characterized at this typical frequency. To start off, the load reflection coefficients were noted for first three harmonics and mapped on the smith chart as shown in Fig.4.20. As we have already identified the cavity reflection coefficients for fundamental, 2nd and 3rd harmonic at loop angle 229, therefore these loads were transformed to transistor's optimal points by deploying transmission lines between the cavity and the 10W-LDMOS power

transistor. As a starting point, ideal transmission lines were used to transfer the natural cavity load points to the transistor optimum locations by tuning their phase lengths and impedance values. After the cavity load points were moved to the transistor optimum locations, these ideal lines were converted to the microstrip lines using RT/duroid5880 substrate (εr=2.2, h=0.51mm, tan (δ=0.0005) and physical lengths and the widths of the lines were calculated using ADS Lincalc function. Harmonic tuning process has been summarized as follows:

- Working from cavity plane in Fig.4.20, a series line (line-1) of 50 degrees electrical length (E) and characteristic impedance (Z_T) of 25 Ω is used to move the fundamental load reflection coefficient towards the optimum transistor point. Then a second series line (Line-2) of E=25 degrees and Z_T=24 Ω moves the fundamental load to the optimal point of PA.
- In case of the 2nd harmonic, the electrical length of the lines 1 and 2 doubles to E=100 degrees and E=50 degrees respectively. This has the effect of moving the 2nd harmonic load towards its optimum.
- The 3rd harmonic current component was observed to be very small for this device, so its impact on drain efficiency is limited as already seen earlier. We are interested in achieving the best possible performance of the PA however, so the ideal 3rd harmonic load was also achieved using the same network.

After tuning the harmonic loads, the circuit was fabricated. The measured performance of the integrated setup was observed to be slightly reduced in comparison to that observed during transistor load-pull measurements. This could be due to the losses associated with the transmission lines and the fabrication tolerance; which are unavoidable in this case. The eventual inverted class-F waveforms obtained at the current generator plane are depicted in Fig.4.21, although the current waveform could be squarer by the addition of multiples of odd harmonics, but the reduced higher harmonic components due to the lower cut-off frequency of Silicon does not allow much freedom for wave-shaping [10]. However, the waveforms obtained at I_{GEN}-plane in this integrated setup are still indicative of inverted class F.

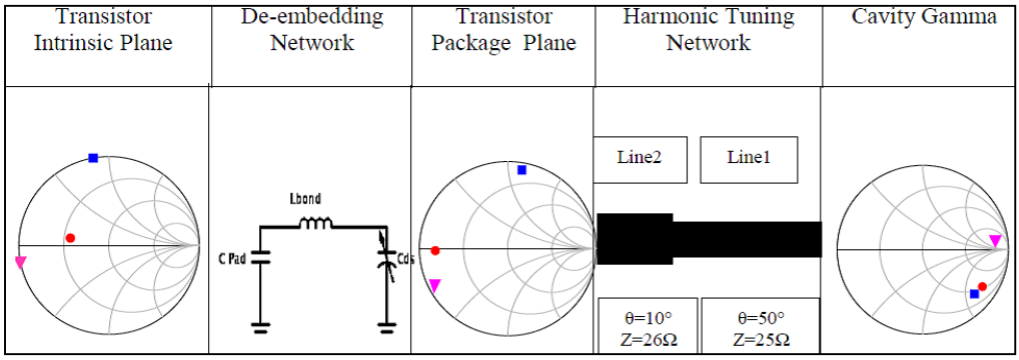

Figure 4.20: Complete harmonic tuning recipe for observing the transferred loads at the package and the intrinsic plane of BLF6G27-10G 10W-LDMOS power transistor at 2.45GHz.

Cavity Impedances at loop angle∠229°			Delay Line-1		Delay Line-2	
● Z_{Fo} (Ω)	■ Z_{2Fo} (Ω)	▼ Z_{3Fo} (Ω)	θ_1	Z_1	θ_2	Z_2
57-j*155	41.6-j*121	350+j*325	50°	25Ω	10°	26Ω

Table 4.3: Harmonic tuning network values for cavity load transformation

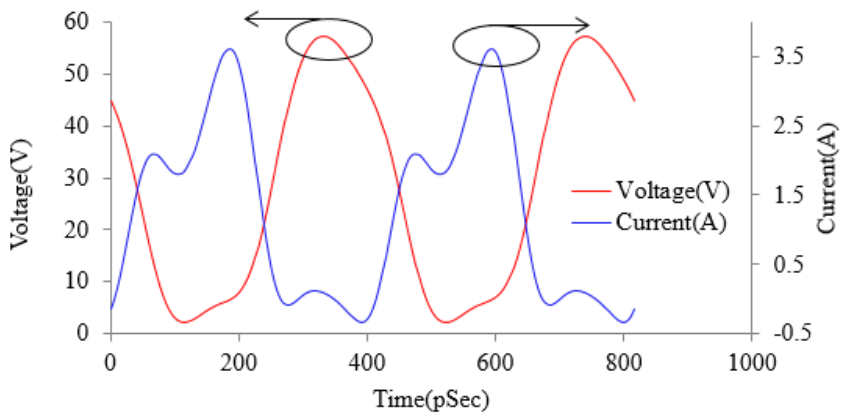

Figure 4.21: Simulated inverted-F waveforms obtained using integrated PA design approach at 2.45GHz

4.5.1 Coupled Line Directional Coupler

In traditional 50Ω systems, the power measurements are taken by using the directional coupler at the output stage of the circuit which is a reputable and authentic way of measuring the reflected and transmitted signal. But there are some disadvantages associated with it as well. For example, its large and bulky structure and 0.2-0.5 dB

power loss limits its usage in portable and compact structures such as the one targeted in this research. Also the traditional directional couplers cannot be used in any other non-50Ω impedance environment.

(The traditional 50Ω solid state microwave heating structure with conventional directional coupler can be seen in appendix-1).

Therefore, to monitor the power performance analysis, a key enabler for describing transistor drain efficiency, a coupled line directional coupler was designed by placing a micrstrip line 1mm apart from the matching delay lines. By using this approach, the matching lines not only act as harmonic tuners but also become part of the coupled line coupler for overall performance analysis. The detailed analysis on the power calibration and design of the coupled line directional coupler will be demonstrated in chapter.5.

4.5.2 Measurements and Test

After designing and simulating, the PCB was fabricated using LPFK milling system and components were soldered and slightly tuned to optimize the overall structure performance. The Vgs=2.5V was set as class-A voltage and VDS set to 28V. The 100µL water filled cavity coupled at loop angle 229 degrees was directly presented as an optimal passive load to the 10W-LDMOS transistor and a power sweep was conducted at 2.45GHz. The coupled portion of the transmitted power was obtained at port-1 where the Port-2 was terminated to 50Ω.

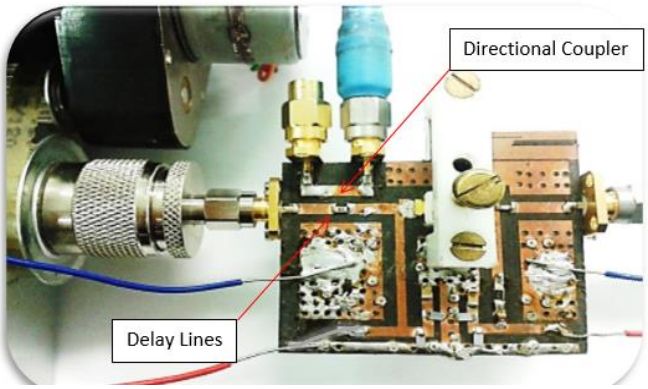

Figure 4.22: Inverse-F PA prototype using simple series lines and coupled line directional coupler at output stage

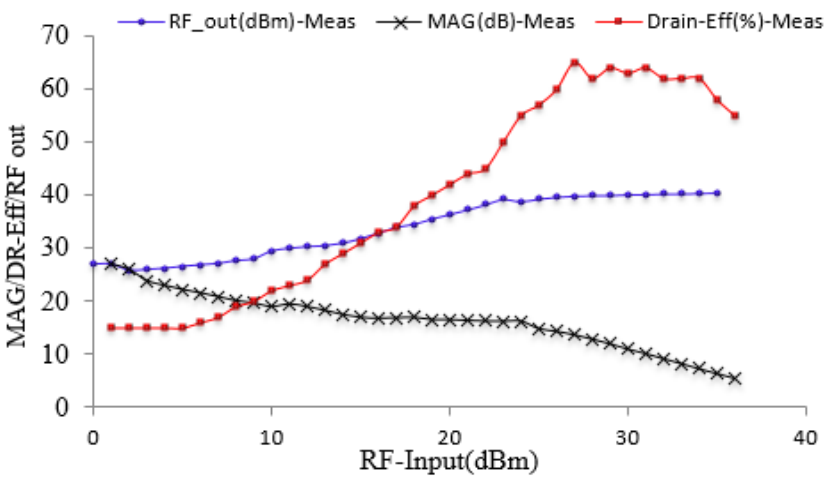

Figure 4.23: Measured PA-Cavity performance.

4.6 Summary

In this chapter a compact and field deployable microwave heating apparatus for portable healthcare applications has been practically demonstrated. This chapter basically introduces a two-way design technique in which firstly by adopting waveform engineering techniques, a high efficiency inverse class-F mode power amplifier has been designed using the natural impedance environment of the water loaded TE011 mode rectangular cavity together with simple series microstrip lines. Secondly, the cavity resonance properties have been preserved at the same time by using the same set of series matching transmission lines which allow the efficient power delivery by minimizing the cavity reflections.

Unlike, traditional high efficiency mode power amplifier design approaches, as shown in Fig 4.1, where the lossy and physically large harmonic tuning networks are deployed between source (transistor) and load (50Ω term); this technique makes direct use of the natural impedance environment possessed by the cavity and transfers the identified cavity reflection loads to the transistor optimum performance points by simple series delay lines.

This novel F^{-1} PA design technique guarantees improved PA performance and significant reduction in the physical size of the structure. To further assure the apparatus compactness, a directional coupler has been added at the output stage by using a coupling line parallel to the main RF output path so that the coupled line directional coupler then allows the overall performance analysis by measuring the

transmitted and reflected waves from the cavity. This PA design technique also eliminates the need to have fixed 50Ω load. Besides the advantages of this heating arrangement it has limitation of working strictly at a single frequency (2.45GHz) which means that this arrangement is suitable to work for one sample with fixed dielectric properties. Any change to the microwave properties of the sample will affect the performance of this setup. Therefore as a future work, same integrated setup can be upgraded to work over broad frequency range using the series delay line approach.

References

[1] Lovleen Tina Joshi, Budha L.Mali, Chris D.Gddes, Les Baillie, "Extraction and Sensitive Detection of Toxin A and B from the Human Pathogen C-difficile in 40 Seconds Using Microwave Accelerated Metal Enhanced Flourescence," Vol 9, Issue 8, Aug (2014)..

[2] Stephen B.Baumann et al, "Feasibility Study of Batteryless Temperature Transponders Using Miniature Microwave Cavity Resonators" *IEEE Trans. Biomedical Engineering*, vol.BME-34, no.9, September 1987.

[3] A. Sheikh, C. Roff, J. Benedikt, P. J. Tasker, B. Noori, P. Aaen, J. Wood, "Systematic waveform engineering enabling high efficiency modes of operation in Si LDMOS at both L-band and S-band frequencies," *IEEE MTT-S Int. Microwave Symp. Digest*, June 2008, pp. 1143-1146.

[4] Aamir Sheikh, "High Power Waveform Engineering,*" PhD thesis, School of Engineering, Cardiff University*, UK, June 2010.

[5] David M.Pozar, *Microwave Engineering*, 3rd Ed, Jhon Willey& Sons, Inc.

[6] Water structure and science (http://www.lsbu.ac.uk/water/microwave_water.html) date accessed March 10, 2015.

[7] Matthew Ayres, Robert Friedhoff, Michael Gray, Owain Jones, "Microwave Heating in a Microfluidic Reactor," Master thesis, *Cardiff University*,2011

[8] Naylon, J. Private Communication. *Cardiff University*: S.n., 2010 - 2011.

[9] J.A.G.Malherbe, *Microwave Transmission Line Filters*, Artech House, Dedham, Mass., 1979.

[10] John L.B.Walker, *Hand book of RF and Microwave Power Amplifiers*, Cambridge University Press 2012.

Chapter.5 INTEGRATED CONTINUOUS MODE POWER AMPLIFIER FOR MICROWAVE HEATING

5.1 Introduction

The research conducted in this chapter significantly expands our previous work by introducing a new solid-state microwave heating arrangement capable of heating samples that differ in volume and temperature, and working efficiently over the functional bandwidth of a cavity resonator. This work differs from our previous work by two main factors; firstly, the cavity used this time is a TM_{010} mode circular cavity and secondly, the load impedance controlling variable is the amount of sample volume to be heated. The natural change occurring in the cavity impedance design space due to the varying water volume can be systematically utilized to formulate a flexible and efficient integrated heating setup.

The work presented in this chapter targets true continuous mode broadband power amplifier design using direct integrated design technique. It will be shown that the selected load points from the cavity design space can be logically arranged at the intrinsic plane of the transistor by series delay lines and transistor built-in package network. This arrangement offers a significant reduction in the OMN complexity whilst the waveform engineering techniques applied in this method, present half rectified voltage and phase shifted current waveforms. To formulate the continuous mode power amplifier arrangement, the impedance environment of TM_{010} mode circular cavity together with stepped microstrip lines and built-in package network has been exploited as a function of the amount of sample to be heated and used systematically to present the optimal loading conditions for a 10W GaN power transistor. This compact setup serves for two important purposes. *Firstly*, it allows transistor efficient and broadband operation under varying loading conditions and *secondly*, the reduced cavity reflections over the targeted bandwidth make the cavity resonator a matched broadband load.

The design process has been divided into five steps as follows:

1. Characterization of 10W-GaN power transistor at 2.45GHz using active harmonic time domain loadpull mesaurement system.
2. Characterization of TM_{010} mode circular cavity resonator under varying loading conditions (different water volumes in this case)
3. Broadband output matching network sysnthesis for systematic transfer of cavity loads at the intrinsic plane of the 10W-GaN power transistor.
4. Non-linear waveform engineering analysis of the integrated setup for amplifier mode identification (continuous-F^{-1}).
5. Fabrication and Measurements.

5.2 GaN Power Transistor Technology and Analysis

Eneregy bandgap is an important property of semiconductor materials where the materials with larger bandgap have the ability to withstand high electric field before the occurance of the voltage breakdown. One such material is Gallium Nitride whose bandgap is 2 to 3 times wider than conventional semiconductors such as Silicon and GaAs [1]. Similarly, thermal conductivity is another important figure of merit of semiconductors that defines the dissipated power handling capability of the devices. The devices with lower thermal conductivity have high risk of damage and also it results in lower RF performance. GaN is a compound semiconductor made of group-III and group-V in the periodic table. The wider bandgap of the GaN (3.4eV) allows it to handle high critical electric field before its breakdown. Consequently, GaN based devices can withstand a large terminal voltage thus resulting in a high output power. Similarly, lower dielectric constant, high thermal condutivity, higher cut-off frquency and high critical electric field of GaN power transistors make them the right choice for high power applications such as power amplifiers.

the following table provides the key electrical properties of different semicoductor materials [1].

Material	E_g (eV)	ε_r	σ (W/°K-cm)	E_c (V/cm)
Si	1.12	11.9	1.5	3×10^5
GaAs	1.43	12.5	0.54	4×10^5
GaN	3.4	9.5	1.3	2×10^6
InP	1.34	12.4	0.67	4.4×10^5

Table 5.1: Different semiconductor materials and their electrical properties

In this microwave heating experiment, we have used a 10W (CLF1G600-10) GaN power transistor as high efficiency microwave energy source. The device has been characterized at 2.45GHz for its F^{-1} mode of operation which can be extended to operate in its continuous inverse-F mode of operation over a wider bandwidth.

5.2.1 DC-Analysis of 10W-GaN Power Transistor

To start with, the transistor is characterized for its DC behavior by generating the family of DC-IV curves. This provides an insight of the knee-voltage, turn-on gate voltage, and maximum achievable output current as shown in Fig.5.1. DC characterization not only provides the cutoff and saturation limiting current range of the transistor but also the stability analysis can be made to avoid unstable portions on smith chart during device RF characterization. To make a stability analysis, the device was biased under different input voltage levels and simulated in ADS. The source and load stability circles were found outside the smith chart under all biasing conditions, which means the device can be presented with any passive load or source impedance during its RF charaterization without worrying for oscillations. To generate the DC-IV curves, the target drain biasing voltage was set to 10V and the gate voltage step was fixed to 0.25V. For each gate voltage, 10W-GaN device was swept until the specified drain voltage range. Starting from the device cutoff point (Vg=-2.7V) to its saturation point (Vg=2V) a fixed gate voltage step of 0.25V was maintained and following set of non-linear curves were generated. It can be seen through Fig.5.1 that the device is capable of delivering a maximum current of 1.3A, nearly half that of the 10W-LDMOS transistor. A reason for this lower output current is the wide bandgap

of the GaN semiconductor compared to Silicon. However, GaN based devices have an added advantage of tolerating higher voltage swings during their active operation without causing the dielectric break down, which is much likely to occure in Silicon based transistors. Therefore, whilst using GaN power transistor, inverted class-F mode of operation can be a right choice for achieving maximum performance out of this RF device. From this analysis, we can also conclude that the high efficiency PA modes where the voltage waveforms can be shaped to have higher swing, GaN transistor may well be the right choice.

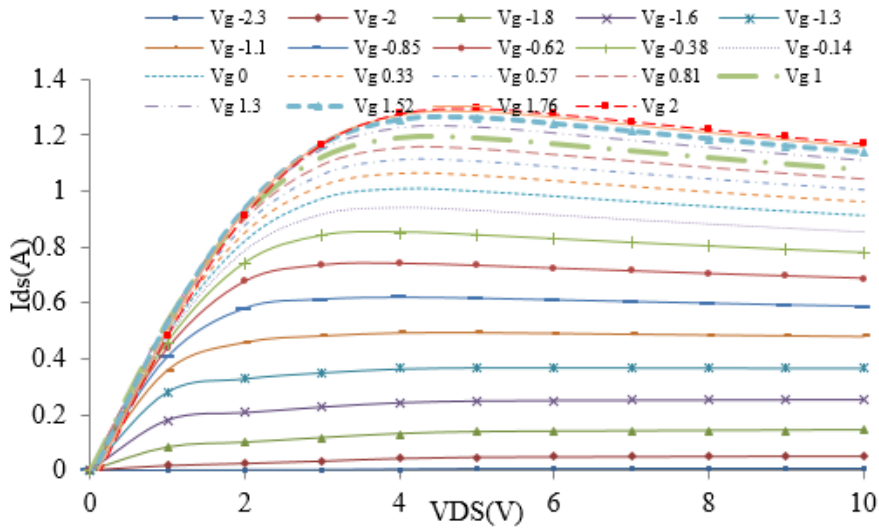

Figure 5.1: Transistor DC-IV Curves for (CLF1G0060-10) Small Signal-Analysis of 10W-GaN Power Transistor.

To accurately predict the intrinsic and extrinsic behaviour linked with the current generator of the 10W-GaN transistor it is very important to know the device behavior in its 'hot' or active state. This is an important step which allows the impedance emulation at extrinsic and intrinsic planes of a transistor. A TRL calibration can allow access to the package plane of the transistor for its biased dependent S-parameter measurements which is necessary to develop the package parasitic model. By developing a large signal package model, the package plane impedances can be translated to the intrinisc plane after fine tuning. The transistor was placed in 50Ω microstrip line test fixture environment for its biased dependent small signal linear measurements. The bias dependent S-parameters were measured at the calibration plane of the test fixture including two 20mm long microstrip lines whilst the hot-state

environment was maintained at VDS=50V, Vgs= -2V, Idq= 50mA, Z_L=50Ω . The 20mm long microstrip transmission lines were deembedded (as we have their deembedding information from chapter 3) and the transistor package plane was accessed. The measured S-parameters were imported in ADS and simulated from DC-6GHz. A comparison of the measured and the parasitic de-embedding network provided by the NXP Inc. shows an excellent agreement upto 6 GHz. Thus by using the parasitic model the package network was deembedded and current generator plane was accessed.

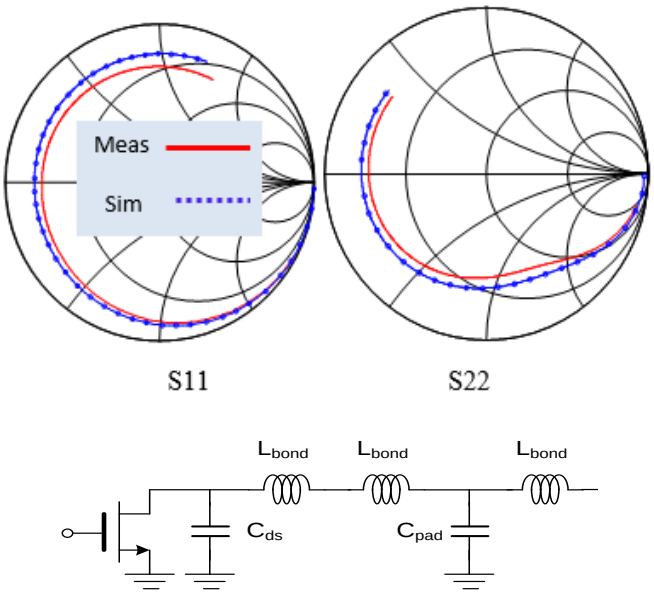

Figure 5.2: (Top) Measured vs simulated biased dependent S-parameter response(DC-6GHz) (CLF1G0060-10) GaN transistor at package plane (VDS=50V, Vgs= -2V, Idq= 50mA, ZL=50Ω), (Bottom) De-embedding network provided by NXP Inc.

C_{DS}(pF)	L_{b1}(nH)	L_{b2}(nH)	C_{pad}(pF)	L_{bond}(nH)
1.25	0.69	0.088	0.42	0.088

Table 5.2: Measured parasitic values of 10W-GaN transistor.

5.3 Large Signal Analysis of 10W-GaN Power Transistor (at 2.45GHz)

To use the transistor as microwave energy source in solid-state microwave hetaing experiment it was decided to initially characterize the transistor for its inverse-F mode of operation at 2.45GHz. The multiharmonic time domain loadpull measurement system was calibrated for 5 haromics whilst fundamnetal at 2.45 GHz. The system was tested and verified in the same way as discussed and demonstrated previously. As the package model of the (CLF1G0060-10) GaN transistor in excellent agreement with the physical device therefore, the measurements were followed by CAD nonlinear simulations to save time and resources.

5.3.1 Gate Voltage Sweep

Gate voltage selection is the starting point of any class of PA design because it fundamentally defines the behaviour of the emerging out voltage and current waveforms out of a transistor. High efficiency modes of PA operation are obtained through waveform engineering by proper utilization of the harmonic components. All classes of operation mainly depend upon the Q-point selection therefore it becomes equally important to see the gate voltage impact on the amplitudes of harmonic current contents. As the transistor is a nonlinear device and the output current strongly depends upon the knee voltage, therefore, it is difficult to estimate the overall harmonics response at a fixed biasing level. To properly gain knowledge of the harmonic contents, gate voltage sweep is necessary. To begin with, the device was simply turned-on and biased to its class-B biasing (Id=0A, Vg=-2.3V, Vd=28V). The biaisng point was selected because of intention to sweep gate voltage upto its class-A point. This would ease the selection of most sutiable gate voltage in terms of harmonic components for targeting F^{-1} mode in which the waveforms are engineered with harmonics utilizations. In F^{-1} mode, a transistor is allowed to draw maximum current during its active operation which can further be increased by a logical addition of even harmonics. The drive signal was set to 1dB compression point i.e., 27dBm and the gate voltage sweep was performed to see the harmonic response of 10W GaN transistor. It is obvious that the 3rd harmonic maxima and the 2nd harmonic minima occurs at -1.6V therefore this input voltage level can be well adopted to shape the voltage and current waveforms from 2nd and 3rd harmonics respectively. Although this

is not the Class-A biasing point which normally should be the prerequisite for inverse-F wave-forming, we do see that increasing the gate voltage to class-A point ≈ -0.85V, a sudden drop in the fundamental and 2nd harmonic drain current appears which probably could be due to input feedback capacitance. The bias dependent feedback capacitance (C_{gd}) in many high voltage power devices has a natural tendency to show its effect in the output currents such as in this case. Therefore, this input voltage cannot be applied to get high performance of the transistor under inverse-F mode of operation.

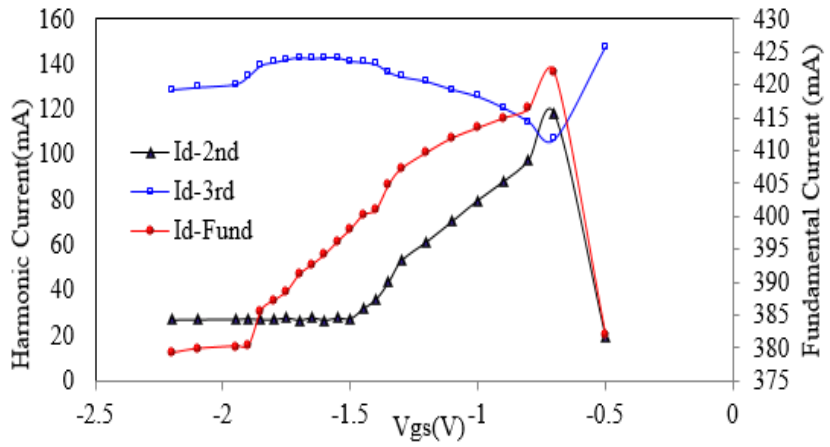

Figure 5.3: Harmonic currents as function of gate voltage

5.3.2 Load Optimization

Impedance load identification and optimization is an important step towards PA design because it allows the best optimum operation of any power amplifier irrespective of its waveform engineering analysis. For example, a quick and rapid method to identify the optimum load impedances is to simply apply the iterative loadpull process at the package plane of a transistor for fundamental and harmonic frequencies. This method can give us the best drain efficiency and output power witin a very short time. Though this method is quite useful in industry environment for quick product evaluation but unfortunately it cannot provide an insight of a transistor during its switching operation. Therefore, it is very important to apply the loadpull techniques at the intrinsic plane of a transistor to properly evaluate its fundamental performance which can be further extended through waveform engineering techniques. In order to reach to the transistor's intrinsic plane, it is very important to negate the effect of transistor package parasitic and apply waveform engineering techniques because at this plane the emerging time domain waveforms are sensible. The termination applied

at this plane are purely resistive and the resulting waveforms are free from the influence of any reactive element. As we have the correct network information of the parasitic elements of 10W-GaN transistor, so we can reliably use this information to de-embed the pacakage network and gain access to I_{GEN}-plane.

After identifying the optimum gate voltage, the device was subjected to RF characterization. 2nd and 3rd harmonics were passively terminated to 50Ω whilst only fundamental load reflection coefficient was spread over the smith chart; all loads were presented at the intrinsic plane. using remotely controlled loadpull system, during first iteration, the narrowed-down high efficiency area was roughly targeted. During the second iteration, the already targeted area was filled with another dense gird of fundamental loads. After this iteration, further high efficiencies were observed. The same process was reapeated several times until the final optimum fundamental load impedance point was observed on the real axis of smith chart. Similarly, to find out the best omptimum fundamental load for output power, the same process was reapted and the optimum load showing highest output power was spotted. In the next stage, harmonic components were targeted to control and shape the output voltage and current waveforms through waveform engineering. To begin with the systematic analysis, the fundamental wave was presented with the identified optimal load and 3rd hrmonic was short circuited. Now using the above stated iterative process the 2nd harmonic optima was located on the smith chart. Finally the fundamental and 2nd harmonics were terminated with their optimum points and the 3rd harmonic optima was located.

Reference Plane	Z_{Fo} Ω	Z_{2Fo} Ω	Z_{3Fo} Ω
Package	55-j*10.25	15-j*2	17+j*143
Current Gen	54-j*0	12+j*7	4+j*70

Table 5.1: Measured load points at package and I-$_{GEN}$-plane

It is important to understand here that the optimum harmonic impedances achieved at the current generator of the 10W-GaN are not exactly at the fixed points on the edges of the smith chart i.e. 2nd open and 3rd short. This could be due to the high sensitivity of the harmonic loads to high frequencies. Because as the frequency increases the 50Ω real load seen by the current generator changes to a complex load at the harmonic

frequencies [2]. Similarly, the influence of drain-sorce capacitance is another unavoidable phenomenon which is due to its nonlinear nature and reactive response to high frequencies. Therefore, it is very difficult to correlate the measured harmonic impedances with the mathematically derived. However, the measured waveforms, and the performance numbers can support the reliable identification of optimum impedance points. Thus, the waveform engineering process in conjunction with load impedance optimization can gaurantee the best possible performance achiveable from a transistor under a certain mode of operation.

5.3.3 RF-Input Optimization

The device was biased at it class AB mode i.e.V_g= -1.6V and first three loads terminated to their optimum impedance points. The next step was to conduct the input RF analysis of the transistor in its F^{-1} mode of operation. The input RF signal level injected to the input terminal of the transistor determines the output voltage and current waveforms. The higher level of the input signal leads to the higher drain current. As is obvious in the Fig 5.4(top), 26dBm is the input drive level where the 3rd harmonic current component is maximum and the 2nd harmonic current component is minimum which is the inverse-F requirement. However, as we further increase the drive level, the transistor reaches its maximum output current saturation limit and no extra current can be drawn beyond this limit. Therefore, we have to choose the optimum level of the 3rd harmonic so that the current waveform can be optimally squared.

Whilst all the other transistor parameters were affixed to their optimum points, the input power sweep was performed and output power, drain efficiency and maximum available gain was measured as shown in Fig 5.4 (bottom).

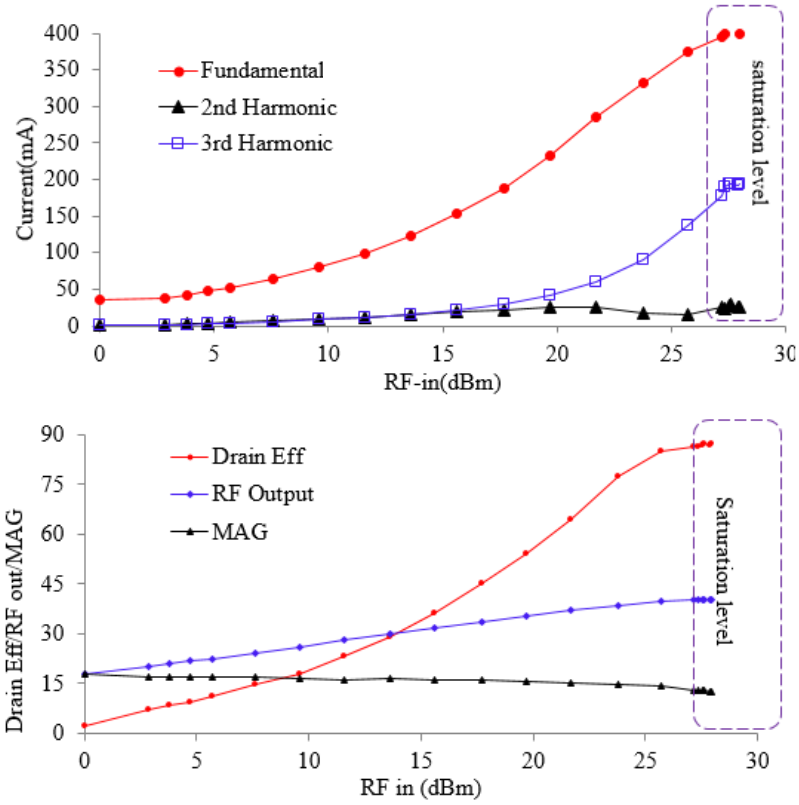

Figure 5.4: (Top) Measured harmonic currents as function of input drive (Bottom)

drain efficiency, output power and gain of the transistor under F^{-1} mode of operation. The package network was de-embedded and the output voltage and current waveforms were shaped at the intrinsic plane by fine tuning the 2nd and 3rd harmonic loads. The 3rd harmonic current component was added to square the current waveform and 2nd harmonic voltage component to half rectify the output voltage waveform as shown in Fig 5.5. this is true that the impedances presented in Table-5.3 do not correspond to the theoratical impedances for inverse-class-F (i.e.$Z_{L2fo}=\infty$ and $Z_{L3fo}=0$) but the waveforms and the performance parameters clearly show that the engineered PA mode belongs to inverted class-F mode of operation.

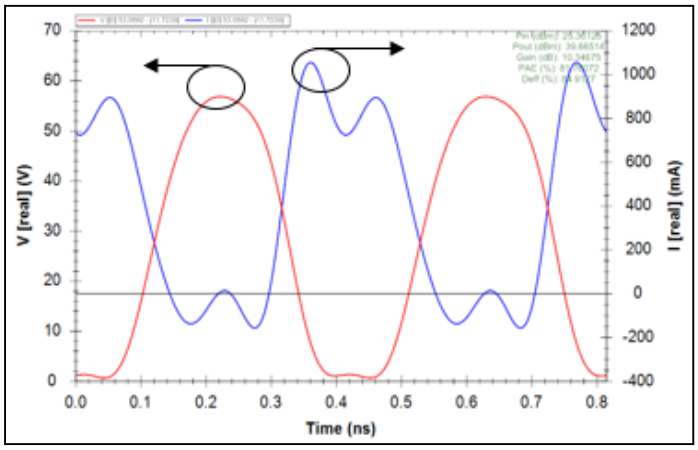

Figure 5.5: Intrinsic voltage and current waveforms

In conclusion, the systematic analysis of a transistor is an important step prior to designing any class of power amplifier for any application. Loadpull characterization leads to a best possible performance out of a transistor. For example, in this section the 10W-GaN power transistor was characterized to operate in its F^{-1} mode at 2.45GHz. The choice for inverted mode of operation was made based on the facts that maximum output current achievable from the transistor is only 1.4 Amperes, so the current waveform can be maximized and squared by adjusting the input RF drive, biasing and 3rd harmonic amplitude. The voltage waveforms can be shaped by adjusting the 2nd harmonic and drain voltage to increase the efficiency and output power out of a GaN transistor. Also, the nature of the GaN based devices to withstand high critical E-Field due to expanded energy bandgap can help avoid device failure for extended time domain voltage waveforms, the fact can be seen in Table-5.1. After applying waveform engineering techniques, it was also observed that, to date, this is the best performance achieved from 10W GaN power transistor at 2.45GHz best according to author's knowledge. The table below provides a quick comparison between the work presented in this section and the works presented earlier.

Transistor Technology	PA Mode	RF output dBm	Drain Efficiency %	Frequency GHz	Year
GaN	F [14]	39	81.9	3.370	2012
GaN	F [15	33.5	90	5.860	2012
GaN	JB [16]	40	80	2	2013
GaN	F [17]	40.3	78.8	2.450	2014
GaN	F^{-1} [present]	40.5	85	2.450	2015

Table 5.4: Summary of frequency VS output performance analysis in different GaN based Power Amplifiers.

5.4 TM_{010} Mode Split Circular Cavity Resonator

In microwave heating, frequencies lying within S-band are the best frequencies for microwave heating. At these frequencies, microwaves penetrate deep inside a water sample and increase its dipole moment that results in increased molecular motion necessary for heating. At these frequencies the dielectric loss factor is maximum, which is an important parameter for microwave heating (refer to Fig.2.1 in literature review). Similarly, a high concentrated E-filed is a key point for heating samples, as according to equation (4.3). It was shown earlier in literature review in Fig 2.8 that cylindrical cavity resonator has ability to concentrate maximum E-field in their axial direction whilst operating in its T_{mn0} mode. However, it is very important to select a right mode of operation because not every T_{mn0} can concentrate E-field in the center of the cylindrical cavity. Therefore, care must be taken while selecting the cavity resonator for microwave heating applications. To allow a sample to be fully exposed to a centralized high intensity E-Field, TM_{010} mode circular cavity is the right candidate in microwave heating applications. The E-field being responsible for heating should be concentrated in axial direction because the sample placed parallel to the Z-axis will experience maximum E-Field and also the depolarization of the sample can be avoided. TM_{010} mode circular cavity is the best candidate for its inherent nature of concentrating E-Field in the center of the cavity where the sample under test should be inserted for heating. In TM_{010} mode cylindrical cavity, the E-Field in the middle of the cavity is maximum and follows Bessel's function of first order. However, as we move away from the center, the field dies out exponentially (see Fig.5.7). In

diagnostic healthcare applications, it is very important that the sample should experience continuous high power pulses to continuously stimulate the sample under test for revealing bacterial DNA information.

The TM_{010} mode split circular cavity previously designed by Daniel Slocomb [3] was used in our microwave heating experiment. To allow the cavity to resonate at 2.5GHz, the circular cavity was designed by substituting following dimensions of the cavity in equation (2.21) in literature review.

Cavity diameter= a=4.6cm

Cavity Height= d= 4cm

It is evident from the equation that by only adjusting the radius of the TM_{010} mode circular cavity, the resonance frequency of an air filled cavity can be adjusted and this is specifically true when we have a split cavity such as in this case. However, the situation changes when a material with different dielectric constant is inserted into the cavity.

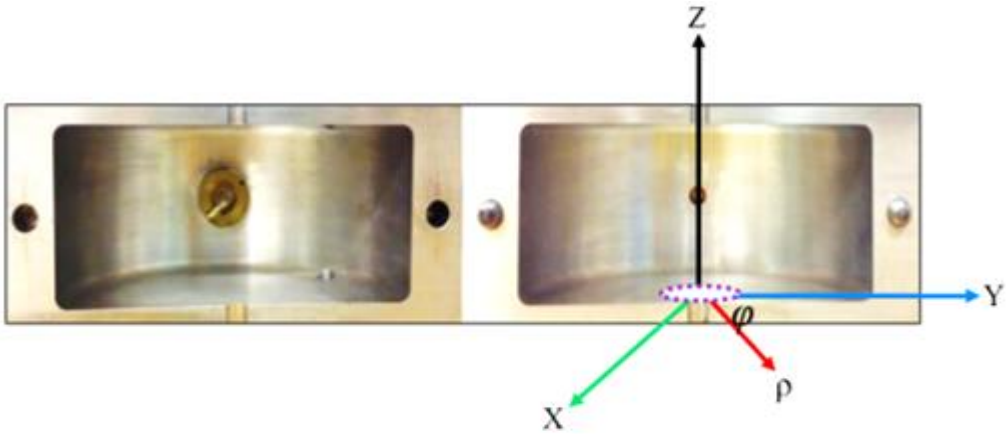

Figure 5.6: TM_{010} mode loop coupled split circular cavity used in the experiment (Design Frequency=2.5GHz)

n	P'_{n1}	P'_{n2}	P'_{n3}
0	3.832	7.016	10.174
1	*1.841*	5.331	8.536
2	3.054	6.706	9.970

TE modes of Circular Waveguide

n	P_{n1}	P_{n2}	P_{n3}
0	*2.405*	5.520	8.654
1	3.832	7.016	10.174
2	5.135	8.417	11.620

TM modes of Circular Waveguide

Table 5.5: m^{th} roots of Bessel's Function for TE and TM modes.

In this case, TM_{010} is the dominant and best suitable mode for circular cavity under the given dimensions because the resonant frequency distance is approximately 1GHz from any other resonating mode as can be seen in Table.5.6. Therefore, any frequency offset within 1GHz can easily be accommodated using the given dimensions.

Resonating	TM_{010}	TM_{110}	TE_{111}	TM_{011}	TE211	TM_{111}	TE_{011}
Resonant Frequency(GHz)	2.4946	3.9748	4.2060	4.5019	4.9070	5.3274	5.4629

Table 5.6: Few of resonant TE and TM modes for Height=40mm and diameter=46mm.

The cavity resonator was coupled into its magnetic field by feeding the cavity through a short circuited square antenna of adjustable side length≈2cm. as already outlined in chapter 4, the coupling strength and resonance of a cavity resonator can be controlled by manually adjusting the loop positioning. This is specifically true when the cavity is loaded with a material of higher dielectric permittivity such as water. In the next

sections it will be shown that how the resonance properties of TM_{010} circular cavity change with different levels of water.

5.4.1 *Q*-Factor of The Split Circular Cavity

For purpose oriented microwave heating applications, the microwave cavities with high *Q Factor* are preferred for their fine resonance behavior at a particular frequency of interest. For example, in case of microwave heating for biomedical applications, the sample holding cavity with low *Q Factor* will have shallow frequency resolution, higher bandwidth and less concentrated E-field that will result in the measurement uncertainty.

The overall *Q Factor* of a sample holding cavity is a sum of the Q_C (*Q* factor due to conducting walls) and Q_d (*Q*-Factor of a dielectric material filling the cavity). Therefore total *Q* Factor of a circular cavity can be found [4] which is the same as the *Q Factor* of rectangular cavity (see equations (2.5-2.9) in literature review).

$$Q_c = \frac{(ka)^3 \eta a d}{4(p'_{nm})^2 R_s} \times \frac{1-\left(\frac{n}{p'_{nm}}\right)^2}{\left[\frac{ad}{2}\left[1+\left\{\frac{\beta a n}{(p'_{nm})^2}\right\}^2\right]+\left(\frac{\beta a^2}{p'_{nm}}\right)^2\left(1-\frac{n^2}{(p'_{nm})^2}\right)\right]} \tag{5.1}$$

$$Q_d = \frac{1}{\tan\delta} \tag{5.2}$$

5.4.2 Field Analysis of The TM_{010} Split Circular Cavity

It is very important to analyze the field distribution of the TM_{010} mode cavity resonator. Finite-element-method for electromagnetic analysis of the complex structures is an efficient way of solving the Maxwell's equations. Variety of intelligent and accurate simulation softwares are available in market which offer quicker and efficient EM solutions . The evident problem, however, with all these softwares is a slower simulation speed due to the high density meshing of 3-D objects. An offline CAD based electromagnetic analysis starts with the meshing of objects under test. The field components are solved by discretizing the model to triangular or square shapes. High density meshing of the models guarantees a higher simulation accuracy and vice versa but the problem is an extremely large computer memory consumption which

sometimes needs termination due to the system hang. Thus the modeling and meshing should be done by properly accounting for the resources and limitations. The EM field analysis was started by adopting the harmonic propagation studies in the RF module of the COMSOL multiphysics software. Harmonic propagation analysis differs from Eigen mode analysis fundamentally by two main factors:

Firstly, it solves the field equations by accounting for the boundary conditions and secondly it requires proper design considerations for the meshing, feeding port, loop coupling structure etc. Therefore, the simulation results obtained through harmonic propagation EM solvers are colser to the real experiments.

A circular cavity with following dimensions was created in the COMSOL.

Cavity Diameter = a=4.6cm, Cavity Height= d= 4cm

As the intention is to heat water sample by loading it in the circular cavity, therefore, the physical dimensions of the Eppendorf tube available in the laboratory were noted down. To begin with, the impedance boundary conditions were applied and the inner doamin of the cavity was set to air (ε_r=2.2). A Nickle coated copper loop structure of radis 1mm and side length 2cm was introduce inside the cavity for adjusting the coupling strength and resonance frequency. This loop was also necessary for controlling the field strength during cavity perturbation. To excite the cavity with a CW signal, a coaxial port of inner conductor of 1mm radius and outer cladding of 2mm radius was designed, where the domain of outer cladding was defined as air (ε_r=1). One end of the coupling loop was connected to the inner conductor of the coaxial port and the other end was short circuited by the cavity wall.

A 20mm long circular tube with conical end was inserted into the cavity from its top end. The material of the tube was set as PTFE (ε_r=2.2) and its inner domain was set to water (ε_r=74) The tube was used for holding the water with maximum volume 300µL. after specifying the materials, boundary conditions and the solver settings, the complete design was discretized by adopting heavy triangular mesh grid. Although this resulted in extremely long simulation time but the simulated results were found as expected and the E-field was found centered showing the sustenance of TM_{010} mode.

The TM_{010} mode preservation phenomenon will be explained in details in the coming section 5.6.4.

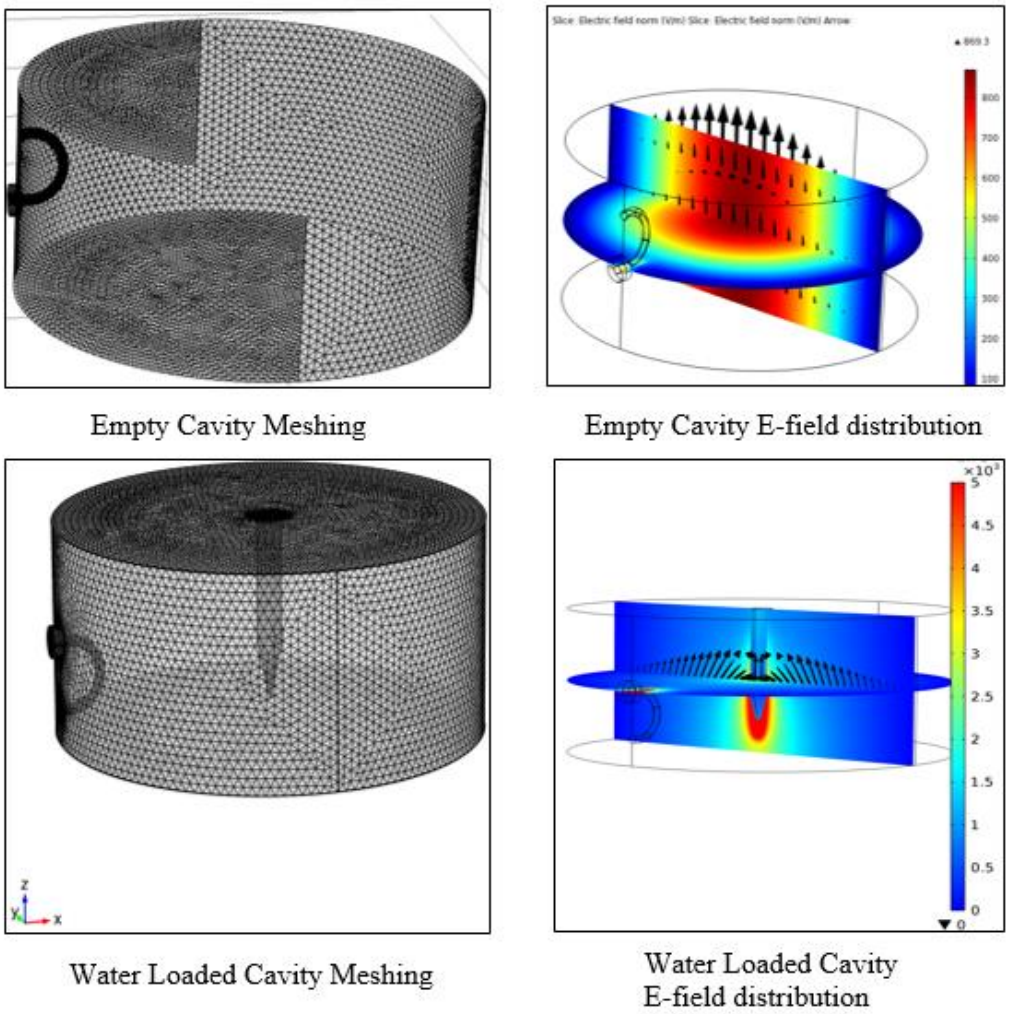

Figure 5.7: Meshing and E-field distribution (V/m) at 2.5GHz in a TM_{010} mode loop coupled circular cavity: (top) Air filled cvity (bottom) cavity filled with 300µL water

5.4.3 Characterization of The Circular Cavity Resonator

After making sure that the sample inserted into the cavity for microwave heating will experience maximum E-Field the next step was to characterize the circular cavity for its resonance and impedance measurements.

Almost all of the materials have their dielectric permittivity greater than 1 therefore, resonance frequency of a cavity resonator decreases when it is loaded with a material, and this is the material perturbation. In order to maintain a good level of coupling, phase and amplitude of the feed into the cavity should be treated very carefully. This can be easily monitored through linear S-parameter measurements. As the intention is

to design a broadband microwave heating structure capable of heating more than one samples therefore, the measurements were taken by loading different volumes of water samples into the cavity resonator. To begin with, a frequency span from 2.34GHz to 7.5 GHz was selected and the network analyzer was calibrated to shift the measurement reference plane from VNA to the input port of the cavity. The purpose for this broad frequency range is to keep track of the fundamental frequency impedance and its integral harmonics with a corresponding cavity material perturbation. Calibration is necessary to record the S-parameters of the cavity only without any influence of the extra cables. The VNA was calibrated for its small signal S-parameter using 8502D keysight Inc. 3.5mm calibration kit. The circular cavity was loaded with 300µL water and connected with the calibrated VNA through a high quality standard coaxial cable as shown in Fig.5.8. The first measurement revealed a significant drop in the *Q* and resonance frequency. This drop was expected because of the high dielectric permittivity of the water sample. Therefore, the coupling level of the cavity was improved by manually adjusting the loop coupling antenna both in the axial and radial direction. It was observed that S11≈-22dB of the cavity can be maintained at 2.365GHz, whilst 300µL water in place. After critically coupling, the n-type connector attached with the loop antenna was screwed and locked to its optimal position for completing rest of the measurements.

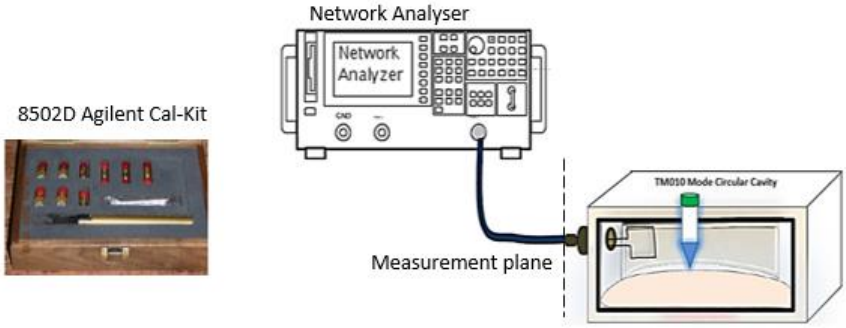

Figure 5.8: S-parameter measurement setup for water loaded circular cavity.

The first S-parameter measurement was taken with 300µL water loaded cavity. For second measurement, 20µL water was reduced from the water filled Eppendorf tube and the S_{11} was re-measured with 280µL water filled cavity. Similarly 3rd measurement was taken with further 20µL water reduction from the tube. The S-parameter measurements were continued following the same process until the last

measurement was taken when the cavity was filled with 100µL. This exercise resulted in 11 S-parameter files of the water filled cavity at room temperature.

After capturing the cavity impedance environment for different volumes of water, the next stage was to import it into the nonlinear CAD environment so that the measured cavity data can be used as passive load together with the power amplifier. Therefore, the measured S-parameter files were combined and arranged into a single *mdif* file format and '*water volume*' was specified as the impedance controlling variable. The post measurement data processing into CAD environment was followed using the detailed method already outlined in Chapter-4. After data import and passive load formation, an S-parameter sweep was conducted to observe the overall resonance and impedance environment of the cavity with varying water volume. The measured results are shown in Fig.5.9 (a) and 5.9(b).

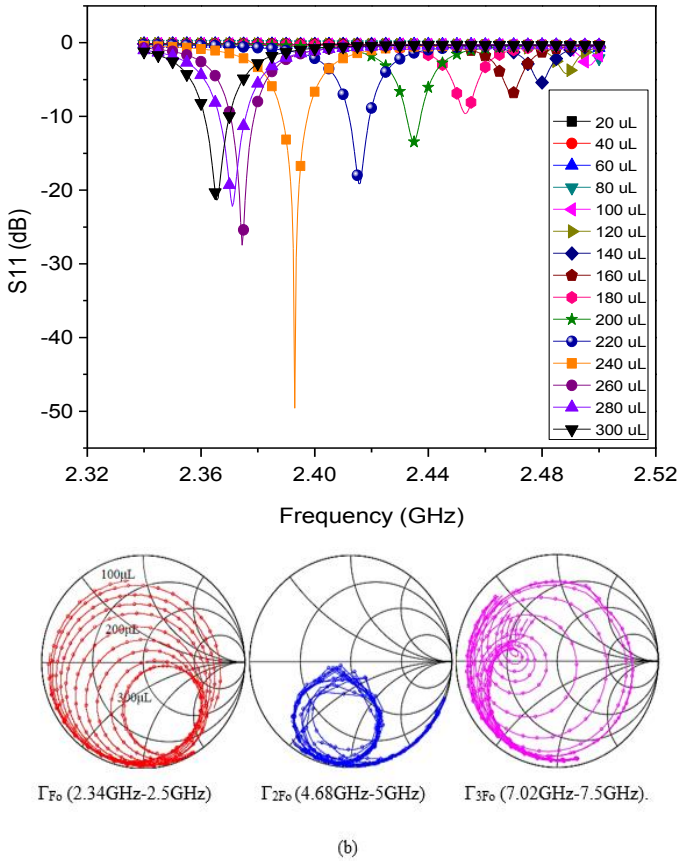

Figure 5.9: Measured TM_{010} mode circular cavity response due to varying water volume (a) Resonance frequency shift (b) Respective impedance change.

The measured results clearly show that the resonant frequency decreases as we increase the volume of the water which is due to sample length impact on cavity resonant properties. For a deeper analysis, this phenomenon can be found in [3] where

the cavity used in this experiment was actually built for material characterization through field perturbation techniques. It can be seen in Fig.5.9 (a) that total resonance frequency shift from 100μL to 300μL is approximately 150MHz which is absolutely within 1GHz range of TM_{010} mode. This means that irrespective of varying loading conditions, the cavity still resonates in TM_{010} mode without interfering with any other neighboring mode so, the E-field in this case will remain focused in the middle of the cavity. Consequently, all levels of water will experience the same intensity of axially concentrated E-field.

Mapping the measured S-parameter response to a smith chart shows that the fundamental frequency impedance changes in a fixed pattern following a clean trajectory which indicates the TM_{010} mode sustenance of the cavity. In contrast, the 2nd and 3rd harmonic loads move on smith charts in a complex way, thus indicating an activation of some of the other interfering resonating modes at these frequencies. Now, the natural impedance change over the fundamental frequency range can be systematically utilized to formulate a directly matched and fully integrated compact heating apparatus. However, to engineer high efficiency waveforms at the intrinsic plane of a transistor, it is equally important to properly account for the harmonic impedances associated with the cavity resonator under varying loading conditions.

Looking at Fig.5.9 (b) reveals that the fundamental and 2nd harmonic load distribution on the smith chart behaves in a deterministic way, and that the harmonic impedance environment, particularly related to the 2nd harmonic has an anti-phased behavior relative to the fundamental loads at the I_{GEN}-plane of the transistor. Consequently, it is possible that the natural changes occurring in the impedance environment of the cavity resonator can be exploited, together with very simple OMN to formulate a continuous mode power amplifier.

As the intention of this experiment is to make a broadband integrated microwave heating structure, a brief theory of the continuous-F^{-1} will be outlined which will help reader in deeply analyzing the continuous-F^{-1} matching conditions in the next parts of this chapter.

5.5 Understanding Continuous-F^{-1} Mode

Recently introduced “continuous modes” allow power amplifiers to operate over significantly wider frequency range by providing systematic fundamental and 2nd harmonic continuous loading conditions to the transistor [5-6]. Literature has revealed

that inverted class-F is one of a number of solutions for obtaining high efficiency operation of the transistor. In this mode, in which the even harmonics are set to open circuit and the odd harmonics to short circuits, results in high *Q*-Factor and narrow bandwidth. Class-F^{-1} can be extended to continuous class-F^{-1} in which the amplifier is engineered to resonate at broad frequency range such that the *Q*-Factor is reduced by spreading it over wider range of frequencies [7]. In continuous inverse-F mode the voltage waveform is half rectified by short circuiting the 3rd harmonic and family of half rectified high amplitude current waveforms is achieved by adding the anti-phase 2nd harmonic set of current components to the fundamental current waveform, as shown in Fig.2.15 in literature review. in this case the performance of an amplifier is spread over a broad frequency range. In the family of power amplifiers, the broadband continuous modes are prefered over narrowband standard high efficiency modes of operation. The first continuous-F^{-1} mode was practically demonstrated by V.Carrubba, et al [8] at Cardiff University in which the GaAs pHEMT was selected to operate in its $C.F^{-1}$ mode at 900MHz using following set of equations.

$$I_{C.F^{-1}}(\vartheta) = I_{dc} - I_1\cos(\vartheta) + I_3\cos(3\vartheta) * (1 - \zeta\sin(\vartheta)) \tag{5.3}$$

Where I_{dc}=0.37, I_1=0.43, I_2=0, I_3=0.06

$$V_{C.F^{-1}}(\vartheta) = 1 + \frac{2}{\sqrt{2}}\cos(\vartheta) + \frac{1}{2}\cos(2\vartheta) \tag{5.4}$$

It can be seen in equation (5.3) that a current waveform is dependent upon the second bracket containing variable parameter ξ. At ξ=0 only the first bracket remains, which gives the squared current waveform due to 3rd harmonic. Now if we look at equation (5.4), there is no term containing ξ, which means that the anti-phaing of the 2nd harmonic load as function of ξ will have no impact on the voltage waveform and it will remain half sinusoidal. However, in practical situations the voltage waveform does vary with the varying current waveform because both voltage and current waveforms are directly related by the knee region of the transistor as can be seen in equation (5.5) [9]

$$I_d(\theta) = V_g . g_m . I_{\max}\left[1 - e^{-\left(\frac{V_{ds}}{V_{Knee}}\right)}\right] \tag{5.5}$$

Where Vgs is the gate voltage, Vds is the drain supply voltage, gm is the transconductance of the transistor, Imax is the maximum available current from the transistor and Vknee is the knee voltage of the device. Generally, during the mathematical analysis of a transistor, the knee voltage effect is neglected so that the drain current is only the function of gate volatge and the device gm profile. But as the knee voltge effect takes place, variation in a current waveform due to the reactive 2nd harmonic also leads to a slightly phase shifted increased half rectified voltage waveform. This can result in increased current and voltage waveforms overlapping area. However, this phenomenon can be addressed predominatnly by adjusting the input drive and gate voltage in-line with the targeted values of ξ within [-1,1] range. Another inevitable factor during matching network synthesis is the harmonic loads sensitivity to the higher frequencies, because at high frequencies the real loads become complex and it becomes difficult to control harmonic impedances for wave-shaping.

Similarly, knee voltage is also a factor which disrupts the output voltage waveform. In the last section of this chapter, knee effect will be visible in output voltage waveform during continuous inverse-F PA formation. Non-'zero-crossing' current waveforms and half rectified voltage waveforms obtained at I_{GEN}-plane guarantee the successful operation of this mode for varying range of $-1 \leq \xi \leq 1$ over the targeted bandwidth.

By applying the following set of equations, continuous-inverse-F waveforms shown in the literature review can be achieved mathematically.

$$Y_{C.F^{-1}} = Y_{opt} * \sqrt{2} i_1 + jY_{opt}\sqrt{2} i_{dc}\zeta \tag{5.6}$$

$$Y_{2,C.F^{-1}} = -jY_{opt} * 2(i_1 + i_3)\zeta \tag{5.7}$$

$$Y_{3,C.F^{-1}} = \propto \tag{5.8}$$

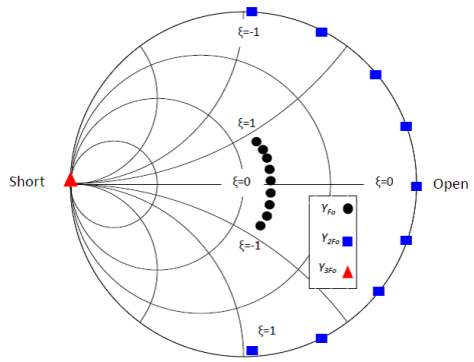

Figure 5.10: Continuous-F^{-1} network topology and I_{GEN}-plane waveforms (admittance chart)

5.6 The Direct Integrated continuous class-F^{-1} Power Amplifier

For direct integration approach it is necessary to outline here that the extra complexity of the matching stubs and filters will lead to a sub-optimal behaviour of the heating apparatus due to the power losses associated with the matching network as well as their large physical size. A correct impedance transformation matching network is a basic requirement for realizing high efficiency PA modes. Low-pass filtering methods using multistage low pass networks stated in [10-11] or stepped impedance transformer stated in [4] [12] can present required loading conditions for high efficiency PA modes designed in 50Ω environment. In our case, we have used a similar stepped impedance transformation approach to match transistor with the selected non-50Ω direct integrated load (cavity) so that the discrete measured load points (cavity) present the continuous mode inverted class-F loading conditions at Igen-Plane of the 10W GaN transistor.

Another great opportunity to reduce the size of an output matching network is to make the built-in package network of a transistor as a part of matching network. The internal, low pass package network of a transistor together with external OMN can present the arranged loading conditions to the current generator. One such technique was prescribed earlier in [13] where the general purpose hybrid continuous mode PA was designed in fixed 50Ω environment. However, the external output matching network together with the package network was extremely large and complicated as shown in Fig.5.11(top).

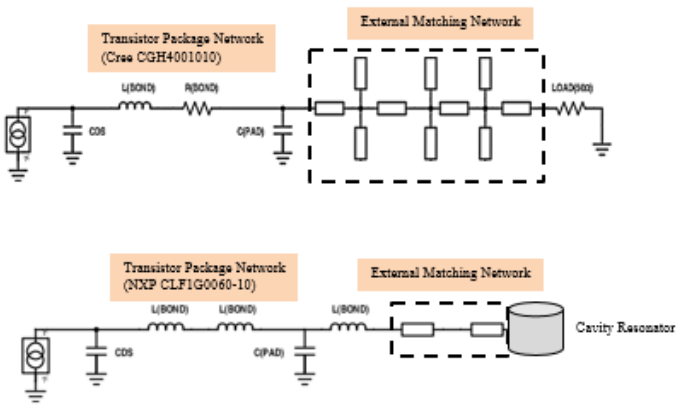

Figure 5.11: Continuous-mode PA design using package network: (Top) general purpose conventional approach, (Bottom) application based direct integration approach.

To design a fully integrated continuous mode PA, we need to directly integrate the transistor to the circular cavity without any extra matching periphery. This means that the circular cavity will be an integral part of the output matching network. In this design technique, the built-in package parasitic network is fixed. Therefore, by a precise selection, the cavity load points from available cavity impedance design space can be arranged at the I_{gen}-plane through delay lines and fixed package network. A continuous class-F^{-1} mode of operation demands an anti-phasing of fundamental and 2nd harmonic loads at the current generator plane of the transistor. This arrangement of reactive loads facilitates the transistor to operate over a wider frequency range. In our case, the cavity loads are spread over a large area of smith chart and distributed over 150MHz bandwidth (2.365GHz-2.5GHz). Therefore, a careful seletion of loads from each distributed circle will allow the amplifier to work over a range of frequencies.

5.6.1 The Integrated continuous class-F^{-1} Harmonic Tuning

The load transformation process was conducted through the interactive ADS match tool which offers a great visualization of '*moving loads'* on a smith chart. The process was started by making a random load point selection together with the stepped series lines of realizable legth and width as part of external matching network. The built-in package network of the 10W-GaN transistor was connected in series with the stepped transmission lines as shown in Fig.5.12. To begin with, cavity load points were carefully selected and transferred to the transistor I_{GEN}-plane togethers with the employed series transmission lines and the fixed package network. After iterative tuning and optimization by using ADS matching tool we were able to present the required continuous-F^{-1} loading conditions over the cavity bandwidth. The lines were tuned and optimized until the fundamental and 2nd harmonic loads were anti-phased at their optimum locations. The simulated results depicted in Fig.5.12 clearly show that by using simple series transmission lines, it is possible to transfer the discrete cavity loads to the optimum points of the transistor realizing a direct integrated continuous mode PA structure.

It is worth mentioning here that it is always not necessarily required fitting the MN behavior to emulate the continuous mode loads cover the full range $-1 \leq \xi \leq 1$ stated in [13]. Therefore, the range $0 \leq \xi \leq 1$ was found easily emulating the continuous mode

F^{-1} loading conditions over the cavity bandwidth (2.365GHz-2.5GHz) as shown in Fig.5.12(a). It is also important to highlight that, the fundamental and 2nd harmonic cavity load points only fulfill the continuous mode F^{-1} loading conditions whereas the 3rd harmonic load is still unaccounted. This is because, 3rd harmonic load is scattering on the smith chart and cannot be perfectly short circuited by a combination of series line and package network. However, an extra short circuited stub designed at 3rd harmonic frequency can short circuit 3rd harmonic thus, giving a perfect continuous-F^{-1} realization. But this will introduce extra power losses and network complexity to the proposed compact and simplified design targeted for portable health-care applications. To determine the impact of 3rd harmonic on the performance of amplifier, 3rd harmonic phase sweep was conducted outside the smith chart and only (1-2%) contribution to the drain efficiency of the PA was observed. Therefore, it was decided to neglect 3rd harmonic load. The simulated results depicted in Fig 5.12(a) clearly show that by using simple series transmission lines, it is possible to transfer the discrete cavity loads to the optimum points of the transistor for making a direct integrated continuous mode PA structure. The impedance numerical values can be seen in Appendix-B .

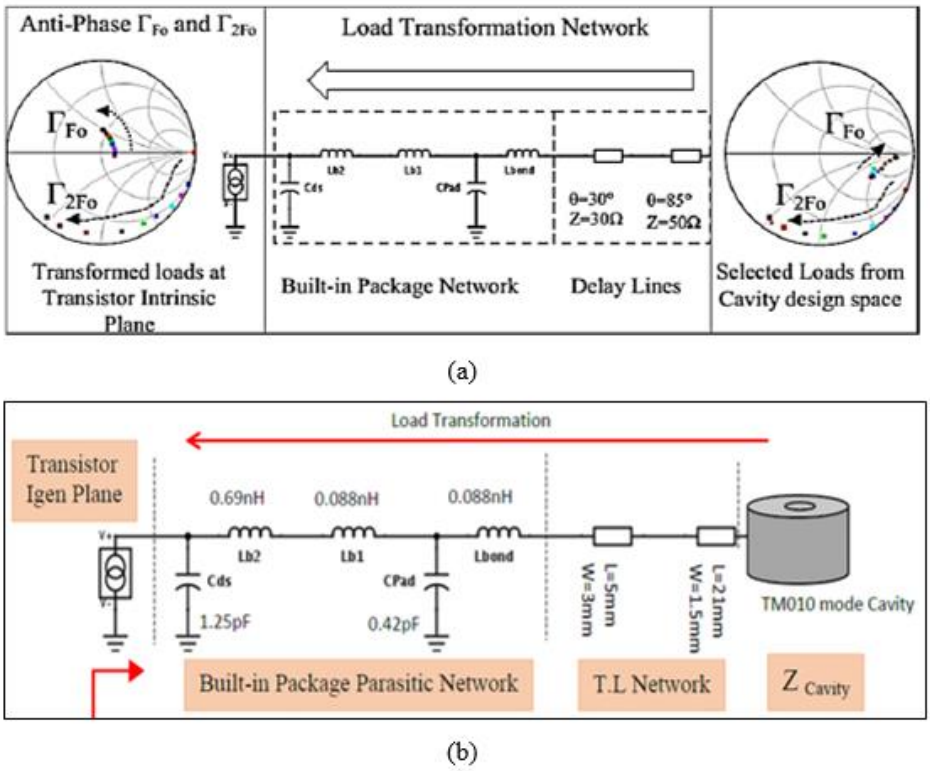

Figure 5.1 2: Harmonic tuning network (a) using ideal lines (b) using microstrip lines.

To form a practically realizable structure, the design was finalized by converting the ideal transmission lines to microstrip lines using RT duroid-5880 substrate (ε_r=2.2,H=0.5mm, Tan(δ)=0.0004) and physical length and widths of the lines were calculated. The final integrated PA design was simulated using ADS harmonic balance simulator and continuous-F^{-1} waveforms were obtained at I_{gen}-Plane as shown in Fig.5.13. For some values of *"ξ"* the waveforms do not ideally represent continuous-F^{-1} PA mode. An obvious reason for this is the sensitivity of current waveforms to the knee votage -effect of 10W GaN transistor as given in equation (5.5). Also, input drive and unaccounted 3rd harmonic load could be the reson as well but, these are still indicatives of continuous-F^{-1} where clearly voltage waveforms are second-harmonic peaking half-wave rectified sinusoidal voltage waveform and current waveforms being extended and phase-shifted.

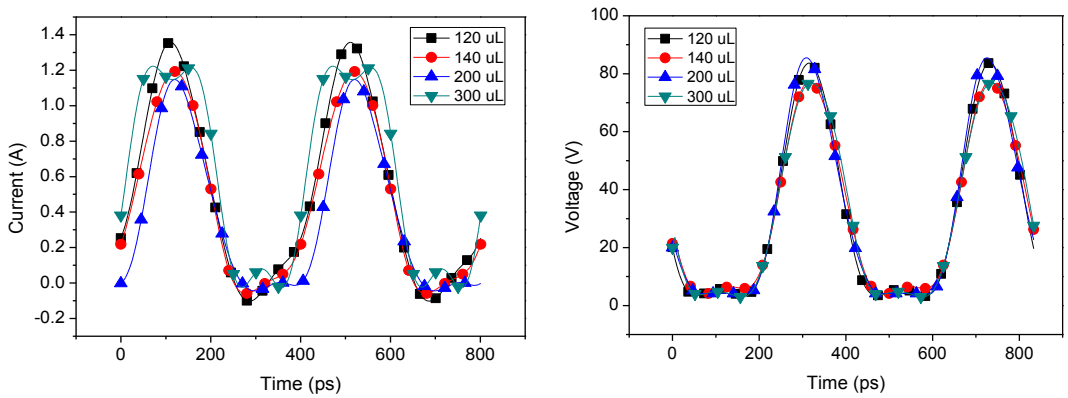

Fig 5.13 Simulated continuous.F^{-1} waveforms obtained following arranged loads at the Intrinsic plane of 10W-GaN transistor using (NXP CLF1G0060-10) transistor package model (Top) current waveforms (Bottom) voltage waveforms.

The efficient RF power delivery into the cavity is another important objective of the integrated health-care apparatus. An efficient and properly designed apparatus not only provides higher PA efficiency but also guides the high power signals to the load (cavity in this case). Thus, after engineering continuous-F^{-1} mode, reflections were observed between cavity and the OMN under varying water volumes. The complete MN including the embedded package parasitic network was simulated separately by presenting the selected cavity loads at right side of the final OMN from 2.3GHz to 2.6GHz. simple S-parameter sweeps were conducted for each of the selected load. Simulation results depicted in Fig.5.14 show that for discrete loading conditions the

return loss of the cavity is closer to -10dB which is quite acceptable because in this case approximately 90% of the power is delivered to the cavity.

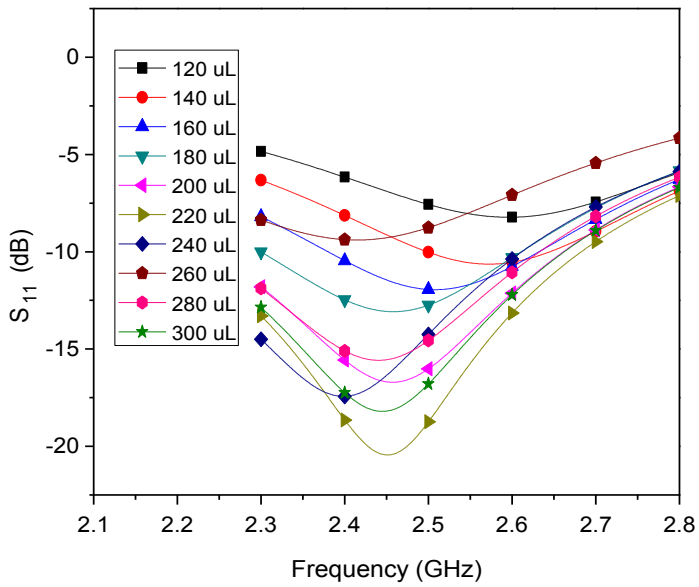

Figure 5.1 4: S11 of the integrated TM_{010} Circular cavity resonator for varying sample volumes.

5.6.2 Directional coupler design and calibration

A properly designed directional coupler is key enabler for realizing a correct degree of mismatch between the source and load. Typical power measurements are taken using conventional standard 50Ω directional couplers where the reflected power from the load is measured and the system performance is monitored (the traditional 50Ω solid state microwave structure with conventional directional coupler can be seen in appendix-1). For one port direct integrated setups, power measurements are very difficult. However, the best possible method for measuring the overall system performance is to couple the output power and monitor its amplitude.

Therefore, a coupled microstrip line of quarter-wave length and 50 Ohm impedance was designed in electromagnetic simulation environment and printed 1mm apart from the main RF-delay lines to couple the delivered RF output power to the load (cavity). The coupling losses during varying water volumes were found to be slightly varying. The possible reason for this variation could be due to the poor directivity of the coupled line directional coupler. Therefore, to best estimate these varying power fluctuations, the measurement activity was followed by ADS simulations of the integrated setup. A neutral RF power probe was inserted in the main RF path to capture

the actual amplified signal, the signal level obtained at this port was set as the standard reference signal. The other power probe was inserted in the coupler's left arm to record the coupled signal appearing at this port. With this arrangement the simulations were conducted and power level appearing at coupler's port was synchronized with the main RF signal by adding the relevant coupling loss. Therefore, the coupled line directional coupler was calibrated for all water volumes by accurately accounting for variable coupling losses. After collecting the information from nonlinear simulations, the measurements were carried on under same conditions.

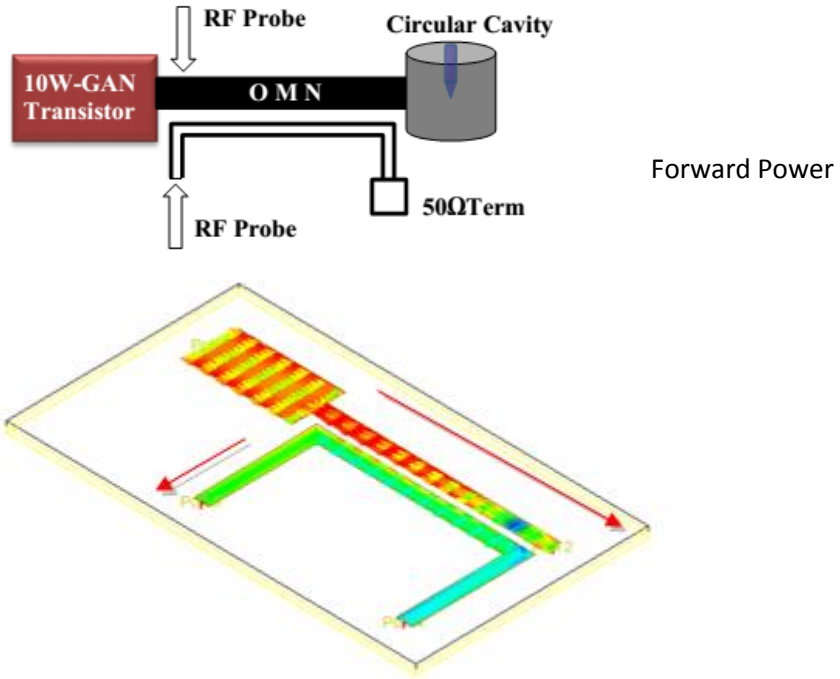

Figure 5.65: Calibration method of coupled line directional coupler
(in electromagnetic simulation environemnt).

After designing the C.F^{-1} integrated structure, the design was fabricated and the PCB board was manufactured. The power amplifier measurements were taken at the couple port of the printed coupled line directional coupler as shown in Fig.5.16

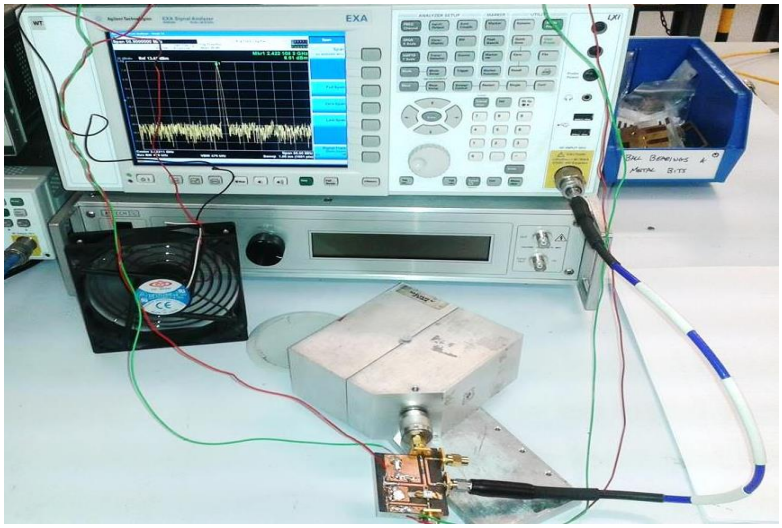

(a)

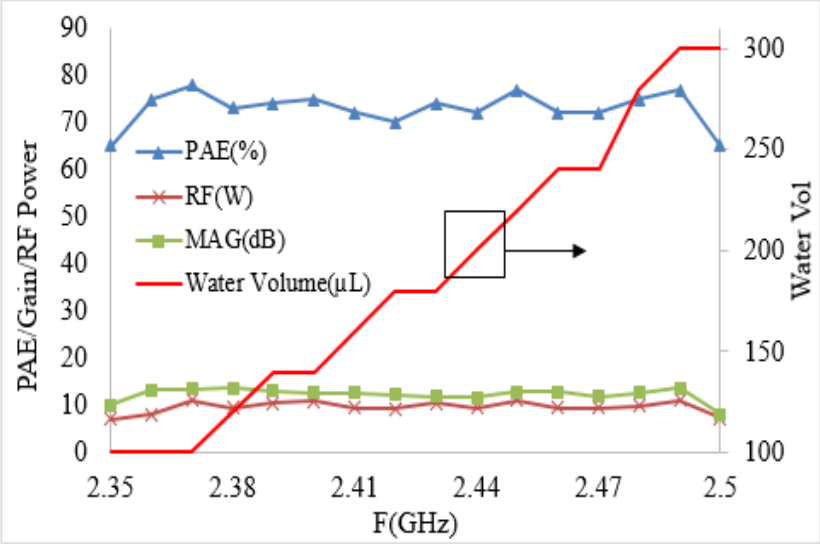

(b)

Figure: 5.16 (a) Microwave heating measurement setup-snapshot (b) Integrated power amplifier measured results (over the cavity functional bandwidth) with varying water volume.

5.7 Summary

In this chapter, a high efficiency and broadband microwave heating structure capable of heating multiple samples of different volumes at a same time have been presented. Such a structure becomes particularly important in the diagnostic healthcare applications, where the DNA of bacteria is released by exposing different sample volumes to continuous high power pulses. This chapter demonstrates the design procedure of a highly efficient compact and continuous mode broadband microwave heating structure. The structure presented in this chapter is capable of delivering high RF power with reduced DC supply and accommodating varying sample volume for

microwave heating. Using the waveform engineering approach the high efficiency continuous inverted-Class-F waveforms have been shaped at the intrinsic plane of the DC-6GHz (CLF1G600-10) GaN transistor. The natural change in the impedance environment of the circular cavity has been accommodated systematically using microstrip delay lines in conjunction with built-in package network. The dircet integrated structure has been designed for high efficiency broadband operation. The extended and phase shifted time domain current waveforms have been shaped by presenting the continuous cavity loads at the transistor Igen plane. The built-in package network together with synthesized stepped microstrip lines allows an anti-phasing of the fundamental and 2nd harmonic load impedances from cavity impedance design space. The ideal transmission lines were converted to microstrip transmisison lines by mapping on to RT-DUROD 5880 substrate. The finally designed power amplifier structure was simulated and 80% drain efficiency, 40dBm output power and 13dB gain was achieved over the functional bandwith of the cavity. To ensure the efficient power delievery, a 50Ω microstrip coupled line directional coupler was mapped at the output stage of the power amplifier to monitor the reflected power from cavity. For accurate measurements, the coupler was calibrated offline in CAD simulation environment and all the coupling losses were accounted. It was demonstrated that the integrated apparatus is capable of hetaing 10 water samples of different volumes at a time with output reflections≤-10dB. The integrated setup was fabricated and tested. The simulated results were found in excellent agreement with the measured ones over the functional bandwidth of the cavity.

To further improve the realiability of the PA structure, the coupled line directional coupler can be calibrated using loadpull measurement system. Due to time limitations, this measurement activity has been left as a future task.

Reference

[1] John L.B.Walker, *Hand book of RF and Microwave Power Amplifiers*, Cambridge University Press 2012.

[2] Amir Sheikh, "High Power Waveform Engineering," PhD Thesis, *Schoolf of Engineering, Cardiff Uinversity UK*, June 2010.

[3] Daniel Slocombe, *"*The Electrical Properties of Transparent Conducting Oxide Composites,*"* PhD Thesis, *Schoolf of Engineering, Cardiff Uinversity UK*, June 2012.

[4] David M.Pozar, *Microwave Engineering*,3rd ed, *John Willey & Sons, Inc.*

[5] V.Carrubb, J.Lees, J.Benedikt, P.J.Tasker, S.C.Cripps, *"* A Novel Highly Efficient Broadband Continuous Class-F RFPA Delivering 74% Average Efficiency for an Octave Bandwidth," *IEEE MTT-S Microwave Symposium Digest*, June 2011, pp.1-4,.

[6] V.Carrubb, A.L.Clarke, M.Akmal, J.Lees, J.Benedikt, P.J.Tasker, S.C.Cripps, "The Continuous Mode Class-F Mode Power Amplifier," *EuMC*, Sept.2010,pp.432-435.

[7] C.Friesicke, A.F.Jacob, "Mode continua for inverse class-F RF power amplifier," *IEEE German Microwave Conference*,March 2011,pp.1-4.

[8] V.Carrubb, A.L.Clarke, M.Akmal, Z.Yusoff, J.Lees,J.Benedikt, S.C.Cripps, P.J.Tasker, "Exploring the design space for broadband Pas using the novel continuous inverse class-F mode," *IEEE EuMC*, October 2011, pp.333-336.

[9] S.C.Cripps, *RF Power Amplifiers for Wireless Communications*, 2nd Edn, Norwood, MA: Artech House, 2006.

[10] G.L.Matthaei,"Tables of Chebyshev Impedance-Transformation Networks of low-pass filter form," *proc.IEEE*,vol.52,no.8, Aug 1964, pp.939-963.

[11] A.G.Malherbe, *Microwave Transmission Line Filters*, Artech House, Dedham, June 1979.

[12] Azeem Imtiaz, Zulhazmi A.mokhti, Jerome Cuenca and Jonathan Lees, "An Integrated Inverse-F power amplifier design approach for heating applications in a microwave resonant cavity," *IEEE Asia Pacific Microwave Conference*, Nov 2014, pp.756-758.

[13] Kenle Chen, Dimtrious Peroulis, "Design of Broadband highly efficient harmonic-tuned Power Amplifier using in-band continuous class(F-1/F) mode transferring," *Microwave Theory and Techniques, IEEE Transactions on*, Vol.60, Issue.12, Dec 2012, pp.4107-4116.

[14] Danish Kalim,Dimitry Pozdaozdniakov and Renato Negra, "A 3.37GHz power amplifier with 77% PAE in GaN HEMT technology," *PhD Research in Microelectronics (PRIME), 2012 8th Conference on*, June 2012, pp.1-4.

[15] Honjo,K, Ryo Ishikawa,Yoichiro Takayama, “Ultra high efficiency microwave power amplifier for wireless power transmission,” *IEEE EuMC, Nov 2012, pp. 1339-1342.*

[16] Taeson Hwang,et al, “Class-F power amplifier with 80.1% maximum PAE at 2GHz for cellular base-station applications,”*WAMICON,2013 IEEE 14th Annual connference, April 2013, pp. 1-3.*

[17] Ying Wang ,et al, “Design of high efficiency GaN HEMT class-F power amplifier at S-band,”*IEEE (APCAP), 2014 3rd Asia-Pacific Conference on, Jul 2014, pp.1157-11585.*

Chapter.6 THE EFFECT OF TEMPERATURE IN SOLID-STATE MICROWAVE HEATING

6.1 Introduction

This chapter considers the impact of temperature on the impedance and resonance environment of a loaded microwave cavity resonator during a microwave heating process. The overall aim of this experimental work is to understand if the temperature dependent changes in the impedance environment of water loaded circular cavity resonator can be accommodated, and in a similar way to volume variation, be exploited during microwave heating. The investigation has focused on the changing microwave properties of water during a representative heating process, where it has been practically demonstrated that a systematic utilization of this change can lead to an efficient, broadband and compact solid-state microwave heating arrangement.

As a sample gets hot, a change in its temperature leads to a change in its dielectric properties. Considering specifically the impact on temperature variation on the microwave properties of water, a number of very interesting phenomena are documented in [1-5], where water samples haven been exposed to both temperature and frequency variations simultaneously, from 0 to 100C and from 1 GHz to THz frequencies respectively (an example can be seen in Fig.6.2).

A water sample placed in a clean impedance environment of a cavity resonator perturbs its resonant properties, an approach called complex material perturbation. It is usual to carry-out material perturbation at a fixed temperature, however, complications arise when the temperature is variable. Therefore, the variations in a water filled cavity complicate its impedance and resonance analysis and it needs proper characterization before any measurement activity.

In the first part of this chapter it will be shown that the resonant properties of a TM_{010} mode circular cavity containing water change with the rise in temperature. The second part shows how this change can be systematically accommodated to design a high efficiency PA working over the functional bandwidth of the cavity during microwave heating process.

The arrangement comprising a TM_{010} mode circular cavity coupled through square loop antenna has been used as temperature dependent load and 10W-LDMOS power

transistor as microwave heating source. Temperature and frequency dependent loads have been presented optimally to the 10W LDMOS power transistor for its efficient operation over the functional bandwidth of the cavity resonator. It has been demonstrated that an adaptive selection of temperature and frequency dependent loads can, not only lead to a reduced cavity reflections but also enables an efficient operation of the PA. The simplest integrated matching structure has been formed by employing simple microstrip series transmission lines together with frequency and temperature dependent impedance loads of the cavity. For performance analysis and size reduction, a microstrip coupled line directional coupler has been printed parallel to the output series lines. Excellent agreement between the simulations and measurements has been observed.

6.2 Design Process

The process of this experiment has been divided as follows:

- Critically couple the 100µL water filled cavity by radially and axially adjusting the inductive loop coupling into the magnetic field inside the cavity, at room temperature.
- Setup the measurement reference plane by calibrating the cavity exactly at its input port so that the S-parameter data of the cavity can be recorded as a function of temperature.
- Place the cavity in the controlled temperature environment so that its temperature can be varied and monitored electronically.
- Vary the cavity temperature in discrete steps and collect the S-parameter data.
- Process the measured data in nonlinear CAD electromagnetic environment to form a temperature dependent passive load (the same method prescribed in chapter 4).
- Within the CAD environment, present the modeled cavity as a synthesized load and use to develop a matching network for the 10W LDMOS transistor, required for making a high efficiency integrated solid-state microwave heating apparatus.
- Verify using a waveform based harmonic load-pull measurement system, and fabricate and test under identified loading conditions and compare the results with the electromagnetic simulations.

6.3 Cavity Resonators and Microwave Heating

Aluminum made single mode resonant cavities are generally designed to operate at low signal levels for material characterization and analysis. For example, composite materials characterization for their applications in electromagnetic screening, radar absorption and plasmonic light trapping etc. [1].

Similarly, the solid-state microwave heating is another very important application where the cavities are driven by high amplitude RF signals. For such applications, the sample to be heated is placed inside the cavity and exposed to high intensity electromagnetic field which then increases its temperature. Therefore, it is necessary that the RF source should be able to generate high power microwave signals to heat the sample within a cavity resonator. RF Power delivered to the cavity, dissipates as heat in the sample and the cavity walls thus resulting in the increased temperature of the sample and the cavity resonator. Temperature is a very important factor that leads to an impedance and resonance change of the microwave cavities during microwave heating.

Most metallic solid objects experience volumetric changes in their shapes after heat absorption which is fine in many traditional heating applications. However, this fact needs careful attention whilst considering high power microwave heating in cavity resonators. For example, shape perturbation in a circular cavity resonator (due to volumetric expansion) will lead to some change in its resonant frequency in accordance with equation (6.1).

It has been observed in this experiment that for well-defined, single mode water loaded circular cavities, there is a bandwidth change per degree rise in temperature which ultimately affects the cavity's resonant frequency and impedance environment. This fact is mainly due to the cavities sensitivity to the water sample temperature, this will be shown later and the chapter will be based on this fact. But, as we are using an aluminum made cavity resonator in our microwave heating experiment therefore, we will also discuss the thermal expansion of cavity resonators during microwave heating in section-2.

6.4 Cavity Perturbations

Perturbation is a useful microwave technique in which the electromagnetic properties of a resonator are disturbed by making some changes in its actual design. These

changes can be made either by modifying the shape of the resonator or by changing the dielectric properties of material inside the cavity. One practical application is to tune the cavity to resonate at a particular frequency by inserting a small metal screw into its volume. This technique can also be used to find out the dielectric constant and Q_d of a certain material under test by measuring the resonance frequency shift [1]. In previous experiments [2], we adopted a technique to find out the impedance and resonance change in rectangular TE_{011} mode cavity by moving the coupling loop antenna and used this method to design integrated microwave heating arrangement. Similarly in [3] we practically demonstrated the cavity impedance shift by different sample volumes and used this natural change to design the microwave heating system. Thus in conclusion, the field environment of a cavity can be perturbed in two ways:

- Material Perturbation
- Shape Perturbation

6.4.1 Material Perturbation

This technique is adopted due to many practical applications linked with cavity perturbations. As we know, the resonant frequency of a circular cavity is dependent upon its dimensions and the material filling the cavity [4] therefore according to equation (6.1) any change in its shape or the complex dielectric constant will lead to a change in its resonant frequency depending upon the resonating mode and the cavity dimensions.

$$f_{nml} = \frac{c}{2*\pi\sqrt{\mu_r \varepsilon_r}} \sqrt{\left(\frac{p'_{nm}}{a}\right)^2 + \left(\frac{l\pi}{d}\right)^2} \tag{6.1}$$

To support the equation (6.1) it is important to understand the dynamic changes in the material due to various parameters associated with time variant microwave irradiations.

6.4.1.1 Applied E-Field and Material Polarization

The dipole moments of water molecules is directly related to the applied alternating electric field. It depends upon the frequency of applied E-field such that the dipole lagging behind the E-field results in energy loss which dissipates power in the form of

heat. As it was shown earlier in chapter 4 that a concentrated alternating E-field is directly related to the power conversion into heat per unit volume, this fact in actuality is due to the phase difference between the E-field and the dipole moment of water molecules.

The applied electric field lags the resulting dipole moments by a phase difference δ so that the higher phase difference results in a higher power loss. Therefore, phase difference, applied electric field and dipole moments define power dissipation in the form of heat [5].

$$|P| = 0.5 * \overline{P}_m * E_{\max} * \omega \sin(\delta) \tag{6.2}$$

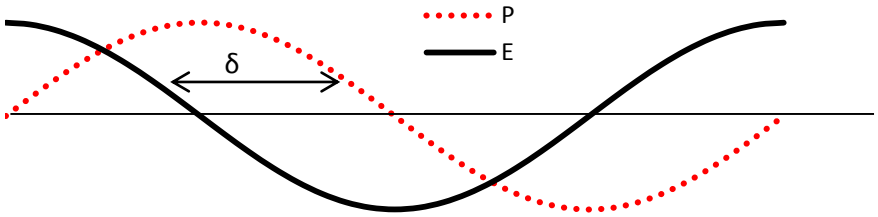

Figure 6.1: E-Field and resulting polarization.

Where $\overline{P}_m$ is the maximum dipole moment resulting by maximum alternating electric field, ω is the frequency of the E-Field and |P| is the power dissipation.

6.4.1.2 Microwave Heating of water

Loss tangent and relaxation time are two very important parameters which are directly related to the electrical properties of a material subjected for microwave heating. These two parameters are primarily responsible for defining the heating efficiency in terms of sample temperature. During microwave heating of water, relaxation time (τ) of water is the time required for water molecules to rotate during an applied electric field [5] and this rotation causes them to collide with each other resulting in inter friction.

$$\tau = \left(\frac{4\pi \times \eta \times r^3}{KT} \right) \tag{6.3}$$

Where r is the molecular radius of water, K is the Boltzmann constant, η is the material viscosity and T is the temperature. From equation (6.3) it is evident that the high

viscosity and larger molecular radius materials have longer relaxation time therefore, such materials require a different frequency of alternating E-filed for efficient heating compared to water for example. Substituting the electrical specifications of water in equation (6.3) results in a relaxation time of 8.27psec at 25C° [5].

Maximum dielectric loss occurs when ω=1/τ, Therefore, for efficient microwave heating, the frequency needs to be carefully selected according to a material under test so that maximum dielectric loss can be achieved. Dielectric loss factor defines the ratio of the electromagnetic energy conversion into heat. Similarly, dielectric loss tangent of a material is another important factor in heating which is given by

$$\tan(\delta) = \frac{\varepsilon_2}{\varepsilon_1} \tag{6.4}$$

Where ε_2 is the loss factor quantifying the conversion of electromagnetic energy to heat and ε_1 describes the polarization ability of the material under applied E-Field. A larger value of tangent loss factor will results in an increased material temperature. As stated in [6], frequency and temperature are two variable parameters that affect the permittivity and the dielectric loss of a material and thus define the microwave heating efficiency and this is specifically true in case of water. To validate this argument, some of experiments were established in [7-8], the water sample was subjected to variable frequency range up to THz and temperature up to 100C. Both parameters were varied linearly and the impact of these two parameters on the resonance properties of water was observed simultaneously as shown in Fig.6.2.

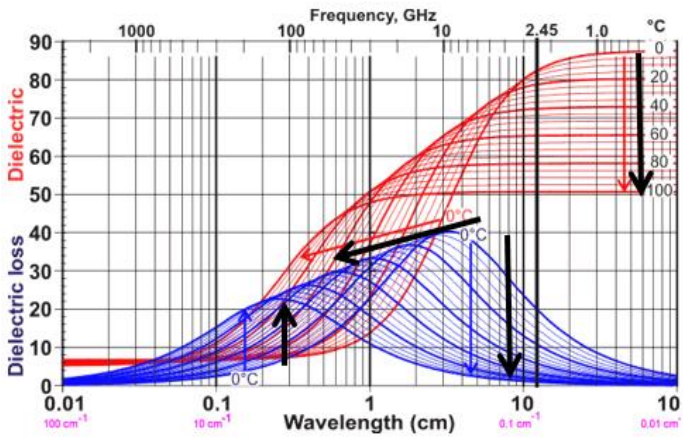

Figure 6.2: Dielectric permittivity and dielectric loss as function of temperature and frequency [5].

It can be observed through Fig.6.2 that starting from very low frequency up to 20GHz, the dielectric loss increases linearly and then, depending upon the temperature, starts decreasing with increasing frequency. It is clear from this characteristic that during microwave heating, the heating efficiency will depend upon frequency selection. In fact, temperature is the second dominant factor that defines the microwave heating efficiency. As the bonding strength between the hydrogen molecules decreases, with increasing temperature this natural phenomenon leads to three interesting facts:

- Lowers the dielectric permittivity of water.
- Due to the decreased hydrogen bonding strength, allows the resonance to occur at higher frequencies (will be experimentally shown later).
- Minimizes the dielectric loss.

Thus if a microwave heating system is designed to operate at a fixed frequency and its surrounding temperature is increased linearly, not only will resonant frequency increase, but also heating efficiency will decrease due to decreasing dielectric loss (see Fig. 6.2). Therefore, to maintain the overall efficiency of a microwave heating system based on a resonant cavity, it is very important to track the "temperature-frequency" relationship during microwave heating. In other words, a correct synchronization between temperature and resonance will keep a microwave heating system matched under all temperature and frequency shifts, and ensure maximum delivery into the sample. It will be practically shown in this experiment that the overall system efficiency of a solid-state microwave heating system can be maintained through dynamic selectivity of temperature and frequency. This is an important study as in the practical application, both volume and temperature of the sample is expected to vary significantly, so being able to design efficient PAs and power delivery systems to accommodate this change is paramount.

To start with, the magnetically loop coupled TM_{010} mode circular cavity designed at 2.5GHz was used for our heating experiment for an obvious reason of centralized high E-field capability detailed in chapter 5.

Initially two measurements were taken at room temperature (T=25C°). The first measurement was taken while the cavity was air filled and the second measurement when the cavity was filled with 100µL water, as shown in Fig.6.3. The critical coupling was maintained by adjusting the short circuited loop antenna.

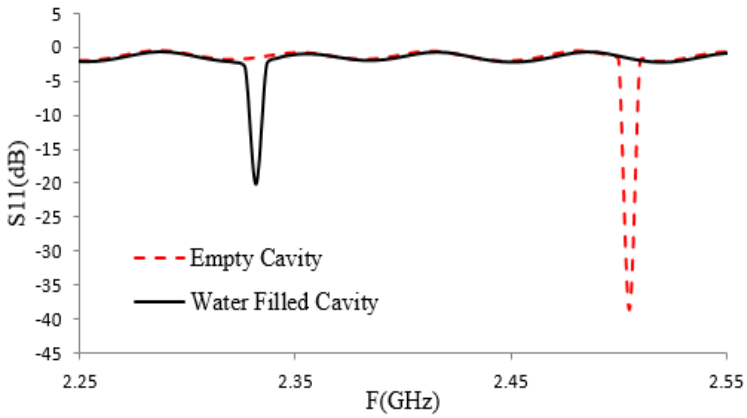

Figure 6.3: Measured resonance behaviour of TM_{010} mode cavity.

Fig.6.3 shows that the resonant frequency of the TM_{010} mode resonant cavity due to high permittivity sample (ε_r=74) has decreased. This result satisfies the inverse relation of frequency and dielectric permittivity as according to equation (6.1). Thus the air filled cavity resonating at 2.5049GHz, now resonates at 2.33165GHz after insertion of a water-filled Eppendorf tube.

6.4.2 Shape Perturbation

To properly account for any possible change in the shape, it is important to consider the temperature effect on the shape of the cavity resonator. According to equation (6.1) any change in the radius or the height of a circular resonant cavity will lead to a change in its resonant frequency depending upon the resonating mode of interest. The following equation adopted in [4] describes how shape perturbation can lead to a definite change in resonant frequency.

$$\Delta\omega = \omega - \omega_0 = -j \times \frac{\oint_{\Delta s} E_0 \times H.ds}{\int_V (\varepsilon E.E_0 + \mu H.H_0) dv} \tag{6.5}$$

Where ΔS is the differential change in the surface area of the object and Δω is the change in bandwidth related to ΔS.

6.4.2.1 Shape Perturbation Due To Thermal Expansion

A change in the volume of an object due to a change in its temperature is called thermal expansion. This is a natural characteristic of any matter, such that when an objects get hot, the kinetic energy of the molecules increase. The increased kinetic energy of the

molecules results in an increased average separation between them that ultimately leads to a volumetric expansion. It is not always true that all the materials expand after absorbing heat energy because some materials have negative temperature coefficient and they contract after heat absorption [9]. There are different forms of thermal expansion, for example in linear expansion the matter expands in the direction of its length due to linear expansion coefficient (length expansion per degree rise in temperature). Similarly in volume expansion, the matter expands as a whole and experiences equal increment in its length, width and height which is due to the volume expansion coefficient (volume expansion per degree rise in temperature).

For solid objects under controlled pressure, the volume expansion coefficient can be calculated using equations (6.6-6.7) [10]

$$\frac{\Delta V}{\Delta T} = \int_{T_1}^{T_2} \alpha_V(T)dT \tag{6.6}$$

$$\alpha_V = \frac{1}{V}\frac{d}{dT}(V) \tag{6.7}$$

Where V is the volume of the object and $\frac{dV}{dT}$ is the rate of change of volume with respect to temperature. Almost all matters have already been catalogued in [11] for their thermal expansion coefficient values. Therefore, if we know the thermal coefficient of a matter, its volumetric change as function of temperature can be calculated using equation (6.7).

For circular cavity resonator, the volume can be calculated using equation (6.8)

$$V = \pi \times a^2 \times d \tag{6.8}$$

Where, *a* is the radius of the cavity, and *d* is the height.

Substituting this value in equations (6.6-6.7) will give the volume expansion with respect to the temperature variation in the circular cavity. Now according to equation (6.1), the resonance frequency of a circular cavity is dependent upon its radius and height. Therefore, following the above set of equations it can be easily concluded that the temperature change in a circular cavity will result in a differential change in its resonant properties depending upon the level of expansion.

However, compared to the temperature dependent material perturbation, the shape perturbation of the cavity is almost negligible. To validate this argument, the experiment was performed in which the impedance and resonance properties of TM_{010} mode circular cavity was closely observed by capturing its temperature dependent S-parameter data over a wide frequency range. The experiment was performed under electronically controlled and thermally isolated temperature environment. The natural change in the impedance environment of the cavity was later accommodated in the PA matching process, to formulate a simplified microwave heating arrangement that will be explained later in this chapter.

6.5 Controlled Heating Arrangement

Microwave cavity resonators are very sensitive to any external interference therefore, the measurement test bench needs to be stable and isolated for ideal measurements. Before starting the temperature dependent impedance analysis of microwave cavity, thermally isolated and electronically controlled heating arrangement was setup and the 100µL water filled TM_{010} mode circular cavity was placed in thermally isolated controlled temperature chamber. Where the complete setup contains:

- MEMMERT oven (thermally isolated heating chamber)
- OMEGA sensor (high sensitivity temperature sensor)
- DAQ (National instrument's *Data Acquisition* device)
- PC
- Microwave Cavity Resonator
- VNA (Vector Network Analyzer)

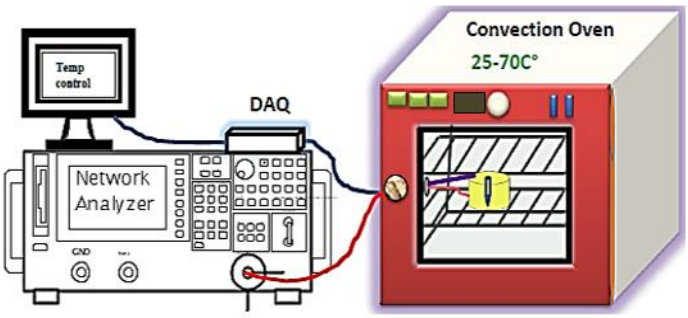

Figure 6.4: Electronically controlled and thermally isolated heating arrangement

6.5.1 Calibration

Calibration is the first step before starting the measurements of the cavity resonator. In this step, the effects of the cable attached between the cavity and the VNA is negated by performing one port standard calibration. An 8502D standard 3.5mm Keysight calibration kit was used to move the measurement reference plane to the single port of the cavity to negate the phase delay incurred by the extra piece of coaxial cable and to capture the true response of the cavity. This is specifically important because we are intending to design the compact microwave heating arrangement by directly integrating the PA with the cavity without introducing any extra network between the source (PA) and the load (cavity), and measuring complex load accurately is key.

6.5.2 MEMMERT Oven

It is a thermally isolated heating chamber with enough inside space to homogeneously heat many samples at a time. It has couple of holes furnished on both side walls to insert extra cables and sensors to attach with the cavity resonator. The simplified temperature controlling click buttons and the digital display make this heating chamber user friendly and straightforward during measurement process.

After calibrating the system, the heating chamber temperature normalization is the second step. The oven was turned on using the main center push button and the water filled TM_{010} circular cavity calibrated to its input port was connected to the VNA and placed in the heating chamber. The initial temperature 27.5C° was selected and then oven was tightly closed. The average time required for homogeneous heat distribution inside the oven is between 25 to 30 minutes. The temperature can be seen through the digital display on the front wall of the chamber. Therefore, the oven was left for approximately half an hour to warm up to 27.5C°.

6.5.3 OMEGA Temperature Sensor

Although the heating chamber has a digital display of the chamber inside temperature but it was observed that there is nearly 1C° error in the temperature when compared with the temperature measured through probe sensor. Therefore, to assure the measurement accuracy, the OMEGA RTD high sensitivity temperature sensor was used to monitor the true inside temperature. The delicate sensor probe clung to the outer surface of the cavity resonator senses the actual temperature change in the cavity

and the Labview program running on the remote PC picks this information through DAQ (data acquisition device). Therefore, the temperature measurement setup consisted of PC, DAQ and temperature sensor allows the most accurate temperature measurements of the TM_{010} circular cavity resonator.

6.5.4 Network Analyzer

Vector Network Analyzer is the external RF measurement instrument used to capture the S-parameter data of the cavity resonator as a function of temperature. The detailed process of capturing the temperature-dependent S-parameters of the cavity resonator has been outlined in the next part.

6.6 TM_{010} mode Circular Cavity Characterization

After setting up the electronically controlled oven, and allowing to stabilize for half an hour, the cavity temperature 27.5C° was observed on the remote PC display.

It is important to mention here that the VNA was calibrated separately three times to cover the fundamental, 2nd and 3rd harmonic frequencies of the cavity resonator. The calibration files were stored in the VNA for their use during measurement activity. The reason for this choice was to accurately pick up all the frequency points for fundamental, 2nd and 3rd harmonic components through frequency high resolution. Also, it was thought that the single mode cavity resonator may show only a very small frequency-impedance shift at harmonic frequencies during temperature variation, so to cover the large frequency span in sufficient frequency resolution, a segmented frequency measurement approach was adopted. Therefore, a single bigger frequency range was divided in 3 segments of adequately large spans. The first frequency span was selected from 2.2GHz-2.6GHz spread over 21000 frequency points so that any resonance frequency shift with a 19 KHz resolution was possible. Similarly, the 2nd harmonic frequency span was selected from 4.4GHz-5.2GHz and 3rd from 6.6GHz-7.8GHz. In this case, each time we increase the temperature, the relevant calibration files have to be used to record the S-parameter data of fundamental, 2nd and 3rd harmonic. The temperature range was selected from 27.5C° to 70C° (Heating Chamber's Limit). To capture the impedance and resonance shift in the well-defined impedance environment of the water loaded circular cavity, the inside temperature of the heating chamber was varied linearly within 27.5C° to 70C°. The first S-parameter

measurement for fundamental, 2nd and 3rd harmonic was taken at 27.5C° using their corresponding calibration files. For second measurement, the temperature was increased by a step of 2.5C° such that the next S-parameter measurement should be taken at 30C°. Therefore, oven temperature was allowed to normalize at 30C° for next 30 minutes. After seeing 30C° on the remotely attached computer display, second S-parameter measurement was taken. For 3rd measurement the temperature was increased further by a fixed step of 2.5C° and measurements were taken at 32.5C°. The temperature dependent measurements were conducted by following the same process until the last measurement was taken at 70C°. This exercise resulted in 54 temperatures dependent S-parameter files of the water loaded TM_{010} mode circular cavity. The S-parameter response was captured individually for fundamental, 2nd and 3rd harmonic frequencies so that the harmonic components can be utilized to shape the voltage and current waveform during integration with the transistor. It is specifically true for F^{-1} mode of operation using Si-LDMOS power transistor. Therefore, to properly account for the 2nd and 3rd harmonic frequency impedances, it is important to have correct impedance information at these frequencies

6.6.1 Post Measurement Data Processing

To allow solid-state microwave heating arrangement in CAD simulation environment, the 54 measured S-parameter files were arranged in a single MDIF (multi-dimensional index format) file where each data set in the file was holding the actual cavity S-parameters at a specific temperature. By following the process already detailed in Chapter-4, the passive load was formed by using ADS S_{1P} data item which was able to load the actual temperature dependent S-parameter files of the circular cavity. The independent variable "*temperature*" was chosen in non-linear circuit simulator environment so that by varying the temperature, the cavity's offline impedance and resonance response can be monitored. Thus, before making a real integration of cavity and power amplifier, it was possible to have a good estimation of how the integrated setup will perform in reality. This setup allowed a straight integration of the cavity with the 10W-Si LDMOS software package model. The measured cavity resonance response of the water loaded cavity over temperature variations (27.5 C° to 70C°) is shown in Fig.6.5.

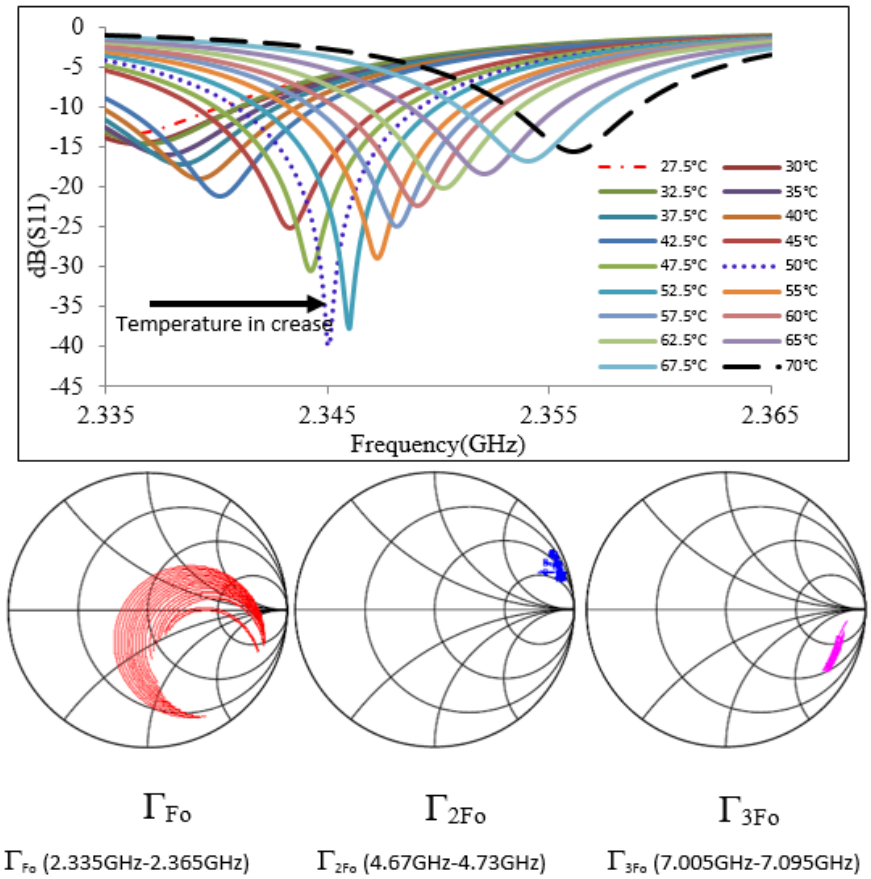

Figure 6.5: Impact of temperature sweep (27.5 C° to 70C°) on the cavity (top) resonance environment (bottom) impedance environment

The results depicted in Fig.6.5 (top) highlight the cavity's resonance shift as function of temperature and also agree with the investigations made in [7-8]. A close observation reveals that from 2.335GHz to 2.365GHz, a total of 30MHz bandwidth is available from (27.5C° to 70C°) with reduced reflections. Therefore, a proper characterization of temperature and frequency allows a proper investigation into the possibility of making the cavity behave as a broadband, continuous load during microwave heating process. Also, this naturally available bandwidth can be utilized to allow power amplifier to operate over that band without introducing any broadband network topology. A mapping of the measured S- parameters on the smith chart shows that the temperature dependent impedance environment of the cavity. Whereas the fundamental is quite active, the harmonics remain relatively static. Therefore, it can be inferred that the material perturbation (water temperature in this case) to the single mode TM_{010} cavity not only leaves the TM_{010} dominant mode unperturbed but also the higher resonating modes as well. As the cavity is working in its TM_{010} mode with next

mode frequency spacing of 1GHz therefore, sustenance of TM_{010} dominant mode will ensure a focused and centralized E-Field distribution over the available bandwidth (30MHz<<1GHz). An efficient direct integrated matching network synthesis is easier when load spread on smith chart is rich, because it gives designer more freedom to systematically select and transfer the loads at I_{gen}-plane of transistor. Now, a closer look at Fig.6.5 shows that the 2nd and 3rd harmonic loads are restricted to a small area of the smith chart which means, a waveform engineering enabled high efficiency mode PA may not be possible to achieve through simplified series matching network. This naturally appearing phenomenon will be discussed in section 6.6.1 during direct integrated PA design.

6.7 Transistor Characterization

The temperature dependent resonance behavior of the cavity presented in Fig.6.5 shows that the TM_{010} mode cavity gets critically coupled at 2.345 GHz where the temperature is 50C°. Therefore, as a starting point, single frequency narrowband integrated power amplifier structure was intended to design. Although, the 10W Si-LDMOS power transistor has already been characterized in chapter. 3 for 900MHz and in Chapter. 4 for 2450MHz through load-pull measurement system and we know the accurate information of its optimum impedance points both at package plane and current generator plane. But to check its response at 2.345 GHz, a rapid approach was adopted this time by using the ADS load-pull simulation template. To start with, the transistor was biased at its class-AB point to allow the transistor to draw sufficiently high drain current. The harmonic load tuner was applied at the package plane and fundamental, 2nd and 3rd harmonics were varied around the smith chart. By following the same process already highlighted in details in previous chapters, nearly the same performance was observed with slight impedance offset than the measured results.

Reference Plane	● $Z_{Fo}\,\Omega$	■ $Z_{2Fo}\,\Omega$	▼ $Z_{3Fo}\,\Omega$
Package	8+j0.65	3+j*30	2-j*15
Current Gen	20+j*0.55	0+j*42	0-j*5

Table 6.1: BLF6G27-10G LDMOS Power Transistor Measured Impedances at package and I_{GEN}-planes

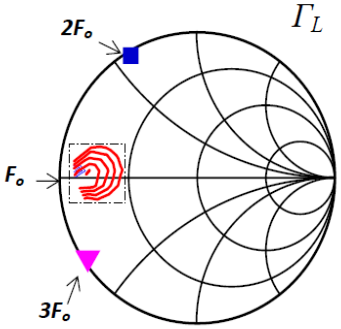

Figure 6.6:impedance load points at the package plane at 2.345GHz.

6.8 Integrated Narrowband F^{-1} Power Amplifier Design

Under optimal solid-state microwave heating conditions, the power amplifier should be subjected to its best output performance and the resonant cavity should be critically coupled for maximum power transfer. Therefore setting up this goal for integrated structure, the temperature and frequency load points were selected where the cavity was critically coupled i.e. Z_{fo}=50Ω as shown in Fig.6.5. Now, after characterizing the transistor at 2.345GHz and locating its optimum impedance points, the next step was to present the cavity as a passive load to the transistor at this frequency so that by applying simplest matching network, the natural cavity impedances could be presented to the transistor. Therefore, at critical coupling point, the impedance points were selected so that they can be transferred to the transistor I_{gen}-plane during integration. In order to formulate the integrated setup, the harmonic tuning techniques using series stepped microstrip lines already referenced in chapter.4 and chapter.5 were applied to transfer the cavity loads to the transistor at the current generator plane. The ideal transmission lines were tuned until the cavity load points were transferred to the transistor $_{Igen}$-plane and the inverse-F voltage and current waveforms were observed.

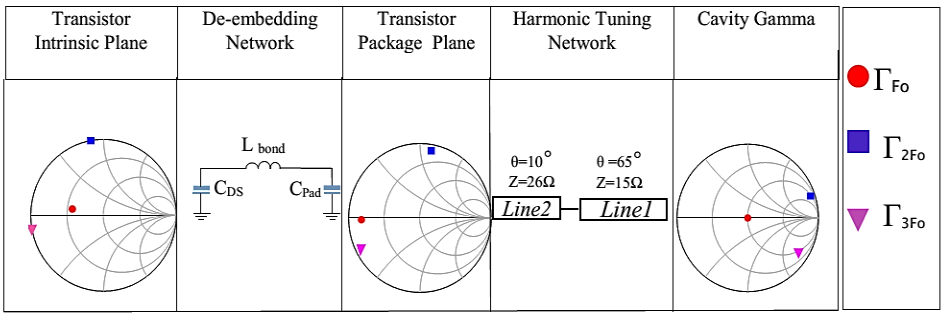

Figure 6.7: Inverse-F Harmonic Tuning Network at F=2.345GHz and T=50C°

The de-embedding network provided by NXP Inc. was used to de-embed the package parasitic network associated with the current generator. The simulation results shown in Fig 6.8 clearly resemble the one obtained in Chapter.4 during inverse-F wave forming. Therefore, this was further verified by observing the inverted class-F waveforms at the I_{gen}-plane as shown in Fig.6.8.

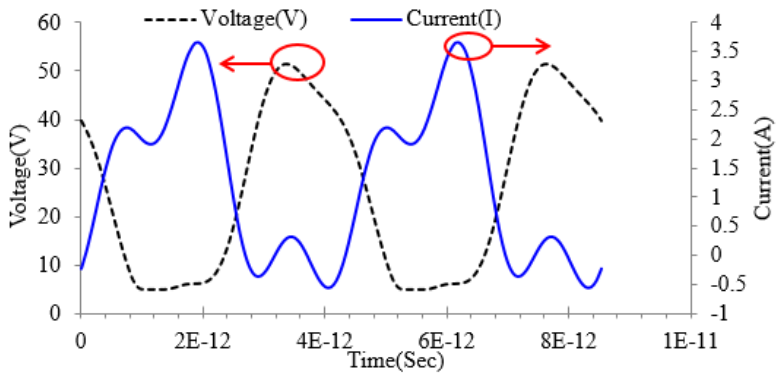

Figure 6.1: simulated Inverse-F voltage and current waveforms at Igen plane

Cavity Impedances at temperature 50C°			Delay Line-1		Delay Line-2	
● Z_{Fo} (Ω)	■ Z_{2Fo} (Ω)	▼ Z_{3Fo} (Ω)	E_1	Z_1	E_2	Z_2
50	150+j*966	107-j*300	65°	15Ω	10°	26Ω

Table 6.2: integrated harmonic tuning network synthesized values.

It is true that the intrinsic waveforms obtained in this case are capable of generating high RF power but it is also true that this integrated structure can only operate at fixed temperature and frequency. Therefore, with the rise in temperature the well-defined fixed cavity loads will displace and the performance of the integrated setup will start degrading. The temperature and frequency dependent natural change associated with the impedance environment of the water holding cavity needs to be fully accounted for so that the robust microwave heating structure could work over the differential cavity bandwidth (30MHz). Therefore, it was decided to design a broadband solid-state microwave heating apparatus capable of accommodating complete temperature range (27.5C° to 70C°) over cavity bandwidth (2.335GHz to 2.365GHz).

6.9 Integrated Broadband Power Amplifier Design

The complex even and odd harmonics generated by the non-linear devices like transistor can be effectively utilized to engineer continuous mode high efficiency output voltage and current waveforms [12]. But unfortunately very complex and lossy harmonic traps are required that result in extra bulk and a cumbersome network synthesis [13]. Therefore, when it comes to a compact, physically small and direct integrated structures, these frequency sensitive harmonic traps are not suitable and cannot perform efficiently.

From impedance design space of the cavity, the selection of load points can be made to systematically transfer at the current generator plane of BLF6G27-10G LDMOS power transistor for continuous mode intrinsic wave-shaping. But it is important to understand here that using temperature and series lines as tuning parameters; it is very difficult to realize a true continuous mode voltage and current waveforms in the PA-Cavity integrated structure. It can be seen in Fig.6.5 that the measured cavity impedance environment for 2nd and 3rd harmonics is very much restricted and we find very narrowband load spread over the smith chart. Thus the temperature dependent impedance environment possessed by TM_{010} mode circular cavity together with simple series lines is not enough to anti-phase the fundamental and 2nd harmonic loads systematically over the targeted bandwidth. Therefore, due to the naturally limited impedance environment and compact matching network restrictions, it is almost impossible to shape the voltage and current waveforms by systematically utilizing the 2nd and 3rd harmonic loads over broad frequency range. However, together with a broadband harmonic tuning network, comprising of series lines and shunt stubs, the harmonic loads can be well arranged over the cavity functional bandwidth but then the benefits associated with the direct integration approach will simply disappear.

Therefore, it was decided to adopt the rapid approach by presenting the inherent cavity broadband loads at the package plane of the transistor using the direct integration method through series lines. Thus the choice was made by setting up two main goals:

1. The power generated by amplifier should be delivered to the cavity by minimizing the reflections as much as possible over the operational bandwidth of the cavity.

2. The power amplifier should be able to work efficiently over the targeted bandwidth by accommodating the frequency and impedance change as a function of temperature.

To finalize the integrated broadband PA structure, it was decided to proceed without targeting the true continuous mode power amplifier due to restricted harmonic loads. Therefore, by using the passive load tuning approach explained in literature review, the measured reflection coefficients of the cavity were varied by varying the cavity temperature and minimum 60% efficiency, 40dBm RF power and 20dB gain was set as targeted parameters. By using the ADS built-in matching tools, the harmonic tuning environment was setup to make a direct offline integrated design. Discrete load points (function of temperature and frequency) were selected and tuned together with series microstrip lines for an efficient transfer to the 10W-LDMOS transistor's package plane. The load transfer strategy is shown in Fig.6.9 where a clear transfer of fundamental, 2nd and 3rd harmonic selective loads can be seen over the available cavity bandwidth. The process of picking up the cavity loads together with series lines tuning was iterated until the simulation results showed an optimal transfer of loads as shown in Fig.6.9. The impedance numerical values can be seen in Appendix-C .

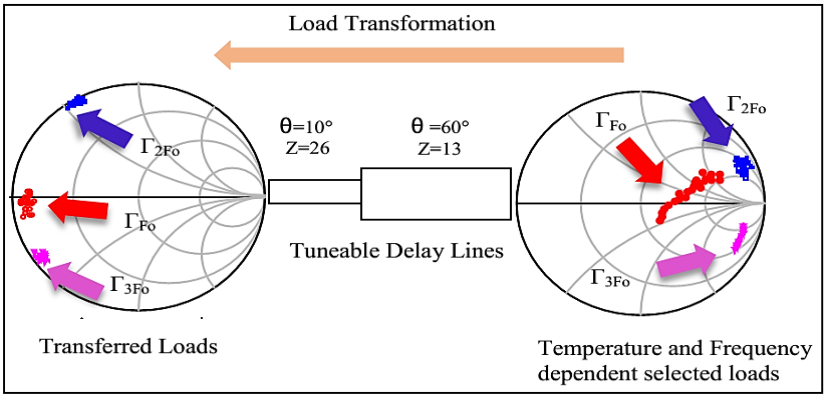

Figure 6.9: Broadband High efficiency tuning network using series delay lines

It is worth mentioning here the selected discrete load points exist at discrete frequencies and temperatures point such that the structure can operate for only discrete conditions. But it was further investigated that the continuous selection of the temperature and frequency can help formulating a broadband microwave heating structure over a continuous bandwidth. In other words a continuous high efficiency of the PA can be maintained by temperature and frequency selectivity. To finalize the

integrated design, the ideal lines were converted to microstrip lines using RTduroid 5880 substrate and lengths and widths of the lines were calculated using ADS Lincalc simulation tool. And since the bandwidth is only 30MHz, the PA was found operating efficiently over this band with the reduced cavity reflections as shown in Fig.6.11.

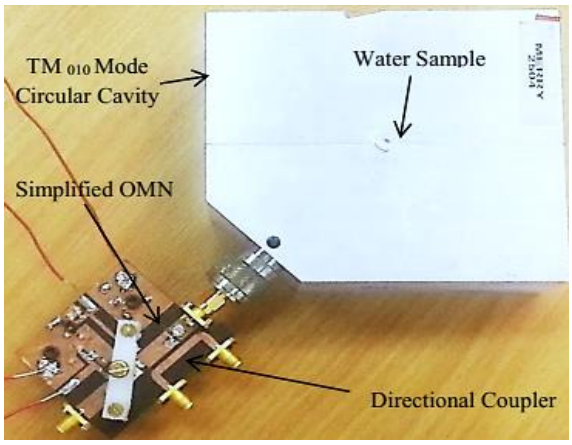

Figure 6.10: Broadband High efficiency integrated microwave heating structure

The benefits associated with the coupled line directional coupler for power measurements have already been outlined in previous chapters. Therefore a 50Ω microstrip line 1mm apart was coupled with the series lines that enabled the reflection and PAE, RF output power and gain measurements of the power amplifier as shown in Fig.6.11. The calibration of the coupled line coupler was conducted by placing the built-in power probes at the main RF path and the coupled arm of the coupler. As outlined in chapter 5, the main RF probe was set as a reference probe because, the power picked at this port will have no influence of any coupling and it will be the original power generated by the amplifier. After capturing the power and calculating the drain efficiency at the main RF path, the coupled power appearing at the coupler was adjusted according to the reference and the calibration procedure was accomplished. The temperature and frequency variations were applied in the real measurement setup and the measurement results achieved at the coupled ports were compared with the simulation results. Performance of the integrated power amplifier as a function of frequency and temperature was measured over the specified range of frequency (2.335GHz to 2.365GHz) and the results were compared with the simulations.

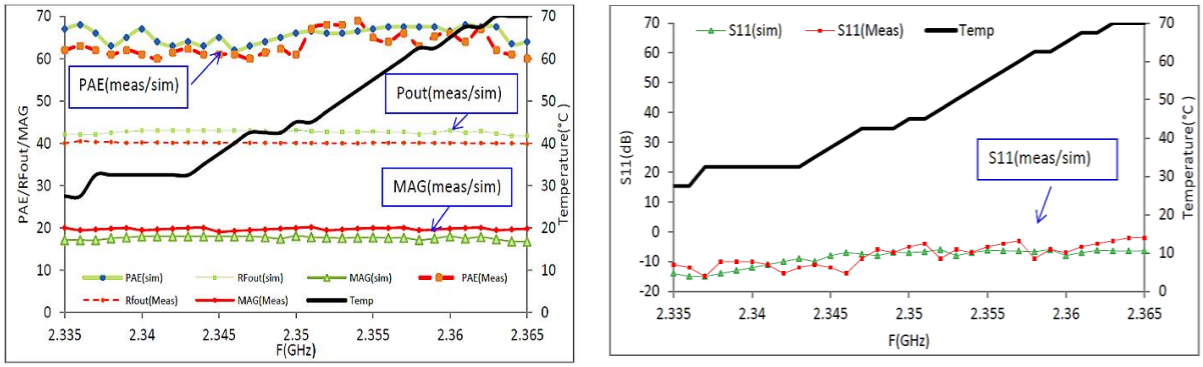

Figure 6.11: Broadband High efficiency microwave heating structure (measurement vs simulations).

6.10 Summary

Temperature is a natural phenomenon of any heating system where it is an important figure of merit in defining the heating system efficiency. For example in conventional microwave ovens, food temperature averaged over time defines its efficiency. But since the magnetron based heating systems are highly inefficient due to uneven and unpredictable microwave energy distribution; therefore solid-state microwave heating is another efficient heating method. It is true that cavity resonators used in Solid-state microwave heating structures possess clean impedance environment that can be exploited to make high efficiency power amplifier modes, but it is also true that these resonators are also sensitive to any perturbation whether it is the shape perturbation or the material perturbation. In this chapter we have shown both cases in which the cavity resonance properties change. The main objective of the experiment presented in this chapter was to observe the changes in the cavity's impedance and resonance behavior with the temperature variations. We found that as the sample holding cavity gets hot, it experiences material perturbation due to the permittivity and dielectric loss decrease which leads to its impedance and resonance change.

Using the load selectivity and the frequency tuning techniques, two integrated structures have been suggested. The first of these is a narrowband solid-state microwave heating structure which can only work at fixed temperature and fixed frequency. The second one is the broadband structure but the PA mode identification is not possible due to restricted harmonic cavity impedance environment. In a broadband design approach, we have accommodated the natural temperature dependent impedance change by employing simple series delay lines between

temperature variant cavity resonator and the 10W LDMOS power transistor such that with the temperature and frequency variations a broadband microwave heating structure can be designed. To realize this setup, this concept was put into practice by fabricating the PCB on RT Duroid 5880 Substrate and directly attached it with the TM_{010} mode circular cavity. The measurement showed excellent agreement with the simulated results.

Reference

[1] Daniel Slocombe, *"*The Electrical Properties of Transparent Conducting Oxide Composites,*"* PhD Thesis, *Schoolf of Engineering, Cardiff Uinversity UK,* June 2012.

[2] Azeem Imtiaz, Zulhazmi A.Mokhti, Jerome Cuenca and Jonathan Lees, "An Integrated Inverse-F power amplifier design approach for heating applications in a microwave resonant cavity," *IEEE Asia Pacific Microwave Conference, Nov,2014, pp.756-758.*

[3] Azeem Imtiaz, Jonathan Lees and Heungjae Choi, "An Integrated Continuous F^{-1} Mode Power Amplifier Design Approach for Microwave Enhanced Portable Health-Care Applications,", *IEEE-MTT-S IMWS-Bio Mini Special Issue,* no.1,vol.1, Apr 2015 US.

[4] David M.Pozar, *Microwave Engineering*,3rd ed, *John Willey & Sons, Inc.*

[5] Water structure and science *http://www.lsbu.ac.uk/water/microwave_water.html)* ,Date accessed March 20, 2015

[6] Akerlof G., Oshry H.I., "Dielectric Constant of Water at High Temperaturs and in Equilibrium With its Vapor," *Chem.Soc.72,* 1950, pp.2844-2847.

[7] J.B.Hasted, Liquid Water: "Dielectric Properties in Water A comprehensive treatise," *Vol 1, Ed.F.Franks,* New York, pp.255-309.

[8] R.Buchner,J.Barthel and J.Stauber, *"The dielectric relaxation of water between 0C° and 35C°,"Chem. Phys. Lett. 306* (1999) pp.57-63.

[9] Miller, W.; Smith, C.W; et al, "Negative Thermal Expansion: A Review," *Journal of Materials Science,* Barcode: 2009JMats. 44.5441M.doi:10:1007/s10853-009-3692-4. ISBN.

[10] Turcotte, Donald L.; Schubert, Gerald (2002). *Geodynamics. 2nd ed.* Cambridge. ISBN. 978-0-521-66624-4.

[11] *http://en.wikipedia.org/wiki/Thermal_expansion*, *Date* accessed March 22, 2015.

[12] V.Carrubb, A.L.Clarke, M.Akmal, Z.Yusoff, J.Lees,J.Benedikt, S.C.Cripps, P.J.Tasker, "Exploring the design space for broadband Pas using the novel continuous inverse class-F mode," *IEEE EuMC, October 2011, pp.333-336.*

[13] Kenle Chen, Dimtrious Peroulis, "Design of Broadband highly efficient harmonic-tuned Power Amplifier using in-band continuous class(F^{-1}/F) mode transferring," *Microwave Theory and Techniques, IEEE Transactions on*, Vol.60, Issue.12, Dec 2012, pp.4107-4116.

Chapter.7 CONCLUSION AND DISCUSSION

A portable, field deployable and physically small solid-state microwave heating structure has been practically demonstarted in this thesis. BLF6G27-10G 10W-LDMOS and (CLF1G0060-10) 10W-GaN power transistors have been used to generate sufficiently high power RF signals, where TE_{011} mode rectangular cavity and TM_{010} mode circular cavies have been used to accommodate the output power for heating. Compactness and field deployment of the apparatus have been the main motivation, and have been assured by simplifying and minimizing the physically large and complex matching networks to only series delay lines between the transistor and the microwave cavity resonators.

As we know, the well-defined impedance environment of the single mode cavities is highly sensitive to any interference whether it is due to the coupling structure, external temperature variation or sample properties variations, such as volume and temperature. In all the cases, the cavity natural impedance environment changes dramatically. For any change; the critical coupling of the cavity resonators is affected and hence the *Q*-factor generally decresaes. Therefore, whether using the cavity resonators for material characterization or for microwave heating it is very important to preserve its resonance and field properties. The cavity perturbantion phenomenon has been used in this work to formulate the integrated microwave heating arrangement. Three experiments were conducted which allowed the efficient Solid-state microwave heating.

The first microwave heating experiment performed using BLF6G27-10G 10-W LDMOS power transistor and the TE_{011} mode rectangular cavity resonantor allowed the formulation of an integrated F^{-1} powe amplifier by using the waveform engineering techniques. The impedance environment of the rectangular cavity was exploited as function of moving loop coupling antenna. The identified cavity impedance points together with simple series delay lines were presented at the I_{gen}-plane of the transistor for intrinsic-F^{-1} wave shaping at 2.45GHz. Thus by using this simplified integrated PA design approach high system efficiency was observed and measurements were found in excellent agreement with the simulations.

During the second experiment, (CLF1G0060-10) 10W-GaN power transistor and TM_{010} mode circular cavity was used to formulate the continuous mode inverted class-F power amplifier structure for solid-state microwave heating. The motivation behind this novel technique was to make a broadband and portable mirowave heating system capable of accommodating more than one sample at a time. Therefore, this concept was exploited by introducing 10 water volume samples in the cavity and its impedance environment was captured as function of water volumes. Impedance change in the cavity as a function of water volumes was accommodated by using series delay lines which presented the optimum continuous-invereted-F loading conditions at the I_{gen}-plane of 10W-GaN transistor. The measured results showed 10W RF power and more than 70% drain efficiency over the cavity's functional bandwidth where the cavity reflections were closer to -10dB.

The third experiment was to observe the impact of sample heating on the impedance environment of the well-defined TM_{010} mode cavity resonator. The motivation was to accommodate this natural impedance change to maintain the higher performance of the integrated structure over the operational bandwidth of the cavity. The impedance environment of the cavity was captured as function of discrete temperature variations from 27.5C°C to 70C° and around 30MHz frequency shift was observed until maximum 70C°. The natural impedance change over 30MHz was accommodated by presenting the optimum loading conditions to the 10W-LDMOS power transistor using microstrip series lines. The measurements allowed maximum 67% drain efficiency over 30MHz bandwith.

In conclusion, high-efficiency PA mode impedances have been achieved by utilizing the natural impedance environment of the sample holding cavity and fundamental, 2nd and 3rd harmonic loads have been transformed to the optimum impedance locations of the transistor by using simple series delay lines. The cavity impedance exploitation and load transformation procedure has been adopted by taking motivation from passive laodpull techniques.

The proposed integrated PA approaches offer solutions to the limitations found in the conventional PA design approaches. Firstly, it replaces the physically large and lossy transmission line matching networks with simple series microstrip lines which not only makes this arrangement more efficient but also guarantees its portability and field deployment; potentially for diagnostic healthcare applications. Secondly, this

approach allows the engineering of the voltage and current waveforms at the I_{GEN}-plane of transistor after de-embedding the package network as obserevd in two experiments. This is necessary because, once the access to the current generator plane is possible, it becomes easier to shape the voltage and current waveforms for high efficiency power amplifier modes of operation. In the proposed integrated Solid-state microwave heating methods, the limitation of the directional coupler has been removed by placing a coupled line directional coupler at the output stage of the integrated setup i.e. parallel to the output delay lines. conclusively, the first ever made Soild-state microwave heating arrangement for biomedical diagnostic applications makes it a field deployable apparatus due to portability, compactness and high efficiency broadband operation.

Chapter.8 FUTURE WORK

Though the solid state microwave heating arrangement presented in this thesis puts forth the foundation of a portable microwave heating structure but there are certain limitations which can be improved to make this physical structure further compact and fully integrated.

8.1 Coaxial Connection Removal

The first possible improvement in this structure can be made by completely removing the coaxial connector so that the heating structure can be made completely independent of any extra side bulk. But then the quenstion comes, how to capture the S-parameter response of just an aluminum box as shown in Fig.8.1.

Figure 8.1: TM_{010} mode Cavity without coaxial connection (a hollow box)

8.2 Measurement Technique

To capture the S-parameter response of the cavity, the following proceduer can be adopted:

1. Close the side hole of the cavity by an aluminum sheet to avoid any microwave power leakage.
2. Design a microstrip line of L=20mm and W=1.51mm printed on RTDuroid 5880 such that one end of the line is connected to VNA and the other end is connected directly with a circular loop antenna opening into cavity. The choice

of microstrip line dimensions is made because we already have the S-parameters of this line extracted through TRL calibration kit outlined in chapter.3.

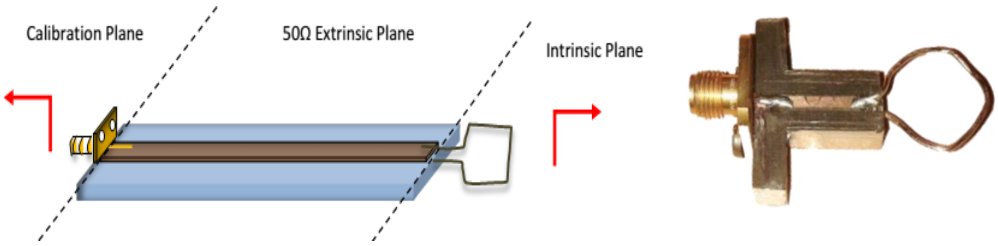

Figure 8.2: Cavity measurement structure

3. Now after setting up this arrangement, the S-parameters of the cavity can be captured (for any of the experiments conducted in this thesis) while the effect of extra 50Ω line is still in place.
4. while the S-parameter data of the cavity including fixture line has been captured, in each of the discrete data file the effect of the 50Ω extrinsic line can easily be removed in ADS. The de-embed component can be used from ADS and the S-parameter file of the fixture line can be loaded to negate its impact from the cavity and fixture measured data. Thus the finally obtained discrete S-parameter files will represent the exact behavior of the cavity only.
5. Now prcosess the data as outlined in chapter 4 and perform nonlinear simulations to formulate a true high efficiency PA-Cavity integrated solid-state microwave heating arrangement.
6. After fabricating the compact matching network, remove the aluminum backed ground so that T.L network remains printed on the independent substrate only for example RTDuroid/5880.
7. Finally bolt down the simplified matching network on top surface of the aluminum made cavity (which will also act as ground to the substrate) and attach the loop antenna directly with the designed matching network as shown in Fig 8.3. While finalizing the completely integrated setup, make sure that the antenna should be normal to the magnetic field for maximum energy transfer.

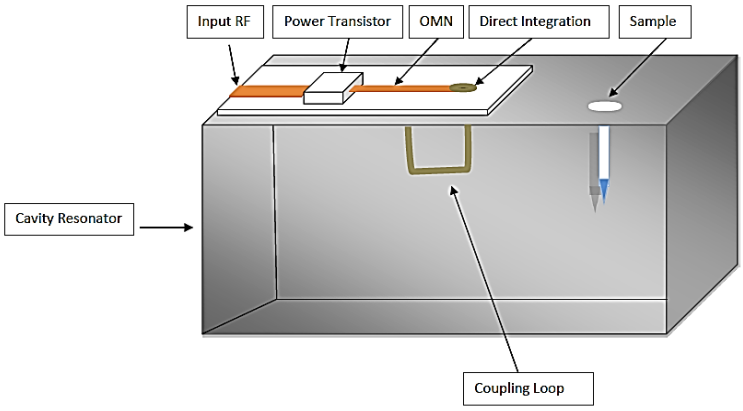

Figure 8.3: Fully Integrated Solid-State microwave heating arrangement

8.3 Coaxial Connector vs T.L connector measurements

To verify this approach, the TM_{010} circular cavity was selected for the initial experiment in which the loop coupling structure attached with the N-type connector was completely removed as shown in Fig.8.1. To measure the response of the cavity; the transmission line coupling structure shown in Fig.8.2 was inserted into the cavity and the orientation of the loop was adjusted and locked for the critical coupling of the cavity. The simple one-port calibration was performed until the SMA connector of the coupling loop and a frequency sweep was conducted to capture the S-parameter response of the cavity and the addional 20mm microstrip line. However, to verify the measurement accuracy of the loop coupling structure, the S-parameter response of the cavity was measured again by N-type connector. The two S-parameter files obtained in this case were imported into ADS citcuit simulator for comparison analysis. It important to note here that the S-parameter response of the cavity measured through the transmission line coupling structure includes the effect of the additional 20mm transmission line. Therefore, it is necessary to remove that effect by de-embedding this additional line. As we already have the de-embedding information of this line through TRL calibration (see section 3.2.2) therefore, the effect of the T.L was removed and the S-parameter response (mag, phase) of the cavity measured in both cases was compared as shown in Fig.8.4. it can be seen that the mesaured response in both cases is in excellent agremment where the resonance frequency shifts by approximately 6MHz. However, this frequency gap can be further reduced by slighly adjusting the loop coupling diameter and repositioning the loop orientation.

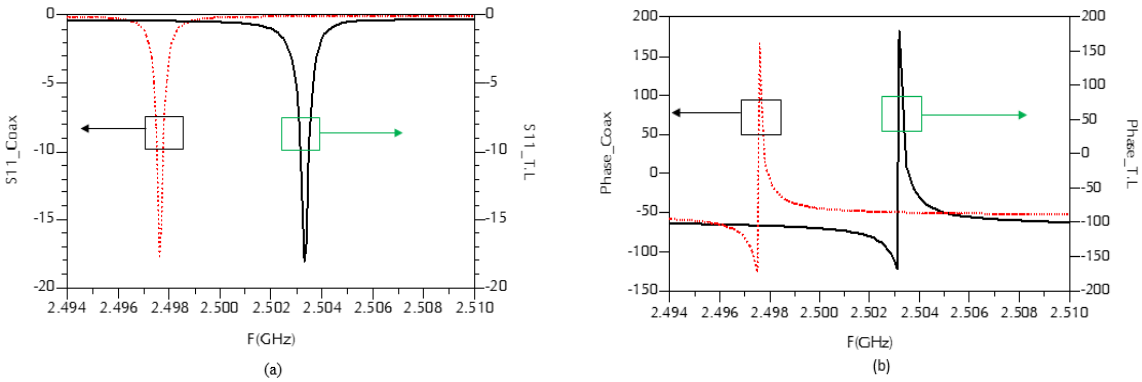

Figure 8.4: Measurement comparison of the air filled TM_{010} circular cavity resonator (a) Reflection loss (dB), (b) Phase response

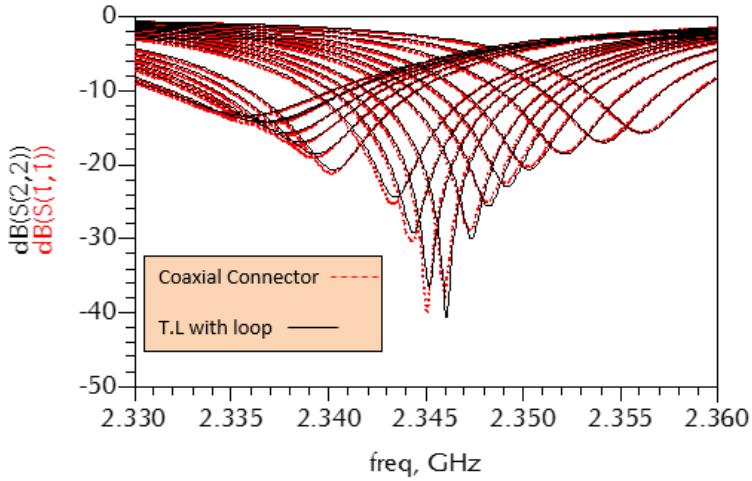

Fig 8.5: Coaxial vs Transmission Line connector measured response (T=27.5C° to T=70C°)

For further verification, the effect of the T.L coupling structure was introduced in one of the experiment conducted in chapter.6. The measured S-parameter files in both cases were superimposed in each other as shown in Fig.8.5. It can be seen that the actual response of the cavity in both cases is almost the same. Therefore, it can be concluded that fully integrated approach proposed in future work and shown through Fig.8.3 can be successfully adopted without requiring an extra side N-type connector. Using this novel technique, the experiments performed in this thesis can be repeated and the proposed microwave heating structures can be completely integrated and further reduced in size.

APPENDIX-A

In this appendix the F^{-1} power amplifiers (10W-LDMOS and 10W-GaN) were designed and fabricated based on loadpull transistor measurement characterization. The designs were conducted at 2.45GHz and the circuits were fabricated on RTduroid/5880 substrate. The motivation was to show the real comparison of the direct integrated Pas with the conventional 50Ω PAs. The physical apparatus sizes in this approach (conventional) and the direct integrated (proposed) have been tabulated below.

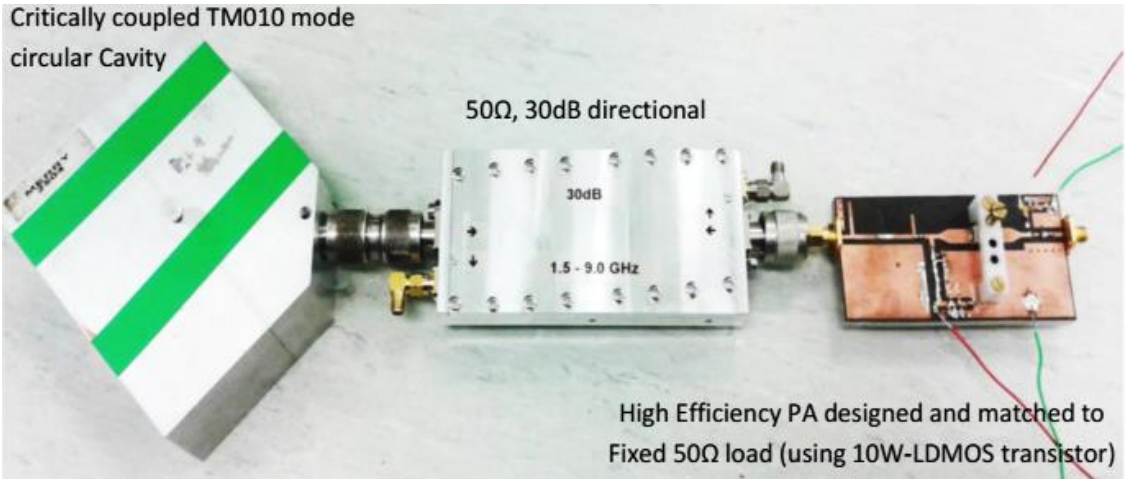

Figure 1: Conventional Solid-State Microwave Heating Apparatus with 10W-LDMOS PA and water loaded TM_{010} mode circular cavity

Figure 2: Conventional Solid-State Microwave Heating Apparatus with 10W-GaN PA and water loaded TM_{010} mode circular cavity

50Ω PA Cm	Directional Coupler Cm	Cavity resonator Cm
L=10, W=5 (using LDMOS)	L=18, W=6.5	H= 4.6, R=4
L=8,W=6 (using GaN)	L=18, W=6.5	H= 4.6, R=4

Table1: physical dimensions of the conventional fixed 50Ω solid-state microwave heating system (RF output stage)

Integrated PA Cm	Directional Coupler Cm	Cavity resonator Cm
L=5, W=4 (using LDMOS)	Printed on the board	H= 4.6, R=4
L=5, W=4 (using GaN)	Printed on the board	H= 4.6, R=4

Table2: Physical dimensions of the integrated non-50Ω solid-state microwave heating system (RF output stage)

APPENDIX-B

The Appendix maintains a table which, on one hand, contains the Impedance values taken from the TM_{010} circular Cavity as a function of water volume and frequency and on the other hand the transformed impedances (by series delay lines) at the package and I_{GEN}-plane of the 10W-GaN Power transistor.

Water Volume(uL)	**Frequency (GHz)**	**Z_{CAVITY}**	**$Z_{Transformed}$ (Power Match)**	**$Z_{Transistor}$ I_{GEN}-Plane**
300	2.376	*132.49-j*93*	18.62+j*19.34	66.3-j*5
280	2.382	*129.45-J*80*	20.18+j*18.12	66.34-j*0
260	2.394	*127.28-J*88*	19.67+j*19.29	66.61+j*13.05
240	2.401	*124-J*76.26*	21.28+j*18.1	64.43+j*17.15
220	2.424	*120-J*90.19*	20.21+j*20.23	62.15+j*34
200	2.442	*150.75-J*82*	17.58+j*16.80	59.2+j*17
180	2.474	*162-J*102*	15.40 +j*1780	56.95+j*19.35
160	2.483	*180-J*105*	14.06 +j*17.23	54+j*20
140	2.491	*227.95-J*125*	11.01+j*16.01	49.85+j*21.8
120	2.499	*306-J*52*	9.32+j*12.23	48.15+j*28

Table: water volume and frequency dependent broadband high efficiency loads presented at cavity and transistor (package/I_{GEN}-plane).

APPENDIX-C

The Appendix maintains a table which, on one hand, contains the Impedance values taken from the TM_{010} circular Cavity as a function of sample temperature and frequency and on the other hand the transformed impedances (by series delay lines) at the package plane of the 10W-LDMOS Power transistor.

Temperature C°	**Frequency GHz**	**Z_{Cavity} (Normalized to 50Ω)**	**$Z_{transformed}$ (Normalized to 50Ω)**
27.5	2.335	*1.27-j*0.412*	The Impedance changes were accommodated by the delay lines and all of the cavity loads were transferred to the near optimum impedance (≈10Ω) at the package plane of the 10W-LDMOS transistor.
27.5	2.336	*1.363-j*0.339*	
30	2.337	*1.377-j*0.251*	
30	2.338	*1.492-j*0.174*	
32.5	2.339	*1.583-j*0.043*	
32.5	2.340	*1.690 –j*0.046*	
32.5	2.341	*1.866 –j*0.176*	
32.5	2.342	*2.034–j*0.282*	
32.5	2.344	*2.509–j*0.510*	
35	2.345	*2.319–j*0.601*	
37.5	2.346	*2.336–j*0.632*	
40	2.347	*2.328–j*0.800*	
42.5	2.348	*2.263–j*0.883*	
42.5	2.348	*2.573-j*1.043*	
42.5	2.349	*2.870-j*1.162*	
45	2.350	*2.211–j*0.960*	
45	2.351	*2.488–j*1.112*	
47.5	2.352	*2.174–j*1.044*	

47.5	2.353	*2.458–j*1.207*	
50	2.354	*2.630+j*1.375*	
52.5	2.354	*2.503+j*1.426*	
55	2.355	*2.433+j*1.481*	
57.5	2.357	*2.410+j*1.582*	
60	2.358	*2.651+j*1.810*	
62.5	2.359	*2.565+j*1.860*	
65	2.360	*2.211+j*1.735*	
65	2.61	*2.363+j*2.011*	
67.5	2.362	*2.509+j*2*	
70	2.365	*2.983+j*2.351*	

Table: Temperature and frequency dependent broadband high efficiency loads presented at cavity and transistor (package plane).